

A STUDY OF OVERVOLTAGE PROBLEMS IN EHV SYSTEMS

**A Thesis Submitted
in Partial Fulfilment of the Requirements
for the Degree of
DOCTOR OF PHILOSOPHY**

**By
N. S. SAXENA**

**to the
DEPARTMENT OF ELECTRICAL ENGINEERING
INDIAN INSTITUTE OF TECHNOLOGY, KANPUR
NOVEMBER, 1981**

MAY 1981

CENTRAL LIBRARY
I. I. T., Kharpur.

Acc. No. **A 82592**

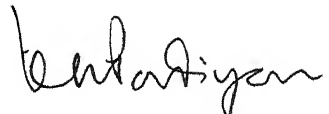
EE-1981-D-SAX-STU

C E R T I F I C A T E

Certified that this work 'A Study of Overvoltage Problems in EHV Systems' by Sri N.S. Saxena has been carried out under our guidance and supervision and that this work has not been submitted elsewhere for a degree.



Dr. R.P. Aggarwal
Professor



Dr. K.R. Padiyar
Professor

Department of Electrical Engineering
Indian Institute of Technology
KANPUR 208 016

A C K N O W L E D G E M E N T

With deep sense of gratitude, I am thankful to Dr. R.P. Aggarwal and Dr. K.R. Padiyar for their valuable guidance and kind cooperation without which this thesis would have not been completed.

I am grateful to Er. B.S.Sharma, Director of Research and Development, U.P. State Electricity Board Lucknow, for his active cooperation and valuable suggestions in the early part of the thesis.

I am thankful to Dr. S.D. Shukla, Director and Dr. V.K. Jain, Professor and Head of Electrical Engg. Department, of H.B. Technological Institute, Kanpur and to Dr. L.P. Singh, Professor of Electrical Engineering, Indian Institute of Technology, Kanpur, for their inspiration, encouragement and cooperation during the course of this work.

I am also thankful to my wife Ranjana for her cooperation and forbearance and to my daughters Sweta and Shikha for their tolerance.

Lastly, I am thankful to Mr. H.R. Verma for his careful typing and to Mr. R.K. Bajpai for his nice sketching.

TABLE OF CONTENTS

LIST OF TABLES	vii
LIST OF FIGURES	viii
LIST OF SYMBOLS	xiii
SYNOPSIS	xvii
CHAPTER I INTRODUCTION	1
1.1. Nature of overvoltages in EHV system	1
1.2. Steady state overvoltages	2
1.3. Dynamic overvoltages	5
1.4. Transient overvoltage - system modelling	8
1.5. Transient overvoltages due to faults	9
1.6. Outline of the thesis	10
CHAPTER II STEADY STATE OVERVOLTAGES	13
2.1. Introduction	13
2.2. Field investigations	14
2.3. Analytical study	17
2.3.1. Steady state analysis	23
2.3.2. Numerical Data and Results for steady state	28
2.4. Pre-steady state (Transient) period analysis	35
2.5. Preventive measures	39
2.6. Conclusion	46

CHAPTER III	DYNAMIC OVERVOLTAGES	48
3.1.	Introduction	48
3.2.	System description	49
3.2.1.	Synchronous generator	51
3.2.2.	Governor system	52
3.2.3.	Excitation system	55
3.2.4.	Transformer	57
3.2.5.	Shunt Reactor	57
3.2.6.	Transmission line	59
3.2.7.	Load	60
3.3.	Network state equations	60
3.4.	Solution Procedure	64
3.5.	Calculation of Dynamic overvoltages	66
3.5.1.	Case study 1 ; Hydro system	66
3.5.1.1.	High side switching	67
3.5.1.2.	Low side switching	73
3.5.2.	Case study 2 ; Thermal system	73
3.6.	Conclusion	78
CHAPTER IV	TRANSIENT OVERVOLTAGES - STATE SPACE AND METHOD OF CHARACTERISTICS	80
4.1.	Introduction	80
4.2.	System analysed	82
4.2.1.	Alternative 'a'	84
4.2.2.	Alternative 'b'	88
4.3.	Comparison of alternatives	94
4.4.	Conclusions	99

CHAPTER V	TRANSIENT OVERVOLTAGES DUE TO FAULTS	101
5.1.	Introduction	101
5.2.	System analysis	103
5.3.	Solution procedure	108
5.4.	System studies	109
5.4.1.	Fault inception overvoltages	110
5.4.2.	Fault overvoltage following load rejection	113
5.5.	Conclusion	118
CHAPTER VI	CONCLUSION	120
6.1.	General	120
6.2.	Review of the significant work	120
6.3.	Scope for further research	122
APPENDIX A	Fourier expression for $f(\phi)$	124
APPENDIX B	Secant method	127
APPENDIX C	Condition of stability	128
APPENDIX D	Generator Equivalent circuit	130
APPENDIX E	System data for dynamic overvoltage study	133
APPENDIX F	Calculation of Initial conditions	140
APPENDIX G	Derivation of Transfer Function relating terminals currents to the component voltages of 'Fourier cosine series'.	143
APPENDIX H	Data for system considered in Chapter IV	144

APPENDIX I	Simulation of transmission line faults.	146
APPENDIX J	Data for source B considered in Chapter V	152
LIST OF REFERENCES		153

LIST OF TABLES

<u>Table No.</u>	<u>Caption</u>	<u>Page</u>
2.1.	Possible voltage solution for fundamental components $L_3 = 1,000$ H and $C_b = 2,000$ pf	31
2.2.	Possible voltage solutions for fundamental components $L_3 = 1,000$ H and $C_b = 2,500$ pf	31
2.3.	Possible voltage solution for fundamental components $L_3 = 700$ H and $C_b = 3,200$ pf	32
2.4.	Occurrence of HV or LV mode with the Angle δ	37
2.5.	Equivalent grading of capacitance ' C_1 ' for various values CBs	42
2.6.	The critical value of L_2 above which the HV mode does not occur for the various values of break point flux ϕ_1	45
4.1.	Comparative statement for Alternative 'a' and 'b'	99
5.1.	Overvoltages on Healthy phases due to fault inception on phase 'a'	111
5.2.	Overvoltages due to load rejection following fault	113

LIST OF FIGURES

<u>Figure No.</u>	<u>Caption</u>	<u>Page</u>
2.1.	Simplified Single Line Diagram of 220 KV Sub-station	15
2.2.	Voltage waveforms Before and After CB Opening	16
2.3.A	v-i characteristic of EMVT	18
2.3.B	Piecewise Linear Approximation of the EMVT v-i characteristic	18
2.4.A	Excitation current wave shape with Secondary energised	19
2.4.B	Excitation current wave shape with primary energised	19
2.5.	Equivalent circuit Representation of the Power System as seen from 220 KV Bus	20
2.6.	Equivalent circuit of the System Neglecting Source Impedance	20
2.7.	Thevenin's Equivalent of the Power System	22
2.8.	ϕ -i characteristic of the VT	22
2.9.	Possible solutions for circuit shown in Fig. 2.7	30
2.10.A	$\sqrt{3}$ x Phase voltage at Bus Along with Third Harmonic component	33

2.10.B	$\sqrt{3}$ x phase voltage at Bus Along with Third Harmonic component	33
2.11(a)	Voltage across EMVT for $\delta = 40^\circ$	37
2.11(b)	Voltage across EMVT for $\delta = 0^\circ$	37
2.12.	Effect of change in L_3 on the probability of HV mode	41
2.13.	EMVT Saturation characteristics obtained from Various Manufacturers	43
2.14.	Typical $\phi - i$ characteristic of the EMVT	44
3.1.	A Typical EHV System	50
3.2.	Circuit Model for 3-phase Stator	50
3.3.	Hydraulic Governor	53
3.4.	Steam Turbine and Governor	54
3.5.	IEEE Type-2 Rotating Excitation System	56
3.6.	Equivalent Circuit of the Transformer	58
3.7.	Equivalent Circuit of the Transmission Line	58
3.8.	Equivalent Circuit of the System	61
3.9.	Interconnection of the System Components for the Digital Simulation	65
3.10.	Variation of V_T , $\Delta \omega$ and E_{fd} with Time (High Side Switching)	68
3.11.	Receiving End Voltages with ES Active (High Side Switching	69

3.12.	Receiving End Voltage with ES Blocked (High Side Switching)	70
3.13.	Receiving End Voltage without any Reactor (High Side Switching)	72
3.14.	Receiving End Voltages with ES Blocked (Low Side Switching)	74
3.15.	Receiving End Voltages with ES Active (Low Side Switching)	75
3.16.	Receiving end Voltages for a Thermal System (High Side Switching)	76
3.17.	Receiving End Voltage of the Thermal System with Increased Line Length	78
4.1.	The System Analysed	83
4.2.	The Equivalent Circuit of the System	83
4.3.	The Transmission Line Model for Alternative 'a'	85
4.4.	The Transmission Line Model For Alternative 'b'	92
4.5.	Receiving End Voltages a Line Energisation (Example - I)	96
4.6.	Receiving End Voltages on Line Energi- sation without Closing Resistance (Example II)	97
4.7.	Received End Voltages on Line Energi- sation with Closing Resistance (Example II)	98

5.1.	System Analysed for Fault Overvoltages	104
5.2.	Equivalent Circuit of the System shown in Fig. 5.1.	104
5.3.	Fault Inception Voltage Waveform at the Sending End of the Line for Case-I and Study-I	114
5.4.	Fault Inception Voltage Waveform at the Send- ing End of the Line for Case-II and Study-II	114
5.5.	Fault Inception Voltage Waveform on Phase 'c' at Sending End of the Line for Case-I and Study - II	115
5.6.	Fault Inception Voltage Waveform on Phase 'c' at Sending End of the Line for Case-II and Study-II.	115
5.7.	Fault Inception Voltage Waveform on Phase 'c' at Sending End of the Line for Case-I and Study-III	116
5.8.	Fault Inception Voltage Waveform on Phase 'c' at Sending End of the Line for Case-II and Study-III	116
5.9.	Fault Overvoltage. Due to Load Rejection on Phase 'b' at the Receiving End of the Line without CB Opening Resistance	117
5.10.	Fault Overvoltage Due to Load Rejection on Phase 'b' at the Sending End of the Line with CB Opening resistance Study-III	117

A-1	Derivation of $f(\varphi)$ from φ	125
D-1	The Generator	131
E-1	The Magnetising Characteristic of the Transformer	137
F-1	Generator vector diagram at steady state	141

LIST OF PRINCIPAL SYMBOLS

(a)	<u>For Chapter - II</u>
e_s	Source voltage
C_l	Total circuit breaker grading capacitance
R	Resistance to account for losses in EMVT and other apparatus connected to bus.
C_b	Bus capacitance
L	EMVT Non-linear inductance
φ	Flux developed in the EMVT core
e_{th}	Thevenin's equivalent voltage
C_{th}	Thevenin's equivalent capacitance
ω	System frequency
δ	Source angle
φ_1	Flux at the first break point of the φ -i characteristic of EMVT
φ_2	Flux at the second break point of the φ -i characteristic of EMVT
L_1	Initial slope of the φ -i characteristic of EMVT
L_2	Second slope of the φ -i characteristic of EMVT
L_3	Final slope of the φ -i characteristic of EMVT
e_L	Voltage across EMVT
$f(\varphi)$	Current through EMVT
A_n	n^{th} sine component of Fourier series for $f(\varphi)$
B_n	n^{th} cosine component of Fourier series for $f(\varphi)$

X_n	Magnitude of n^{th} Harmonic of φ
θ_n	Phase shift between n^{th} harmonic and the fundamental component of φ
(b)	<u>For Chapters III, IV and V</u>
I_g	Dependent current source of the generator model
L_g	Inductance matrix representing generator stator
E_{fd}	d-axis field voltage
ω	Speed
δ	Power angle of the generator
x_d	d-axis reactance at steady state
x_q	q-axis reactance at steady state
x'_d	d-axis transient reactance
x'_q	q-axis transient reactance
x''_d	d-axis sub-transient reactance
x''_q	q-axis sub-transient reactance
T_{do}	Open circuit time constant of d-axis with 'h' winding open.
T'_{do}	Open circuit time constant of d-axis with 'h'winding shorted
T_{qo}	Open circuit time constant of q-axis with 'k' winding open.
T'_{qo}	Open circuit time constant of q-axis with 'k' winding shorted.
H	Inertia constant
D	Damping constant

ϕ	flux linkage with the suffixed winding
P_m	Mechanical power
P_e	Electrical power
i_1	Terminal current of the generator
v_T	Terminal voltage of the generator
R_2	Resistance to account copper loss in T_1
L_2	Leakage inductance of the transformer T_1
R_9	Resistance to account major part of the core loss in T_1
R_1	Resistance to account part of the core loss in T_1
ϕ_1	Flux linkage of T_1
R_5	Resistance to account for losses in sending end reactor
L_5	Inductance of the send ing end reactor
R_6	Resistance to account for losses in receiving end reactor
L_6	Inductance of the receiving end reactor.
i_3	Current of the sending end reactor
i_4	Current of the receiving end reactor
R_3	Line resistance
L_3	Line inductance
C_1	Half of the line capacitance
R_4	Resistance to account for copper loss in T_2
L_4	Leakage inductance of the transformer T_2
R_8	Resistance to account for major part of the core loss in T_2

R_7	Resistance to account for part of the core loss in T_2 .
φ_2	Flux linkage of T_2
i_L	Load current
e_k	Voltage of the sending end of the line
e_m	Voltage at the receiving end of the line
i_{km}	Terminal current at the sending of the line
i_{mk}	Terminal current at the receiving end of the line
e_f	Voltage at the fault point
i_f	Fault current
i_{kf}	Current from node 'k' to 'f'
i_{fk}	Current from node 'f' to 'k'
i_{mf}	Current from node 'm' to 'f'
i_{fm}	Current from node 'f' to 'm'
I_k	Current source at node 'k' depending on past history
I_m	Current source at node 'm' depending on past history
I_{fa}	Current source at node 'f' depending on past history of line Section 'a'.
I_{fb}	Current source at node 'f' depending on past history of line Section 'b'.
C_s	Source voltage of the source B.
R_s	Source resistance of the source B.
L_s	Source inductance of the source B.
R_b	Circuit breaker resistance

SYNOPSIS

A STUDY OF OVERVOLTAGE PROBLEMS IN EHV SYSTEMS

by

N.S. Saxena

Ph.D.

Department of Electrical Engineering
Indian Institute of Technology, Kanpur
July, 1981

With the increase in power demand, the present trend is to transmit large amount of power over long distance lines at extra high voltage (EHV). In EHV systems, the insulation level is decided by overvoltages caused due to switching and/or faults rather than lightening. A poor choice of insulation level will either increase the cost of the system or will increase risk of failures due to faults initiated by flashovers. Therefore a proper insulation level should be chosen which requires the knowledge of the nature and magnitudes of various overvoltages caused by different system conditions. Since the magnitude and time duration of various overvoltages is different, therefore, they stress the insulation in different manner.

There are three distinct periods during which the overvoltages occur, viz.,

- a) A surge period during which the travelling wave effects predominate and in which the line is represented by its surge characteristics. The transient (surge) overvoltages are caused by line energisation/re-energisation or fault initiation.
- b) A dynamic period which is transitional between the surge period and the steady state and is characterized by the voltage variation contained in an envelope which varies aperiodically with time.
- c) A steady state period during which the voltage is periodic but usually is distorted due to various harmonic components. When the power system is terminated by a transformer, steady state overvoltage may occur at the transformer terminals due to switching operation. The transformer non-linear characteristic plays a dominant role in this phenomena and the system is said to be in a 'ferro-resonant' mode.

The objective of this thesis is to study all the above mentioned overvoltages. Suitable techniques for digital simulation have been evolved for their evaluation which consider more detailed system representation than reported before in the literature.

Steady state overvoltages are studied first. The field investigation of an electromagnetic voltage transformer (EMVT) failure while being de-energized by a circuit

breaker (CB) fitted with grading capacitors across its contacts is described. This phenomena has been analyzed using the principle of 'Harmonic Balance' and it is shown that the failure was due to ferro-resonance phenomena. Also the analysis for the pre-steady state period is carried out using state space techniques. This is to give insight into initial conditions which might give rise to the steady state overvoltages. Based upon the data collected for several makes of EMVTs and CBs fitted with grading capacitors, remedial measures have been suggested to avoid such incidents.

Dynamic overvoltages following load rejection have been considered next. The methods reported in the literature for the evaluation of such overvoltages are approximate. Usually the digital simulation is employed to predict the variation in magnitude and frequency of the internal voltage of the machine and this information is used subsequently on the transient network analyzer (TNA) to predict ferro-resonant overvoltages. The digital simulation ignores the network transients but can predict the phenomena of self excitation. In this thesis, this two stage computation is combined in a single digital simulation program, which incorporates not only the network transients on a 3-phase basis but also the synchronous machine representation in detail. The prime mover-governor is also considered along with the exciter and voltage regulator. The nonlinearities

due to transformer and machine saturation are included. It is believed that this is a more accurate approach, and can be used to determine if the phenomena of self excitation and/or ferro-resonance can occur in a single simulation. This is illustrated with the help of the case studies of both hydro and thermal machines feeding a load through a long EHV line. The effectiveness of the voltage regulator in controlling the overvoltages due to ferro-resonance is also demonstrated.

Transient overvoltages are considered next. The method of characteristics as given by Dommel is recognized to be most efficient for the calculation of the transmission line transients, since the equations involved are algebraic rather than differential. However this method requires iterative solution at each time step if nonlinearities are present in the network. The state space techniques are more efficient in handling nonlinearities. In this thesis the alternative of (1) employment of state space techniques for both the network and the transmission line and (2) the combined use of state space techniques for the network and the method of characteristics for the transmission lines, have been examined. It is found out that the second approach is usually superior in terms of computation time.

The transient overvoltages caused by fault initiation are also considered. The transmission line model using the method of characteristics due to Dommel is extended to

simulate the initiation of a fault at any point of the line. The generator dynamics is represented, and the results are compared when the generator is represented by a constant voltage source. It is demonstrated that the overvoltages are greater if the generator dynamics is included in the simulation. It is found that the opening of the CB at the receiving end in trying to clear the fault aggravates the overvoltage problem and it can be controlled through the use of CB opening resistors. It is also found in this case that the overvoltages are higher at receiving end when the fault is closer to the receiving end.

Finally, the thesis concludes with the highlights of the work reported in the area of overvoltages in EHV systems and projects the scope for further work.

CHAPTER - I

I N T R O D U C T I O N

1.1. NATURE OF OVERVOLTAGES IN EHV SYSTEMS

With the increase in power demand and the economic necessities to locate generating stations in remote areas, the present trend is to transmit the bulk power over long distance extra high voltage (EHV) lines. In an EHV system, the insulation level is determined by overvoltages caused due to switching and/or faults rather than lightening. A poor choice of insulation level will either increase the cost of the system or will increase the risk of failures due to faults initiated by flashovers. Therefore a proper insulation level should be chosen, which requires the knowledge of the nature and magnitude of various overvoltages caused by different system conditions.

Following a disturbance, there are **three distinct** periods during which the overvoltages occur, viz.,

- a) A surge period during which the travelling wave effects predominate and in which the line is represented by its surge characteristics. The transient (surge) overvoltages are caused by sudden switching or fault inception.

- b) A dynamic period, which is transitional between the transient and the steady state and is characterised by the voltage variation contained in an envelope which varies aperiodically with time.
- c) A steady state period during which the voltage is periodic but usually is distorted due to various harmonic components. When a power system is terminated by a transformer, steady state overvoltages may occur at the transformer terminals due to switching operation. The transformer non-linear characteristic plays a dominant role in this phenomena and the system is said to be in a 'ferroresonant mode'.

We give below a review of the significant work already done in the above areas along with the modifications and additions implemented in this thesis. The steady state overvoltages have been studied first, followed by dynamic and transient overvoltages respectively.

1.2. STEADY STATE OVERVOLTAGES

As already mentioned in Sec. 1.1, steady state overvoltages may occur when a system is terminated by a transformer. The combination of the circuit parameters may be such that upon switching, the phenomena of ferroresonance takes place. This is particularly true when air circuit breakers with grading capacitors are used for switching operation. Such overvoltages have been reported to result

in damage both to the electromagnetic voltage transformer (EMVT) and the power transformer [24,25,32,33,41].

The problem has been analysed in the past either by using (a) state space technique [18,42] or (b) dual input describing function technique [13,35].

The non-linearity arising due to the transformer saturation is approximated either by an exponential function [18] or by a piece-wise linear model [42].

In state space technique, a set of first order non-linear differential equations are solved on the digital computer. If the solution is carried out for a sufficiently long time, the steady state solution can be obtained. The steady state solution consists of the fundamental and higher harmonics. However, this method does not provide any direct information regarding the harmonic components. The nature of the solution also depends on the initial conditions as it may not always lead to overvoltages. If one wants to examine the effect of several system parameters, then the simulation of all possible initial conditions with different combination of system parameters becomes a laborious if not an impossible task.

Swift [13] has employed dual input describing function technique which is popular in control systems theory. In this technique a small perturbation is considered

and the describing function is obtained assuming the non-linearity to be a third degree polynomial. Only the fundamental frequency component of the solution is obtained since the overall system is assumed to be a low pass filter. The condition of the instability i.e. ferroresonance jump is obtained by calculating the critical magnitude of disturbance for which the Nyquist diagram encloses the minus one point. Prusty and Sanyal [35] generalised the Swift's technique so that the non-linearity can be approximated by an n^{th} degree polynomial. The drawback of the Swift's technique is that the magnitude of the overvoltages predicted does not include the effect of harmonics. Also it gives the critical value of the disturbance for which the overvoltages will occur, but no information is available about the system initial conditions which lead to the ferroresonant mode.

In this thesis, the principle of 'Harmonic Balance' [2,3] is used to determine the steady state overvoltages. The method gives the magnitudes of both the fundamental and harmonic components separately. It gives various possible modes of the operation and their stability can also be examined. The proposed method is shown to give excellent agreement between the results obtained from the analysis and actual field test of a practical system. By collecting the data for several makes of circuit breaker and electromagnetic voltage transformers, we have carried out detailed investigation

in an attempt to suggest remedial measures to prevent the occurrence of such overvoltages. It is shown that if the transformer saturation characteristic can be controlled to a reasonable extent, such overvoltages do not occur.

1.3. DYNAMIC OVERVOLTAGES

Sometimes situations may arise ~~that due to sudden~~ load rejection, an unloaded EHV line is left connected to over-speeding generator(s). This situation can lead to excessive overvoltages in the system. Essentially such overvoltages are of fundamental frequency with harmonic components and may persist for a few seconds. They can become dangerous if the generator self-excitation takes place due to excessive line charging and/or when ferroresonance takes place due to the transformer saturation. The magnitude of such overvoltages is influenced by the generator dynamics, excitation system, prime mover governor, line and transformer constants and saturation characteristics of the transformer. and generator. Therefore, all the components described above need to be modelled accurately for the correct evaluation of dynamic overvoltages.

Demello et.al [4] employed an electronic differential analyzer for the determination of dynamic overvoltages. They represented the generator in details including amortisseur circuits, using the Park's equations. The excitation system

was represented in detail while the prime mover governor was represented approximately by a speed versus time curve. Besides the above approximation, the electrical network was represented on a steady state basis. While the method could predict the generator self-excitation, it was not capable of predicting ferroresonance, since the network transients were ignored.

Aggarwal et al [26,27] employed state space approach to study this problem. The system was represented on a single phase basis, which is not adequate when the non-linear elements are considered. The rise in frequency and generator internal voltage was represented by an approximate method. The non-linearity due to transformer saturation was considered by piecewise linear approximation. While the method was capable of predicting the ferroresonance, it could not predict the generator self-excitation.

Clerici and Didriksen [23] employed digital simulation to predict variation of the magnitude and frequency of the generator internal voltages and this information was subsequently used on a 'Transient Network Analyzer' (TNA) to determine dynamic overvoltages. The digital simulation, where the network transients were ignored, could predict the generator self-excitation and the TNA could simulate the network transients including ferroresonance. However, the process required a two stage computation.

In this thesis we have employed digital simulation technique, which incorporates not only the network transients on three phase basis but also the generator in complete details including amortisseur circuits. Its excitation system and prime mover governor are also represented in detail. The non-linearities due to transformer and generator saturation are also included. The synchronous generator is modelled by a dependent current source in parallel with a constant inductance as given by Ramshaw and Padiyar [28]. The time varying coupling in the machine inductance matrix is replaced by a dependent current source. The concept of dummy rotor coils is used to eliminate dynamic saliency and thereby avoiding the inversion of time varying matrix at each step of integration.

It is believed that this is a more accurate approach for the determination of dynamic overvoltages and can predict the phenomena of self-excitation and/or ferroresonance in a single stage simulation. This is illustrated with case studies for both hydro and thermal generators feeding a load through a long EHV line. The effect of the excitation system in controlling the overvoltages due to ferroresonance and self-excitation is also demonstrated.

1.4. TRANSIENT OVERVOLTAGES - SYSTEM MODELLING

The transient overvoltages can arise in an EHV system either due to internal causes such as switching or fault inception or due to external causes such as lightening discharges. It is a well known fact that the EHV systems are designed from the consideration of overvoltages due to switching [5, 14] or fault inception [15,16,17]. The calculation of these overvoltages requires the representation of the transmission line on a distributed parameter basis and hence is quite complex. There are several method [6,7,8,9, 10,,11,12] for the transmission line modelling, among them the method of characteristics suggested by Dommel [11,21,31] is perhaps most widely used. Using this model for the transmission line, the resulting equivalent circuit for the EHV system is purely resistive and hence can be easily solved. Dommel [21] proposed 'Compensation Method' when non-linearities due to the transformer saturation etc. have to be considered. However, the method becomes very slow due to its iterative nature when there are several non-linearities.

The non-linearities can be better handled with the use of state space techniques. Therefore, in this thesis, two alternatives of the system modelling have been considered viz., (a) to interface the transmission line model based on

the method of characteristics with the state space model for the rest of the system and (b) to employ the state space model for the transmission line as well along with the rest of the system. It is shown that the Alternative 'a' is superior to Alternative 'b' in terms of the computation time.

1.5. TRANSIENT OVERVOLTAGES DUE TO FAULTS

The transient overvoltages which are considered important for the insulation design for EHV systems are due to line energisation/re-energisation [5,14,27]. With further increase in the system voltage, the safety margins are reduced due to economic reasons. This requires that the line energisation/re-energisation voltage should be controlled to a lower value which is achieved mainly by circuit breaker closing resistors. In such cases the overvoltages due to fault inception and subsequent load throw-off may become more important [16,23]. The study of such overvoltages requires detailed generator representation especially for the salient pole machine [1]. In earlier TNA studies [16,22,23], the detailed generator representation was not possible. A method to interface the detailed generator model with the electromagnetic transients program was given by Brandwajn and Dommel [39]. The method employed Park's equations for the simulation of the generator and a few approximations were made to avoid the re-triangularisation of the network matrix at each integration

step due to the time dependent generator inductance matrix introduced by dynamic saliency.

The generator representation employed in **this thesis** has been discussed in Sec. 1.3. It may be noted that this representation gives constant inductance matrix without making any approximation. Based upon the model derived from considerations discussed in Secs. 1.4, the study of over-voltages due to fault inception and subsequent load throw-off have been carried out. The effect of the detailed generator representation, number of generators and the location of the fault have been studied.

1.6. OUTLINE OF THE THESIS

Chapter-II deals with the determination of steady state overvoltages. The failure of an electromagnetic voltage transformer in a practical system while being de-energised by a circuit breaker fitted with grading capacitors has been studied. The field investigations subsequent to the damage and the analytical study performed using the principle of 'Harmonic Balance' have been presented. The field and analytical results obtained are shown to be in close agreement. The analysis of the pre-steady state period is also carried out to get an insight into the initial conditions which give rise to the steady state overvoltages. This analysis is done

using the state space techniques. Based upon the data collected for several makes of electromagnetic voltage transformers and circuit breakers fitted with grading capacitors, remedial measures have been suggested to avoid such incidents.

Chapter - III deals with the determination of dynamic overvoltages following load rejection. A digital simulation technique for the evaluation of such overvoltages has been presented, which not only accounts for the network transients on three phase basis but also includes the detailed generator representation along with its excitation system and prime mover governor. The non-linearities due to transformer and generator saturation are also considered. The simulation technique is capable of predicting the self-excitation and/or ferroresonance in a single simulation. Both the hydro and thermal systems are considered and the effectiveness of an excitation system in controlling the overvoltages due to self excitation and/or ferroresonance is illustrated.

Chapter IV deals with some modelling aspects for the determination of transient overvoltages. The method of characteristics is more popular in determination of transient overvoltages. However **when the EHV system has several non-linear elements**, the state space technique may be more convenient. Thus, two alternatives have been considered viz., (a) to interface the method of characteristics for the transmission

line representation with the state space model for the rest of the EHV system and (b) to use the state space model for the entire EHV system including the transmission line. Both the alternatives have been studied and it is concluded that Alternative (a) is superior to Alternative (b).

Chapter V deals with the transient overvoltages caused by fault inception and also subsequent load rejection. The method of characteristics is extended to simulate the fault at any point on the transmission line. The fault inception overvoltage are studied for both detailed and simplified generator representation. The effect of the number of generators operating in parallel and fault location is also studied. Subsequent to the above studies, the overvoltages on load throw-off, while the fault (at various location on the line) is still present, are obtained. The effectiveness of the circuit breaker opening resistors in controlling such overvoltages is demonstrated.

Chapter VI concludes with a review of the significant work done in this thesis and scope for further work.

CHAPTER II

STEADY STATE OVERVOLTAGES

2.1. INTRODUCTION

Steady state overvoltages may occur when a system is terminated by a transformer. The combination of the circuit parameters may be such that upon switching the phenomena of ferro-resonance takes place. This is particularly true when air circuit breakers with grading capacitors are used for switching operation. Such overvoltages have been reported to result in damage both to the electromagnetic voltage transformer (EMVT) and power transformer [24,25] and, thus, have been the cause of concern.

The main approaches adopted so far in the literature to study this problem have already been reviewed in Chapter I, where the shortcomings of the state space and describing function techniques for steady state solutions have been given.

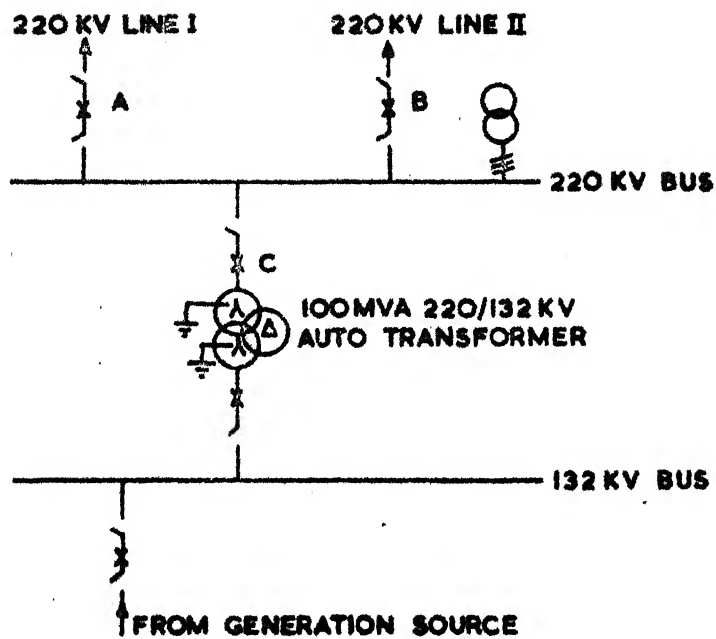
In this thesis, we have adopted the principle of 'Harmonic Balance' [2,3] for studying steady state overvoltages. We were fortunate enough to analyse the failure of a 220 KV electromagnetic voltage transformer (EMVT) which occurred in the U.P. State Electricity Board (UPSEB) system in India. Subsequent to the damage, field investigations were carried out to simulate what actually happened and is given in **S**ection 2.2.

2.2. FIELD INVESTIGATIONS

A 220 KV bus EMVT installed at a 220 KV substation (whose single line diagram is given in Fig. 2.1) got damaged when the 220 KV bus was to be completely **de-energised** from all sources of supply by opening C, the last circuit breaker (CB) (associated bus isolators remaining closed) when other CBs (A and B) had already been opened.

The damaged EMVT was replaced by an EMVT of the same make and design and the sequences which resulted in damage to the earlier EMVT were ~~re~~-enacted and it was observed that when the last CB was opened to disconnect the source of supply, the voltage instead of falling to an anticipated low value, some times **shot** to a high value of 380 KV.

The observed voltage waveforms before and after opening of the CB are shown in Figs. 2.2A, 2.2B and 2.2C. From Fig. 2.2A, it would be seen that on opening the CB at point A, there is a transient period before the voltage settled to a steady state value of 380 KV RMS from point B onwards. The transient period was found to vary as seen from Figs. 2.2A and 2.2B. Figure 2.2C shows a case when the voltage settled to a low value of 70 KV RMS. These results were also repeated with an additional loading of 9 Ohm resistor connected across EMVT secondary to dampen




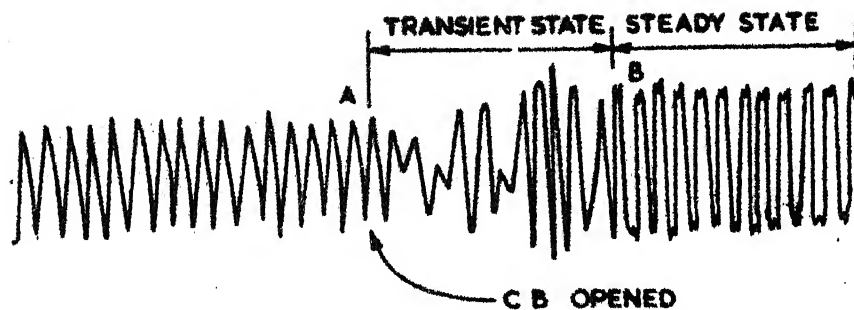
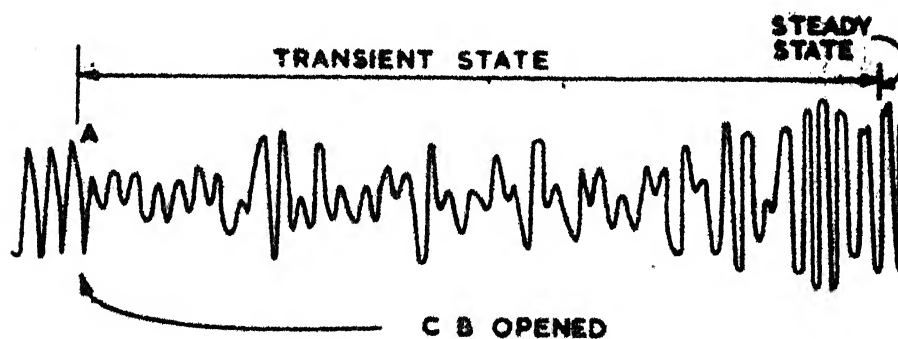
1. X DEPICTS AIR BLAST CIRCUIT BREAKER
2. — DEPICTS ISOLATORS
3.  DEPICTS EMVT (ONE ON EACH PHASE)
4. ALL ISOLATORS WERE IN CLOSED POSITION

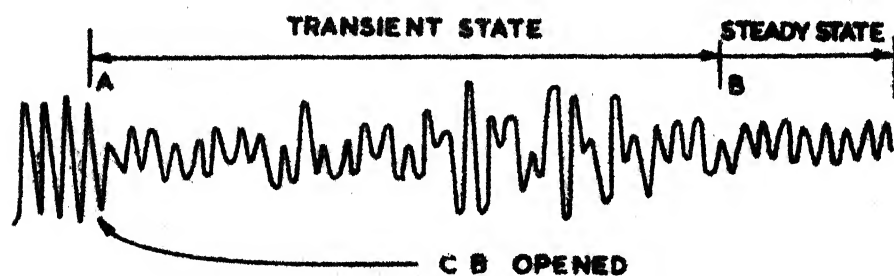
FIG. 2.1 SIMPLIFIED SINGLE LINE DIAGRAM OF 220 KV SUB-STATION.



(A)



(B)



(C)

2.2 VOLTAGE WAVE FORMS BEFORE AND AFTER C B OPENING.

the oscillations but no significant change in results was observed.

The $v-i$ characteristic of the EMVT as shown in Fig. 2.3A was obtained from the field test. The piece-wise linear approximation was used later in the analytical study. It may be noted that the slope L_3 is not known from the field data and, therefore, is a variable.

The oscillograms of the exciting current upto the operating voltage range when excited from the secondary and the primary side are given in Figs. 2.4A and 2.4B respectively. Since $v-i$ characteristic of the EMVT is nonlinear, these waveforms are rich in harmonic content.

2.3. ANALYTICAL STUDY

The equivalent circuit representation of the power system as seen from the 220 KV bus is given in Fig. 2.5.

The various quantities shown in Fig. 2.5 are as follows :

- e_g = Source voltage
- R_g and X_g = Source resistance and reactance respectively
- C_g = Circuit breaker grading capacitance
- R = Resistance to account for losses in the EMVT and connected apparatus at the bus plus the bus loss itself.
- L = EMVT nonlinear inductance.

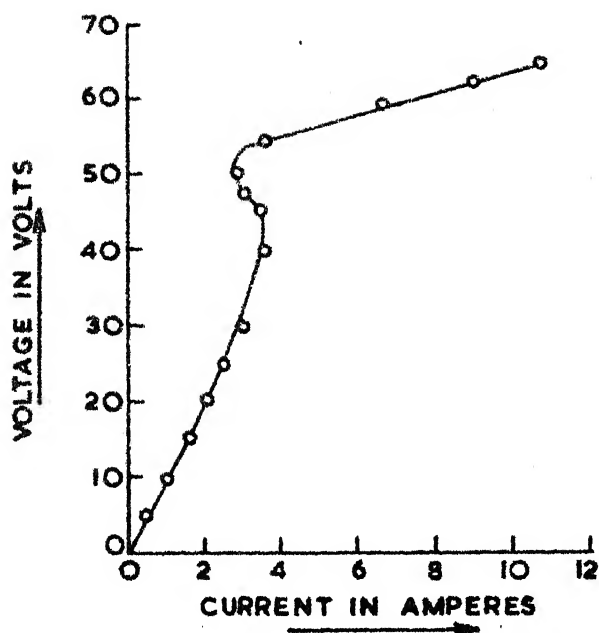


FIG. 2.3A v-i CHARACTERISTIC OF EMVT.

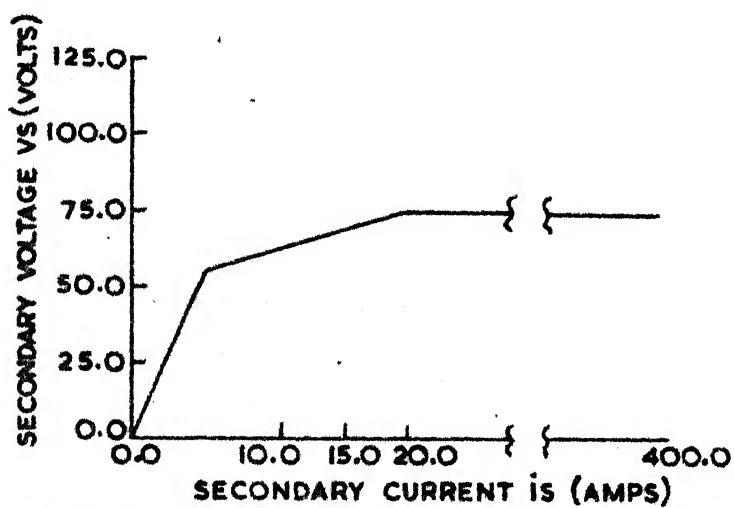
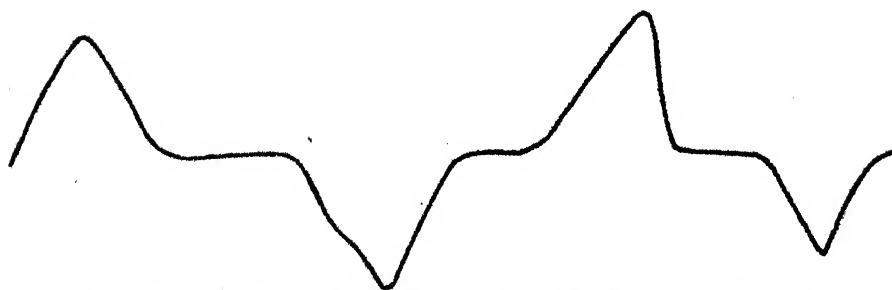


FIG. 2.3B PIECEWISE LINEAR APPROXIMATION OF THE EMVT v-i CHARACTERISTIC.



**FIG. 2.4A EXCITATION CURRENT WAVE SHAPE
WITH SECONDARY ENERGISED.**



**FIG. 2.4B EXCITATION CURRENT WAVE SHAPE WITH
PRIMARY ENERGISED.**

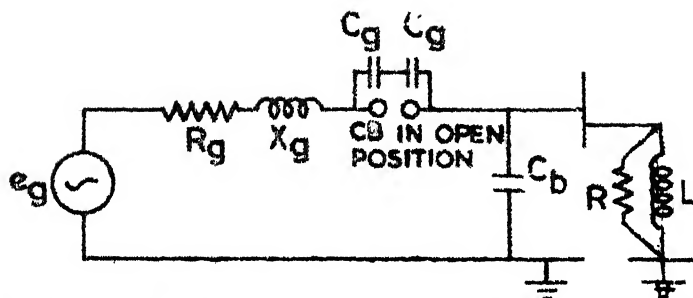


FIG.2.5 EQUIVALENT CIRCUIT REPRESENTATION OF THE POWER SYSTEM AS SEEN FROM 220 KV BUS.

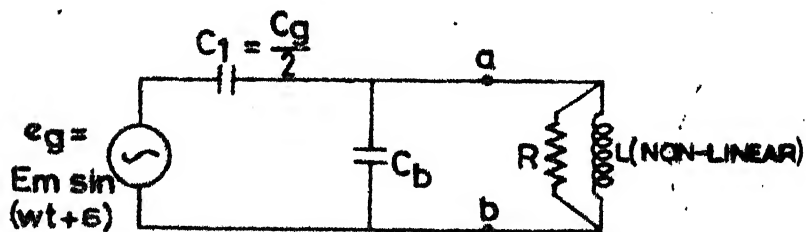


FIG.2.6 EQUIVALENT CIRCUIT OF THE SYSTEM NEGLECTING SOURCE IMPEDANCE.

If we neglect the source impedance, the equivalent circuit of the system is as shown in Fig.2.6. The system to the left of the terminals 'a' and 'b' is represented by its Thevenin's equivalent and the resultant system is as shown in Fig. 2.7.

The objective is to find the voltage across L of the EMVT when the CB is opened. This can be done by solving for flux ' ϕ ' developed in the EMVT core since the voltage is the derivative of flux. Therefore, the $v-i$ characteristic of the EMVT given in Fig. 2.3B is converted to a $\phi-i$ characteristic (Fig. 2.8) as seen from the primary side.

$$\frac{d\phi}{dt} + \frac{1}{C_{th}} \int i_C dt = e_{th} \quad (2.1)$$

$$i_C = i_R + f(\phi) \quad (2.2)$$

$$e_R = R \cdot i_R = e_L = \frac{d\phi}{dt} \quad (2.3)$$

If we take

$$e_{th} = E_{th} \sin(\omega t + \delta) \quad (2.4)$$

Then equation (2.1) can be written after differentiation as

$$\frac{d^2\phi}{dt^2} + k \frac{d\phi}{dt} + \frac{1}{C_{th}} f(\phi) = G \cos(u+\delta) = g \quad (2.5)$$

where,

$$k = \frac{1}{RC_{th}} \quad (2.6)$$

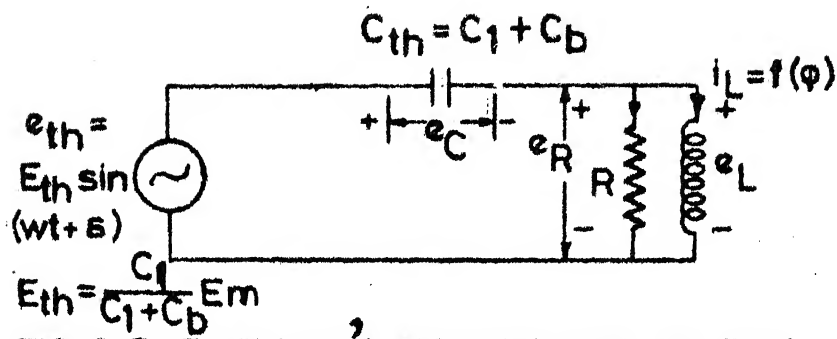


FIG. 2.7 THEVENIN'S EQUIVALENT OF THE POWER SYSTEM.

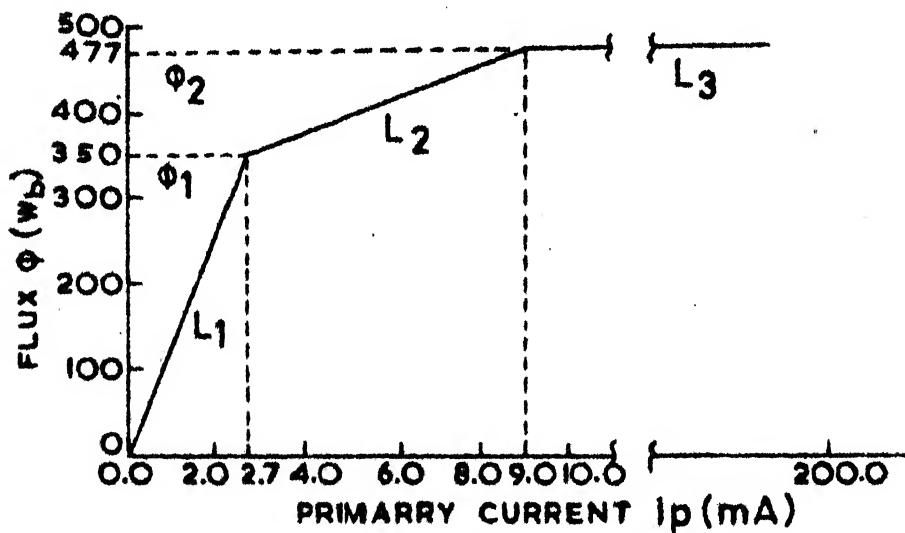


FIG. 2.8 ϕ -I CHARACTERISTIC OF VT.

$$G = \omega e_{th} \quad (2.7)$$

$$u = \omega t \quad (2.8)$$

Both steady state and pre-steady state period analysis of the system were done. The steady state analysis is given in Section 2.3.1 and the pre-steady state period analysis is given in Section 2.4

2.3.1. Steady state analysis

We wish to solve eqn.(2.5) for the steady state flux ϕ , as the derivative of flux ϕ is the desired voltage across EMVT. Since the equation is nonlinear, the flux ϕ and the magnetising current $f(\phi)$ can both have harmonic components besides the fundamental. The principle of 'harmonic balance' [3] is used to solve for the flux ϕ . For the time being, we will concentrate on the fundamental component and determine the harmonic components later, we can assume ϕ of the form

$$\phi = X \cos u \quad (2.9)$$

As seen from eqns. (2.5) and (2.9), δ is the phase difference between the forcing function g and the flux ϕ .

Substituting eqn. (2.9) in eqn. (2.5), we get

$$- \omega^2 X \cos u - k\omega.X.\sin u + f(\phi)/C_{th} = G_c \cos u + G_s \sin u \quad (2.10)$$

where,

$$G_c = G \cos \delta \quad (2.11)$$

$$G_s = G \sin \delta \quad (2.12)$$

The term $f(X \cos u)$ in eqn.(2.10) is a periodic function of time and hence it can be resolved by Fourier series and written as

$$f(\varphi) = A_0 + \sum_n [A_n \sin(nu) + B_n \cos(nu)] \quad (2.13)$$

Since flux φ is an even function of time, therefore, $f(\varphi)$ will also be an even function of the time. This can be seen from Fig. A-1 in the Appendix. Therefore, the sine components of $f(\varphi)$ will be zero. Further, since the steady state $f(\varphi)$ does not have dc component, A_0 is also zero. As we are for the moment considering only the fundamental component, $f(\varphi)$ can be written as

$$f(\varphi) = B_1 \cos u \quad (2.14)$$

An expression for B_1 has been derived in Appendix A. As seen from eqn.(A.8) and Fig. A-1 it is a function of X (peak amplitude of flux φ), break point fluxes φ_1 and φ_2 and slopes L_1 , L_2 and L_3 (see Fig. 2.8). Substituting eqn. (2.14) in eqn.(2.10) and collecting the coefficients of $\cos u$ and $\sin u$ separately and equating them we get,

$$-\omega^2 X + B_1/C_{th} = G_c \quad (2.15)$$

$$-k\omega X = G_s \quad (2.16)$$

where,

$$G^2 = G_c^2 + G_s^2 \quad (2.17)$$

Equations (2.15) and (2.17) can be solved for flux amplitude X iteratively by 'Secant' method (Appendix B).

The steps to be followed are as follows :

1. Assume two values for X viz. X_a and X_b .
2. Obtain the corresponding values of B , from eqn. (A.8).
3. Obtain the corresponding values of G viz. G_a and G_b from eqns. (2.15) and (2.17).
4. Obtain a refined value of X from eqn. (B.4)

$$X_c = \frac{X_a \cdot f(X_b) - X_b \cdot f(X_a)}{f(X_a) - f(X_b)} \quad (2.18)$$

where,

$$f(X_a) = G - G_a \quad (2.19)$$

$$f(X_b) = G - G_b \quad (2.20)$$

The value of G in above is accurately known from eqn. (2.7).

5. Check if $f(X_c) < \epsilon$ ($= 0.005$). If yes stop, else continue.
6. Replace X_a by X_b and X_b by X_c .
7. Go back to Step 1.

Analysis with Harmonic Components Included

If the harmonic components are included, then the expression for flux is

$$\varphi = X_1 \cos u + \sum_{n \neq 1} X_n \cos(u + \Theta_n) \quad (2.21)$$

where,

Θ_n = Phase shift between fundamental and n^{th} harmonic.

The above can be written as

$$\varphi = X_1 \cos u + \sum_{n \neq 1} [X_{nc} \cos(nu) + X_{ns} \sin(nu)] \quad (2.22)$$

where

$$X_n^2 = X_{nc}^2 + X_{ns}^2 \quad (2.23)$$

$$\Theta_n = \tan^{-1}(X_{ns}/X_{nc}) \quad (2.24)$$

The Fourier series expression for $f(\varphi)$ has already been given in eqn.(2.13). The coefficients A_0 and A_1 are zero for the reasons as given for the case when harmonic were not considered.

Therefore,

$$f(\varphi) = B_1 \cos u + \sum_{n \neq 1} [B_n \cos(nu) + A_n \sin(nu)] \quad (2.25)$$

where,

$$B_n = \frac{2}{\pi} \int_0^\pi f(\varphi) \cdot \cos(nu) du \quad (2.26)$$

and

$$A_n = \frac{2}{\pi} \int_0^\pi f(\varphi) \cdot \sin(nu) du \quad (2.27)$$

In the case with no harmonics considered, an explicit expression for B_1 was given in eqn.(A.8). However, it is not possible in this case to get explicit expressions for A_n and B_n . We must resort to numerical integration of eqns.(2.26) and (2.27) respectively to get these values.

If eqns. (2.22) and (2.25) are substituted in eqn. (2.5) and the coefficients of various cosine and sine terms are equated for various values of n , then for $n = 1$ we will get the same eqns. as for the case without harmonics, i.e. eqns. (2.15) thru (2.17) and for $n \neq 1$ we will get

$$-n^2\omega^2 X_{nc} + nk\omega X_{ns} + B_n/C_{th} = 0 \quad (2.28)$$

$$-n^2\omega^2 X_{ns} - nk\omega X_{nc} + A_n/C_{th} = 0 \quad (2.29)$$

Equations (2.28) and (2.29) are re-written as

$$X_{nc} = c_2 A_n + c_1 B_n \quad (2.30)$$

$$X_{ns} = c_1 A_n + c_2 B_n \quad (2.31)$$

where

$$c_1 = \frac{1.0}{C_{th}(k^2 + n^2\omega^2)}, \text{ and} \quad (2.32)$$

$$c_2 = \frac{k}{n\omega} \cdot c_1 \quad (2.33)$$

The iterative scheme to get X_1 , X_n and θ_n is as follows :

1. Assume X_n ($n \neq 1$) as zero, correspondingly A_n and B_n will be zero.

2. Obtain B_1 from eqn.(2.26) by numerical integration (trapezoidal rule has been used in the present study).
3. Obtain a value of X_1 iteratively by 'Secant' method as explained in analysis without harmonics.
4. For $n \neq 1$, obtain A_n and B_n from eqns.(2.26) and (2.27) with above value of X_1 .
5. Calculate X_{nc} and X_{ns} from eqns.(2.30) and (2.31) respectively.
6. Re-compute X_1 iteratively with above values of X_{nc} , X_{ns} , A_n and B_n .
7. Re-compute X_{nc} and X_{ns} from the value of X_1 obtain in step 6.
8. Repeat steps 6 and 7 until the successive values of X_1 , X_{nc} and X_{ns} are within a specified ϵ ($=0.005$).
9. Calculate X_n and Θ_n from eqns. (2.23) and (2.24).
10. Calculate fundamental and harmonic components of the voltage by substituting, X_1 , X_n and Θ_n in eqn.(2.21) and then differentiating it with respect to time.

2.3.2. NUMERICAL DATA AND RESULTS FOR STEADY STATE

Now we give the actual data and the results for the field test case. As mentioned earlier, C_b includes the EMVT capacitance, the bus capacitance and the various bushing capacitances connected to the bus. The EMVT capacitance may be taken as 600 to 800 pf [18]. The 220 KV bus is 108 meters

long having ACSR conductors of 36 mm diameter and spacing of 4.5 m. Since there is uncertainty in the values of various bushing capacitances, a range of values of C_b is taken from 2,000 to 3,200 pf [25].

The numerical values of various parameters shown in Fig. 2.6 are taken as

$$C_1 = 1,300 \text{ pf}$$

$$E_m = \frac{\sqrt{2} \times 220}{\sqrt{3}} = 179.6 \text{ KV}$$

$$\omega = 314.15 \text{ rad/sec for 50 Hz system.}$$

The value of R has been neglected, **since its effect** on steady state solution is very small as verified by computer studies but not reported here. It is also reported in [34]

For L, the $\phi - i$ characteristic is as shown in Fig. 2.8. Since the field test data is available only for the slopes $L_1 = 1.3 \times 10^5 \text{ H}$ and $L_2 = 2.02 \times 10^4 \text{ H}$, the slope L_3 has to be assumed. The results are reported for two values of L_3 viz. 1000 H and 700 H respectively.

The calculated results for typical values of C_b and the slope L_3 are given in Tables 2.1, 2.2 and 2.3. Both the fundamental and the harmonic components are given in the Tables. It may be observed that there are three possible solutions. This may also be seen from Fig. 2.9, which depicts the condition that the source voltage e_{th} must be

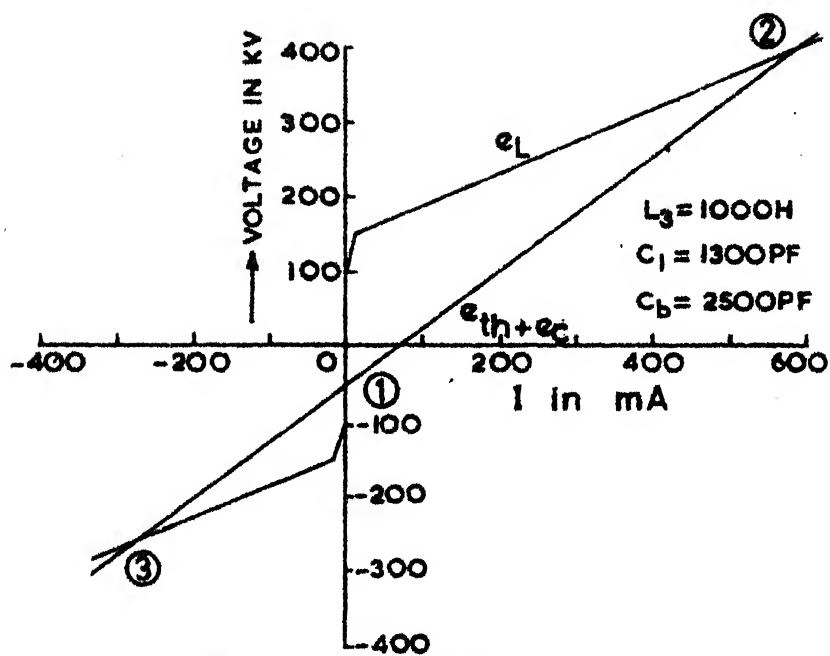


FIG. 2.9 POSSIBLE SOLUTIONS FOR CIRCUIT SHOWN IN FIG. 2.7.

TABLE - 2.1

Possible voltage solution for fundamental and harmonic
components

$$L_3 = 1,000 \text{ H}$$

$$C_b = 2,000 \text{ pf}$$

Sol. No.	Funda- mental	3rd Harmonic		5th Harmonic		7th Harmonic	
	V_1	V_3	θ_3	V_5	θ_5	V_7	θ_7
1	88.75	0	0	0	0	0	0
2	364.40	51.2	2.4	1.8	13.2	3.2	164.4
3*	263.40	34.2	-178	5.0	-172	1.6	-14.4

* Unstable solution

TABLE - 2.2

Possible voltage solution for fundamental and harmonic
components

$$L_3 = 1,000 \text{ H}$$

$$C_b = 2,500 \text{ pf}$$

Sol. No.	Funda- mental	3rd Harmonic		5th Harmonic		7th Harmonic	
	V_1	V_3	θ_3	V_5	θ_5	V_7	θ_7
1	76.8	0	0	0	0	0	0
2	394.5	50.6	2.4	4.1	161.0	2.1	156
3*	290.9	37.5	-172	2.9	-165	2.3	-11

* Unstable solution

TABLE - 2.3

Possible voltage solution for fundamental and harmonic components

$$L_3 = 700 \text{ H}$$

$$C_b = 3,200$$

Sol. No.	Funda-mental	3rd Harmonic		5th Harmonic		7th Harmonic	
	V_1	V_3	θ_3	V_5	θ_5	V_7	θ_7
1	64.7	0	0	0	0	0	0
2	340.8	62.5	2.3	1.5	60.5	3.5	167
3*	273.4	40.6	-178	5.1	-171	2.1	-12.6

* Unstable solution.

equal to $e_C + e_L$ (Fig. 2.7). In the first solution, the network appears as an inductive load. In the second solution it appears as a capacitive load and the third solution is unstable as verified later. Regarding the high voltage (HV) mode, Figs. 2.10a and 2.10b show the typical voltage waveforms across the EMVT for two different cases. These waveforms tally well with those observed in the field (Figs. 2.2a and 2.2b).

Test for stability

Stability of the solution is tested by means of the conditions derived in the Appendix C (eqns. C-9 and C-10). The procedure for testing the stability of a particular solution X_1 is given below :

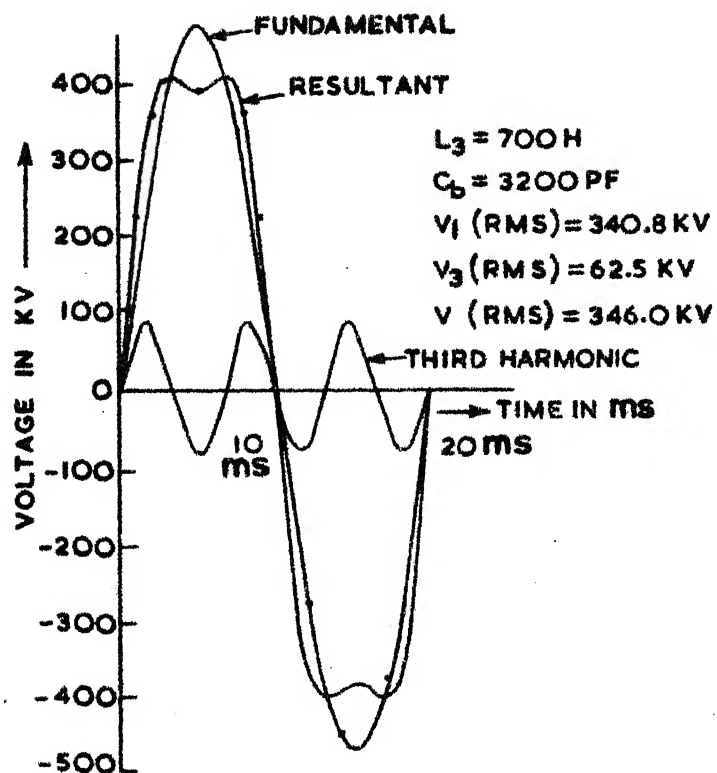


FIG. 2.10A $\sqrt{3} \times$ PHASE VOLTAGE AT BUS ALONG WITH THIRD HARMONIC COMPONENT.

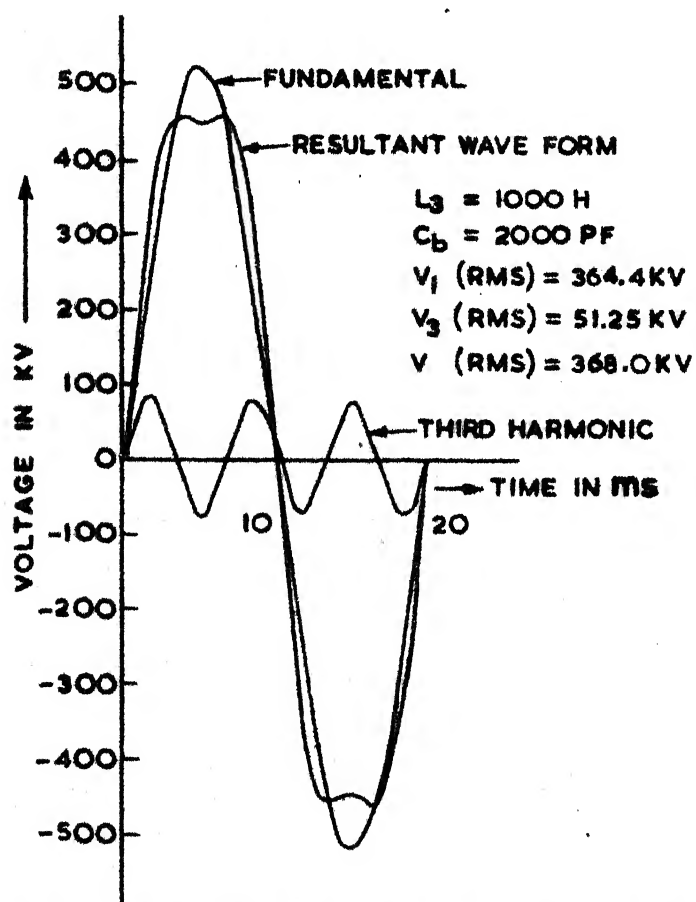


FIG. 2.10B $\sqrt{3} \times$ PHASE VOLTAGE AT BUS ALONG WITH THIRD HARMONIC COMPONENT.

1. Calculate the angle δ by

$$\delta = \tan^{-1}(G_s/G_c)$$

where G_c and G_s are calculated from eqns. (2.15) and (2.16) respectively.

2. Calculate X_o and Y_o from X_1 and δ .

$$X_o = X_1 \cos \delta$$

$$Y_o = X_1 \sin \delta$$

3. Take the small perturbations in X_o and Y_o and obtain the partial derivatives $\frac{\partial M}{\partial X}$, $\frac{\partial M}{\partial Y}$, $\frac{\partial N}{\partial X}$ and $\frac{\partial N}{\partial Y}$ respectively. Let they be represented by [P]

4. Substitute [P] in eqns. (C-9) and (C-10) and find out whether the inequality conditions are satisfied or not.

We illustrate the procedure by an example.

$X = -168.0$ is the solution for the fundamental component of flux which corresponds to Case I in the Table 2.3. Since we have neglected the resistance R (Fig. 2.6), the angle δ and K will be zero.

Then eqns. (C-4) and (C-5) become

$$M = -\omega^2 X + B_1/C - G \quad (2.34)$$

$$N = -\omega^2 Y + A_1/C \quad (2.35)$$

Since δ is zero, we have $X_o = -168.0$ and $Y_o = 0$. Substituting these values in eqns. (2.34) and (2.35) we get

M_0 and N_0 . These turn out to be zero since X_0 and Y_0 are the components of X_1 which is the solution. Now, if we perturb X_0 and Y_0 by an amount of 10, we get

$$X'_0 = X_0 + 10 = -158.0$$

$$Y'_0 = Y_0 + 10 = 10.0$$

then

$$\frac{\partial M}{\partial X} = \frac{M(X'_0, Y_0) - M_0}{X'_0 - X_0} = -0.10 \times 10^7$$

and

$$\frac{\partial N}{\partial Y} = \frac{N(X_0, Y'_0) - N_0}{Y'_0 - Y_0} = -0.97 \times 10^6$$

Similarly

$$\frac{\partial M}{\partial Y} = 0 \quad \text{and} \quad \frac{\partial N}{\partial X} = 0$$

Substituting the above in eqns. (C-9) and (C-10) we find that the inequalities are satisfied, and hence, the solution $X_0 = -168.0$ is stable.

2.4. PRE-STEADY STATE (TRANSIENT) PERIOD ANALYSIS

So far we have considered the steady state solution of eqn.(2.5) and have shown that two possible steady state stable modes are possible viz., HV mode and the LV mode. For studying the pre-steady state behaviour and the value of the initial conditions which will result in one or the other mode, the state space technique as given below is used.

Let the state variables be

$$y_1 = \varphi \quad (2.36)$$

$$y_2 = \dot{\varphi} \quad (2.37)$$

Then from eqns (2.5), (2.36) and (2.37) we get

$$\dot{y}_1 = y_2 \quad (2.38)$$

$$\dot{y}_2 = -k y_2 + \frac{f(y_1)}{C_{th}} + G \cos(u+\delta) \quad (2.39)$$

It may be noted from eqn.(2.37) that y_2 is the EMVT voltage which we wish to determine. The set of first order differential eqns. (2.38) and (2.39) are solved by modified Euler method. The initial conditions $y_1(0)$ and $y_2(0)$, which in Fig. 2.6 is the instance when the circuit breaker opens, are given by

$$y_1(0) = -\omega E_m \cos \delta \quad (2.40)$$

$$y_2(0) = E_m \sin \delta \quad (2.41)$$

where δ is the angle of the source voltage at the instant of the CB opening i.e. $t = 0$

The values of the angle δ between 0 to 180 degrees need to be considered to examine all possible cases (it should be obvious that the value of δ from 180 to 360 degrees will not give different results). The numerical values of the circuit parameters as given in Sec. 2.3.2 were used for pre-steady analysis except for the value of loss resistance R , which is taken equal to 0.68×10^7 ohm

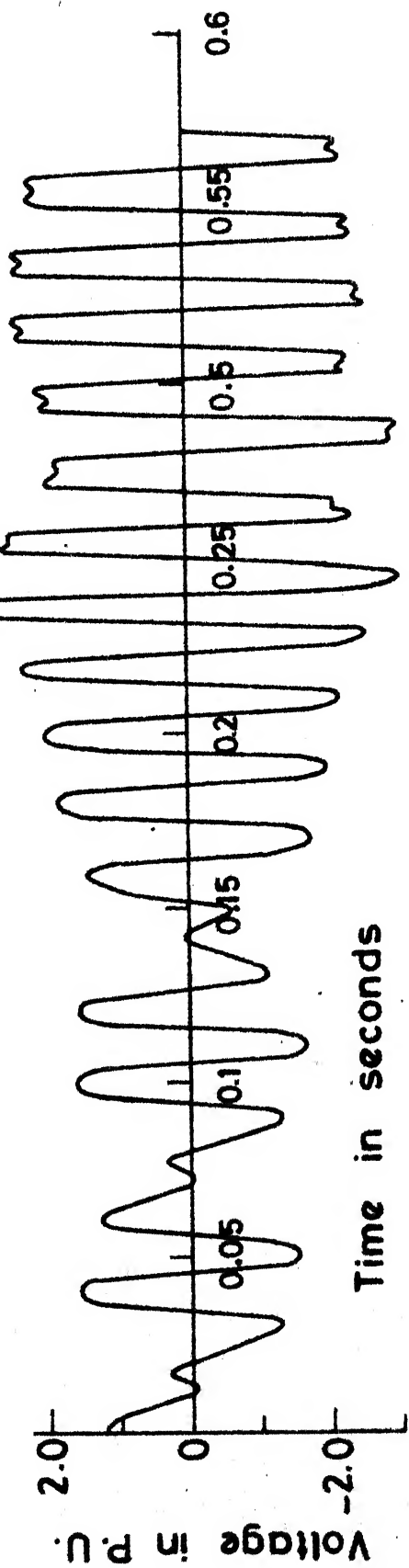


Fig. 3.11 (a) Voltage across EMVT for $\delta = 40^\circ$.

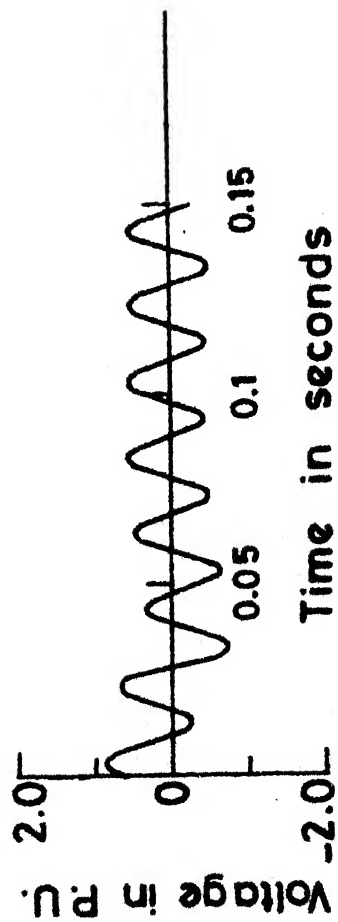


Fig. 3.11 (b) Voltage across EMVT for $\delta = 0^\circ$.

(corresponding to a loss of 2.38 KW per phase). It may be pointed out that this loss accounts for the EMVT, additional equipment at the 220 KV bus and the bus itself. It was observed if the losses were assumed to be somewhat larger ($R = 0.5 \times 10^{-7} \Omega$) the steady state voltage always settled down to the KV mode. If the losses were taken to be somewhat smaller ($R = 1.5 \times 10^{-7} \Omega$), the steady state could not be reached even though the computations were carried out for a long time. Figures (2.11a) and (2.11b) show the waveforms of the voltage across the EMVT for the values of δ equal to 40 and 0 degree respectively. These figures may be compared with Figs. (2.2a) and (2.2c) obtained from the field investigations. There is a very close agreement both in magnitude and shape between the field and the analytical waveforms. The analysis was carried out for other values of δ between 0 to 180 degrees in step of 10 degrees. Some values of δ gave rise to the HV mode, while others gave rise to the LV mode.

TABLE - 2.4

Occurrence of HV or LV mode with the angle δ .

S.No.	1	2	3	4	5	6	7	8	9
δ in degrees	0	10	20	30	40	50	60	70	80
Mode	LV	LV	LV	LV	HV	LV	HV	HV	LV

S.No.	10	11	12	13	14	15	16	17	18
δ in degrees	90	100	110	120	130	140	150	160	170
Mode	HV	LV	LV	HV	HV	LV	LV	LV	LV

2.5. PREVENTIVE MEASURES

Two references [24,33] have come to our knowledge, where several incidents similar to that reported by us are given. Overvoltages due to ferro-resonance are also reported in [22,23,25,34,41]. Some of the preventive measures suggested are :

(a) To have a sequence of switching operations, such that the capacitive coupling between the source and the de-energized bus through CB grading capacitance is avoided [41].

However, any such recommendation which concerns with restriction on the operating procedure, may be difficult or not advisable to implement.

(b) To connect a saturable reactor in parallel with the EMVT secondary [32]. This recommendation needs to be examined in terms of its technical feasibility, economics and burden on the EMVT.

(c) To connect a resistance in parallel with the EMVT secondary [3]. As mentioned in Section 2.2 a resistance of 9.0Ω in the secondary (R_{sec}), which corresponds to $0.36 \times 10^8 \Omega$ as seen from the primary side, was connected.

However, this did not prevent the occurrence of the HV mode. In Sec. 2.4, if the value of resistance (R) to simulate the losses was taken as $0.68 \times 10^7 \Omega$, then the HV mode did occur. While, if the value of R was taken as $0.5 \times 10^7 \Omega$, then the HV mode did not occur. Of course, these values of R are indicative only, since the circuit parameters like L and C etc. will also influence the results. The main point to note is that while R is of the order of 10^7 , R_{sec} is of the order of 10^8 . Since R and R_{sec} are in parallel, unless R_{sec} is reduced considerably, its influence on the occurrence/non-occurrence of the HV mode will not be significant. If R_{sec} is reduced further, the burden on the EMVT secondary may not be acceptable. Also the continuous heat loss due to R_{sec} may be too large for a practical design, if R_{sec} is installed within the EMVT.

It is obvious that it will be better if the steady state overvoltages are controlled by a suitable design of the EMVT saturation characteristic itself rather than the auxiliary means listed above. To examine this situation, various values of the saturation slope L_3 (Fig. 2.8) were considered. For each value of L_3 , the source angle δ was varied between 0 and 180 degrees to find out when the HV mode did occur. The result of this study is shown in Fig. 2.12. It is seen from the Figure that if L_3 is greater than 775 H, HV mode did not occur for any value of the angle δ . This

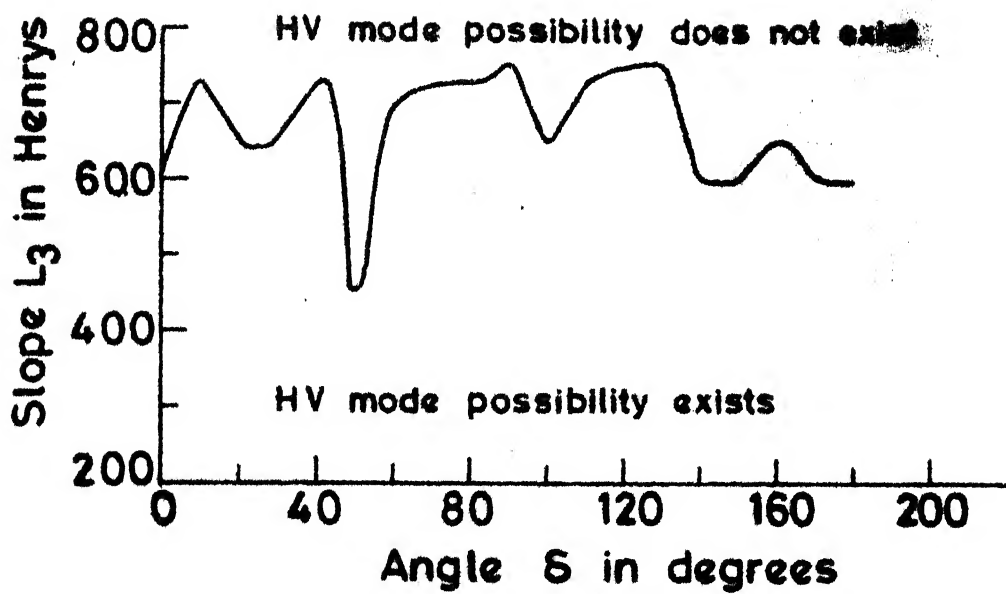


Fig. 2.12 Effect of change in L_3 on the probability of HV mode.

confirms our contention that if the EMVT saturation characteristic can be controlled, then the problem of steady state overvoltages along with its possible damage can be avoided.

In order to study the problem in greater detail the data for values of CB grading capacitance and EMVT saturation characteristic for several makes was collected. Table 2.5 gives the values of C_1 for several makes of CBs. It may be noted from the Table that the range of C_1 is from 250 pf to 1,300 pf. The saturation characteristics

TABLE - 2.5

Equivalent grading capacitance ' C_1 ' for various makes of CBs.

S.No.	Make of CB	Grading capacitance in pf. C_1		
1.	Oerlikon FS9C3	4x1,000	=	250
2.	Magrini 245 MHM	2x1,000	=	500
3.	BBC type DLF	2x2,600	=	1,300
4.	BHEL, India	4x2,000	=	500
5.	Russian	4x2,000	=	500

of the various makes of the EMVTs are shown in Fig. 2.13, and as observed, they differ widely. To take an extreme situation it was assumed that $L_2 = L_3$ in Fig. 2.8. This means that the EMVT saturation characteristic can be approximated by two straight line segments as shown in Fig. 2.14.

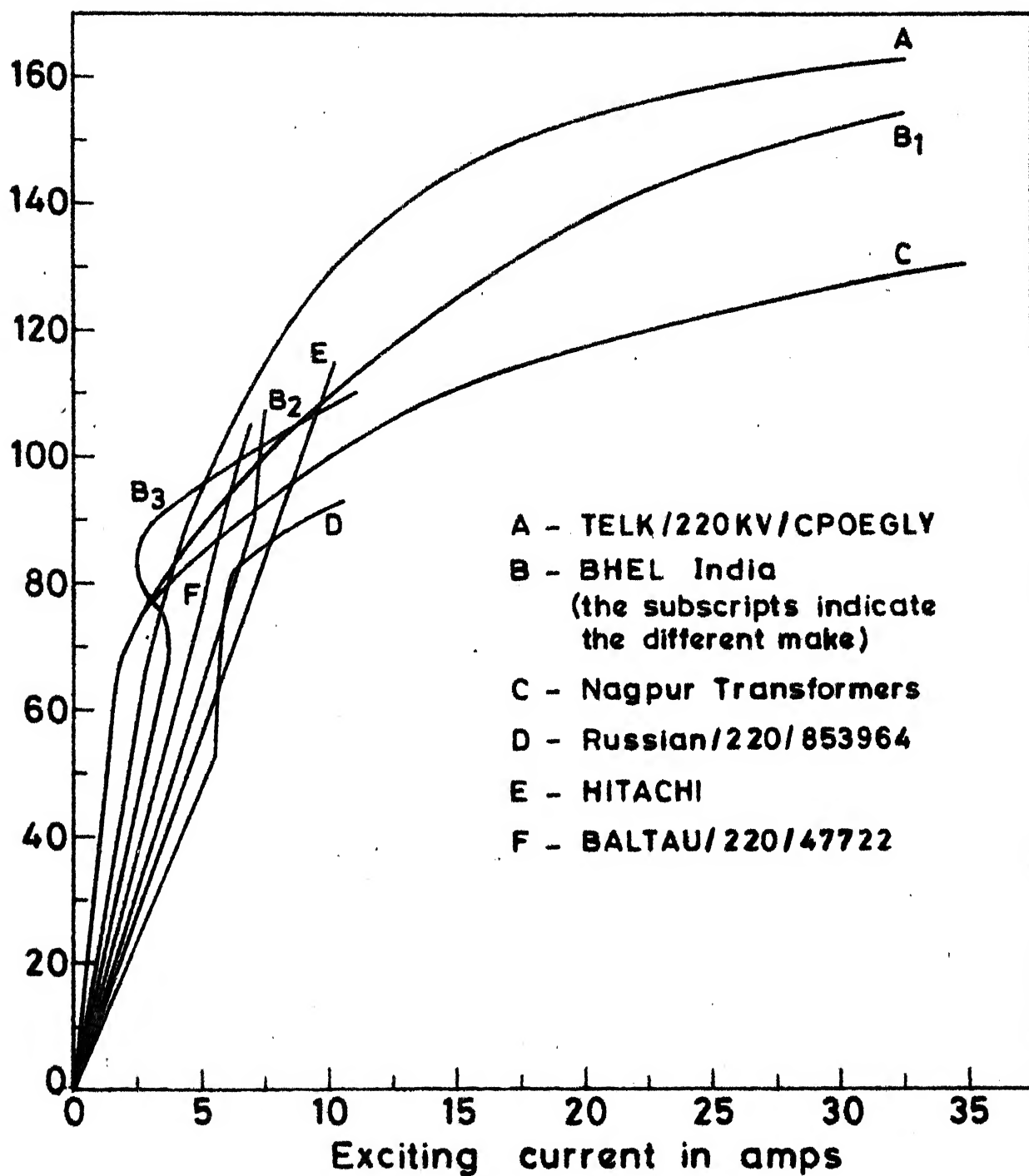


Fig.2.13 EMVT saturation characteristics obtained from various manufacturers.

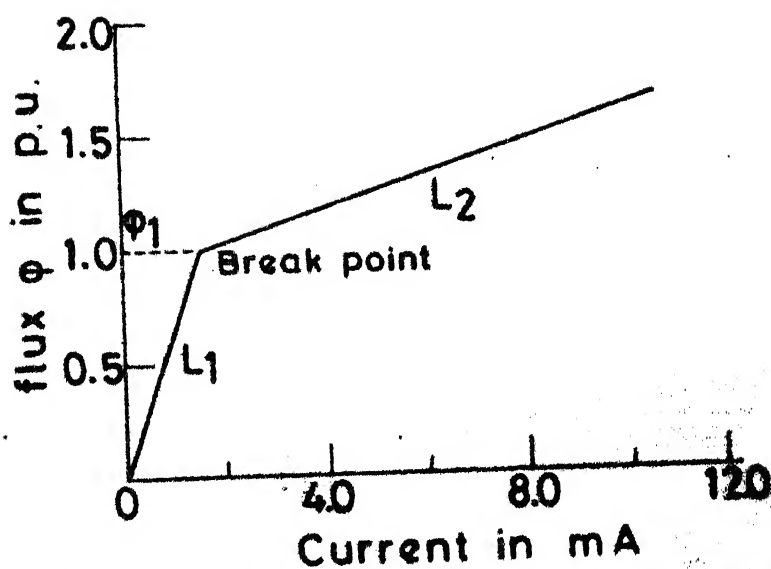


Fig. 2.14 Typical ϕ - i characteristic of the EMVT.

A number of computer studies were done to find out the critical value of L_2 above which the HV mode did not occur for the values of the angle δ from 0 to 180 degrees in steps of 10 degrees, keeping L_1 and C_1 fixed. Table 2.6 shows the results for $L_1 = 1.3 \times 10^5$ H and $C_1 = 1,300$ pf (which are the values from the field test case reported earlier). As already mentioned, 1,300 pf is the maximum value for C_1 . A number of additional computer studies were carried out when the lowest value of C_1 i.e., 250 pf, was taken, keeping L_1 at the same value as before.

TABLE - 2.6

The critical value of L_2 above which the HV mode does not occur for the various values of break point flux ϕ_1 .

S.No.	Break point flux ϕ_1 in p.u.	Critical L_2 in Henries
1.	0.9	1,200
2.	1.1	1,000
3.	1.3	650
4.	1.5	300

It was observed that HV mode did not occur even if L_2 was reduced to a very low value of 300 H as shown in Table 2.6. This points to the fact that the system with higher value of C_1 is more prone to overvoltages. This has also been reported by Tsirel and Palyakov [41].

It is clear from Table 2.6 that if the saturation characteristic of the EMVT is controlled, then the over-voltages can be prevented. The higher the break point, lower can be the value of L_2 . However one point is clear from the Table, compared to the slope $L_1 = 1.3 \times 10^5 \text{ H}$, the slope L_2 is very small (300 to 1,200 H) irrespective of the break point. Hence, as long as the EMVT saturation is moderate upto the maximum voltage expected across the EMVT, the problem of steady state overvoltage should not arise. Some manufacturers recommend [37,47] break point of 1.2 to 1.3 p.u. as in the event of a single line to ground fault the voltage on the healthy phases may rise to 1.2 to 1.3 p.u.

2.6. CONCLUSION

Steady state overvoltage may arise while switching a system which is terminated by a transformer. The actual damage to a 220 KV EMVT has been analysed. Subsequent to the damage, field investigations were performed and waveforms of voltages across the EMVT for the pre-steady and steady state periods were recorded. Analytical study using the principle of 'Harmonic Balance' has been employed to determine the steady state overvoltages. It is established that the overvoltage occurred due to ferro-resonance phenomena. The validity of the method of analysis is verified by the fact that the steady state voltage waveforms, both in

magnitude and shape, are in close agreement with those obtained in the field.

The pre-steady state analysis has been carried out using the state space technique. The validity of the analysis is confirmed by the fact that the waveforms obtained in the field and those obtained by analysis matched very well. This part of the analysis has also given a better insight on how to prevent steady state overvoltages from occurrence. Based upon the data collected for various makes of the CBs and EMVTs and a number of computer studies, it has been established that the steady state overvoltages can be kept to a low value if the EMVT saturation is controlled.

CHAPTER III

DYNAMIC OVERVOLTAGES

3.1. INTRODUCTION

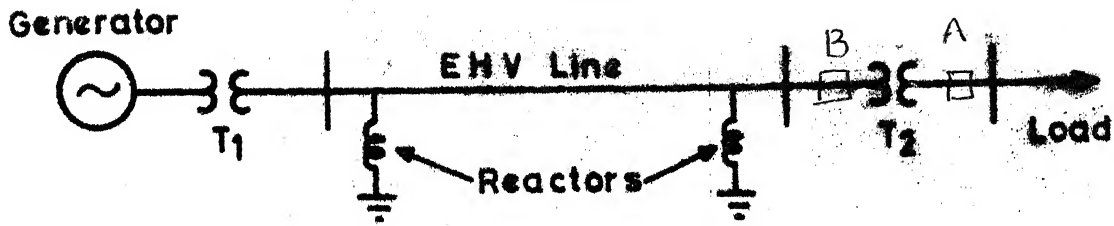
In a power system, a situation can arise that due to sudden load rejection, an unloaded EHV line is left connected to an over-speeding generator(s). This situation can lead to excessive overvoltages (called 'dynamic overvoltages') in the system. Essentially such overvoltages are the fundamental frequency overvoltages with harmonic components and may persist for a few seconds. These voltages can become dangerous if the generator self-excitation takes place due to excessive line charging including series capacitors if any, and/or due to ferro-resonance which may occur because of the transformer saturation. These overvoltages are also influenced by the synchronous generator dynamics, voltage regulator, prime-mover **governor** and network parameters. Therefore, all the above factors should be included for a realistic evaluation of the dynamic overvoltages.

In the methods reported in literature, usually digital simulation is employed to predict the variation in magnitude and frequency of the internal voltages of the generator(s) and this information is used subsequently on the transient network analyzer (TNA) to determine dynamic overvoltages.

The digital simulation neglects the network transients but can predict self-excitation. In this Chapter the above referred two stage computation is combined into a single digital simulation, which incorporates not only the network transients on a 3-phase basis but also the generator representation in detail. The prime-mover governor is also represented along with excitor and voltage regulator. The non-linearities due to the transformer and generator saturation are also included. It is believed that this is a more accurate approach and can be used to determine in a single simulation, if the phenomena of self-excitation and/or ferro-resonance can occur. This is illustrated with the help of case studies for both hydro and thermal systems feeding a load through a long EHV line. The effectiveness of the excitation system and shunt reactors in controlling the overvoltages is also studied.

3.2. SYSTEM DESCRIPTION

An isolated system consisting of a generator supplying load through a long EHV line has been used for the analysis and is shown in Fig. 3.1. When the load is rejected at the receiving end, the unloaded EHV line is left connected to the over-speeding generator. The receiving end transformer T_2 will be left connected to the system if it is 'low side switching', i.e., circuit breaker A is opened. On the other hand, if it is 'high side switching', i.e., breaker B is



T₁ = Sending end transformer

T₂ = Receiving end transformer

Fig. 3.1 A typical EHV system

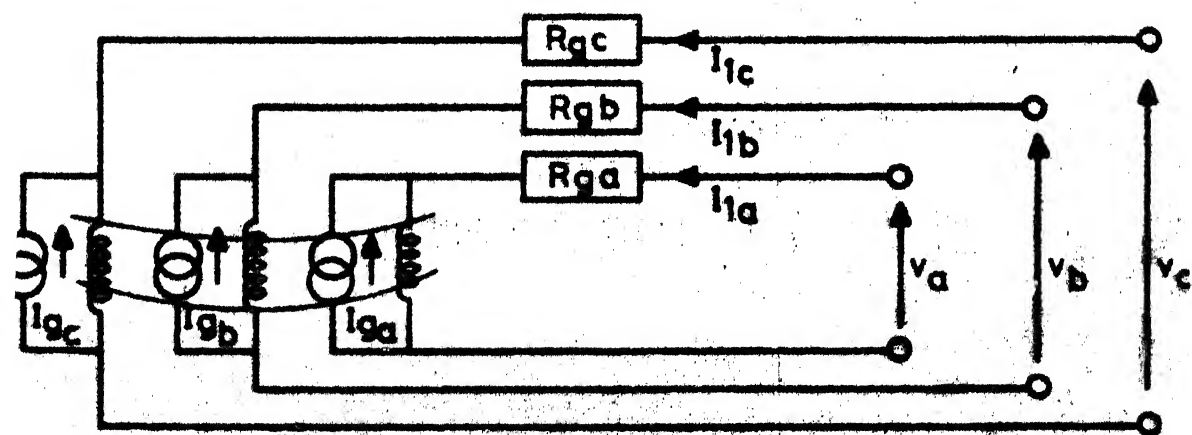


Fig. 3.2 Circuit model for 3-phase stator

opened, then the transformer T_2 is not left connected to the system.

The study of dynamic overvoltages upon load rejection will require the detailed representation of all the power system components shown in Fig. 3.1, which is given in the following sub-sections.

3.2.1. Synchronous Generator

The stator of the synchronous generator is modelled [28] by a dependent current source I_g in parallel with an inductance L_g as shown in Fig. 3.2. It may be noted that I_g is a 3×1 vector and L_g is a 3×3 matrix.

Such representation can handle both the symmetrical and unsymmetrical networks equally well. The time varying coupling between the rotor winding and the stator windings is replaced by a dependent current source and hence the inductance matrix L_g is adjusted to be constant even in the presence of saliency. The transient or the sub-transient saliency is handled by introducing dummy coils on the rotor d or q axes. The major advantage of this circuit model of the synchronous generator is that the formulation of the system equations is facilitated. Also, as the inductance matrix L_g shown in Fig. 3.2 is a constant, this results in simplification of the computations involved in the integration of machine equations. The details of the mathematical formulation are given in reference [28], whereas the generator

winding arrangement and the final equations are given in Appendix - D for ready reference.

The generator saturation is considered by reducing its field voltage. The reduction in field voltage E_{fd} is given by

$$E_{fd} = K_1 \cdot e^{K_2(E_p - K_3)} \quad (3.1)$$

where

$$E_p = x_d'' \sqrt{I_d^2 + I_q^2} \quad (3.2)$$

The coefficients K_1 , K_2 and K_3 will depend upon the saturation characteristic of the generator.

3.2.2. Governor system

The block diagrams of the typical hydraulic and thermal governors [46] used in the study are shown in Figs. 3.3 and 3.4 respectively. The state equations are as follows:

For Hydraulic Governor

$$\dot{x}_{h1} = \frac{1}{T_s} [\omega_{ref} - \omega - (-x_{h2} + \delta G_h) - G_h \cdot \sigma] \quad (3.3)$$

$$\dot{x}_{h2} = \frac{1}{T_r} [-x_{h2} + \delta G_h] \quad (3.5)$$

$$\dot{x}_{h3} = \frac{1}{T_w} [G_h - 2(x_{h3} - G_h)] \quad (3.6)$$

under the restriction that

$$\dot{G}_h \min < \dot{G}_h < \dot{G}_h \max \quad (3.6)$$

$$\text{and } G_h \min < G_h < G_h \max \quad (3.7)$$

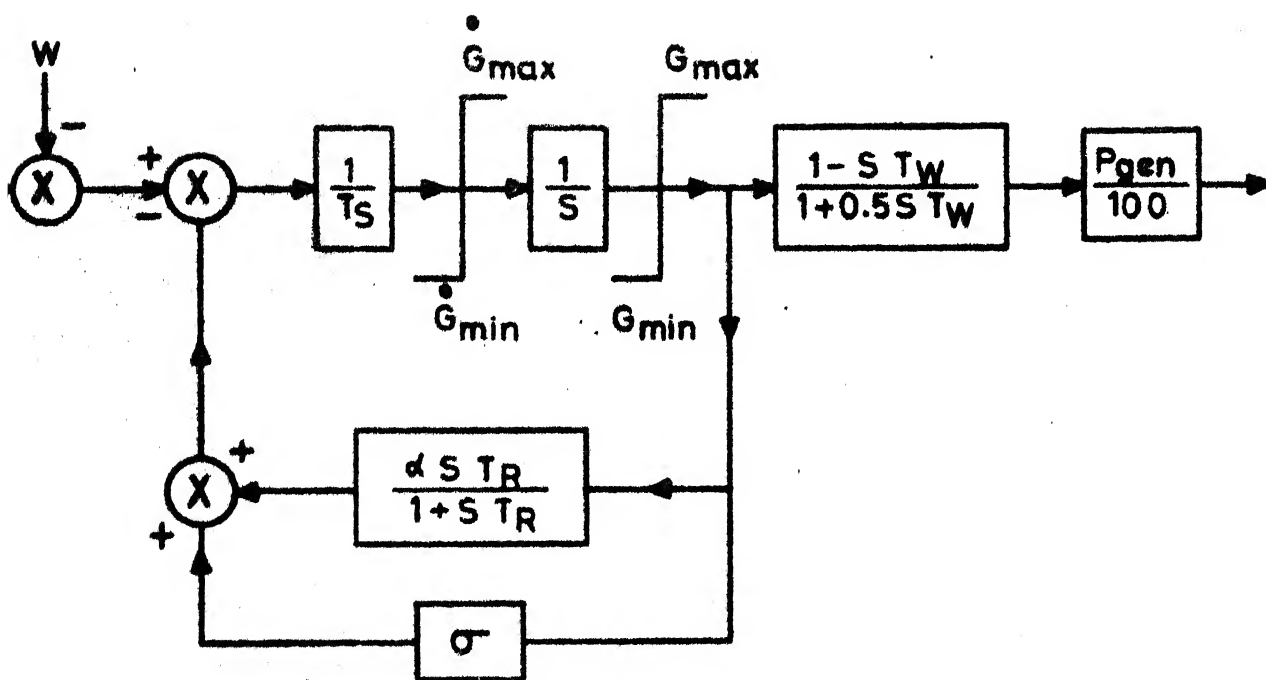


Fig . 3.3 Hydraulic governor

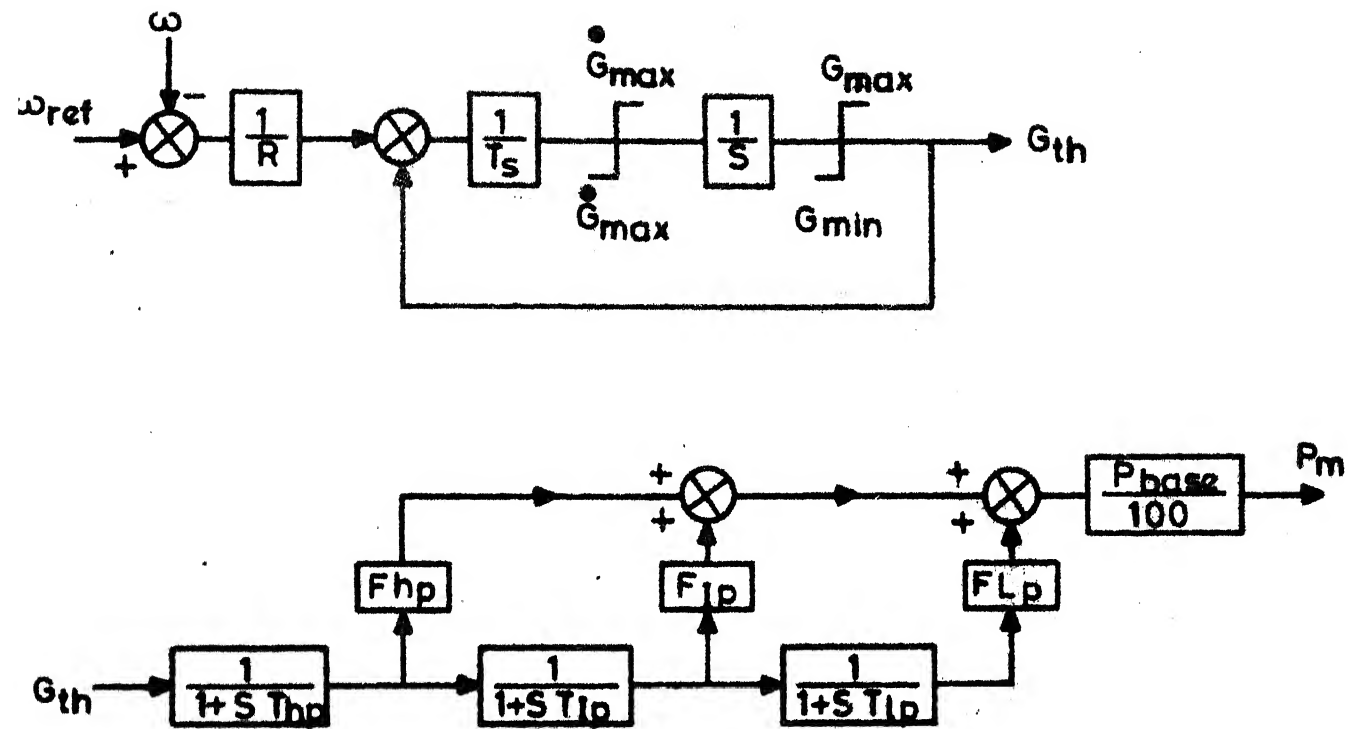


Fig.3.4 Steam turbine and governor .

For Thermal Governor

$$\dot{X}_{s1} = \frac{1}{T_s} [(\omega_{ref} - \omega)/R - G_{th}] \quad (3.8)$$

$$\dot{X}_{s2} = \frac{1}{T_{hp}} [G_{th} - X_{s2}] \quad (3.9)$$

$$\dot{X}_{s3} = \frac{1}{T_{ip}} [X_{s2} - X_{s3}] \quad (3.10)$$

$$\dot{X}_{s4} = \frac{1}{T_{lp}} [X_{s3} - X_{s4}] \quad (3.11)$$

under the restriction that

$$G_{th \min} < \dot{X}_{s1} < \dot{G}_{th \max} \quad (3.12)$$

$$\text{and} \quad G_{th \min} < X_{s1} < G_{th \max} \quad (3.13)$$

3.2.3. Excitation system

The system considered is IEEE type - I rotating excitation system [45], whose block diagram is given in Fig. 3.5. The state equations for the excitation system are as follows :

$$\dot{E}_{fd} = \frac{1}{T_e} [-K_e \cdot E_{fd} + X_{e1} - S_e \cdot E_{fd}] \quad (3.14)$$

$$\dot{X}_{e1} = \frac{1}{T_a} [-X_{e1} + K_a (V_{ref} - V_T - X_{e2})] \quad (3.15)$$

$$\dot{X}_{e2} = \frac{1}{T_f} [-X_{e2} + K_f \cdot \dot{E}_{fd}] \quad (3.16)$$

under the restriction that

$$V_R \min < X_{e1} < V_R \max \quad (3.17)$$

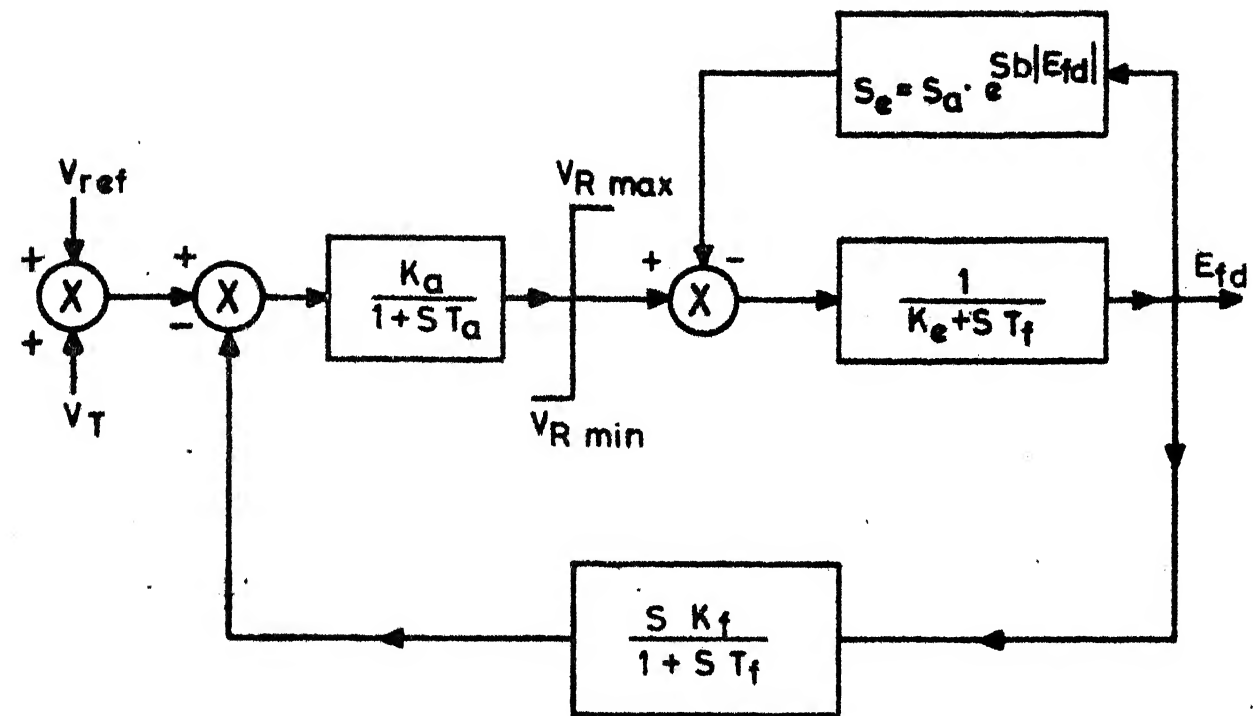


Fig .3.5 IEEE Type-I rotating excitation system.

3.2.4. Transformer

The equivalent circuit of the transformer is shown in Fig. 3.6. Its leakage inductance is represented by L_{lt} and the series resistance R_{lt} accounts for the copper loss. The magnetising inductance is represented by L_{mt} , which is non-linear due to the transformer saturation. The manufacturer usually provide the transformer $v-i$ characteristic, which can be converted into the $\phi-i$ characteristic. The $\phi-i$ characteristic is approximated by straight line segments, so that the slope L_{mt} is piecewise linear, as given in the Appendix-E. The resistances R_c and R_p account for core losses. Since the core losses are voltage dependent, the major part of these losses is accounted for by R_p . The resistance R_c is considered in series with L_{mt} to facilitate the decay of d.c. current which exists during transient condition. This may otherwise not decay fast enough if the source resistance and the transformer resistance R_{lt} are small in value or are neglected. The value of R_c can be chosen so that the ratio of the magnetising reactance (X_{mt}) at rated voltage and frequency to R_c is 20. However, a lower value of R_c giving rise to a higher ratio does not change the results significantly.

3.2.5. Shunt Reactor

The equivalent circuit of the shunt reactor is simply a resistance (R_r) in series with inductance (L_r). The value

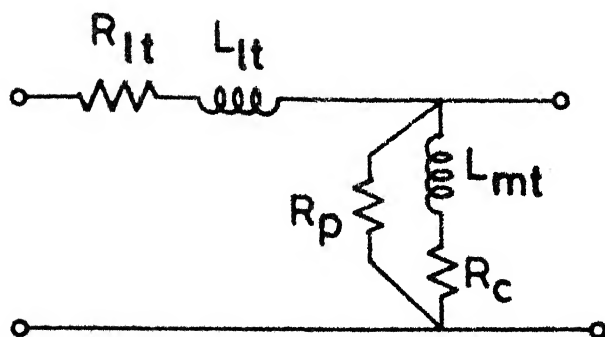


Fig.3.6 Equivalent circuit of the transformer.

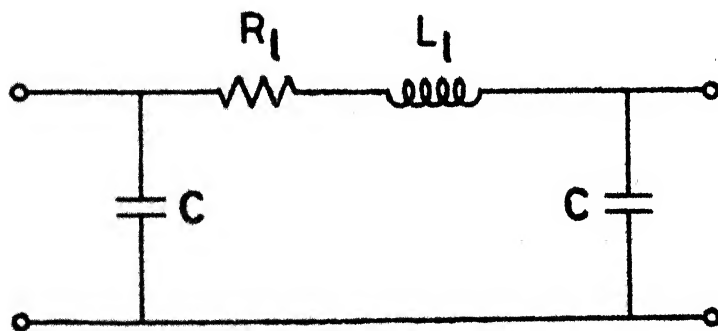


Fig.3.7 Equivalent circuit of the transmission line.

of the L_r depends upon the reactor size. The resistance R_r is so chosen that the ratio of X_{Lr} (reactor reactance at rated voltage and frequency) to R_r is 300 to 400 ~~[48]~~. A non-linear reactor can also be considered. In that case the value of L_r will not be a constant and its representation will be piecewise linear similar to that of the transformer magnetizing inductance L_{mt} .

3.2.6. Transmission Line

The transmission line is represented by an equivalent π as shown in Fig. 3.7. The series resistance R_1 , series inductance L_1 and half line charging capacitance C are 3×3 matrices for 3-phase representation. If the line is transposed, then these matrices are symmetric.

As an example, the form of L_1 is

$$L_1 = \begin{vmatrix} L_{s1} & L_{m1} & L_{m1} \\ L_{m1} & L_{s1} & L_{m1} \\ L_{m1} & L_{m1} & L_{s1} \end{vmatrix} \quad (3.18)$$

where L_{s1} and L_{m1} are self and mutual inductances.

Normally the transmission line data is given in terms of its positive and zero sequence series inductances L_+ and L_0 respectively. The values of L_{s1} and L_{m1} in terms of L_+ and L_0 are given by

$$L_{s1} = \frac{1}{3} (2 L_+ - L_0) \quad (3.19)$$

$$L_{m1} = \frac{1}{3} (L_o - L_+) \quad (3.20)$$

The form of the matrices R_1 and C is similar to that of the matrix L_1 .

3.2.7. Load

The load is represented by a current source whose magnitude and phase angle depend upon the amount of loading and the power factor. The load rejection is simulated by opening a particular phase whenever the current source value goes to zero in that phase.

3.3. NETWORK STATE EQUATIONS

Based upon the equivalent circuits given in Section 3.2 for the various components, the system of Fig.3.1 is represented by the equivalent circuit shown in Fig. 3.8. In the Figure the R 's, L 's and C 's are 3×3 matrices while i 's, v 's and ϕ 's are 3×1 vectors. The state variables are the currents i_1, i_2, i_3 , and i_4 ; voltages v_1 and v_2 and fluxes ϕ_1 and ϕ_2 .

The set of first order differential equations describing the system are

$$(L_g + L_2) \dot{i}_1 = v_1 - (R_2 + R_g)i_1 - L_g \dot{i}_g \quad (3.21)$$

$$L_3 \dot{i}_2 = v_1 - v_2 - R_3 i_2 \quad (3.22)$$

$$L_5 \dot{i}_3 = v_1 - R_3 i_3 \quad (3.23)$$

$$L_6 \dot{i}_4 = v_2 - R_6 i_4 \quad (3.24)$$

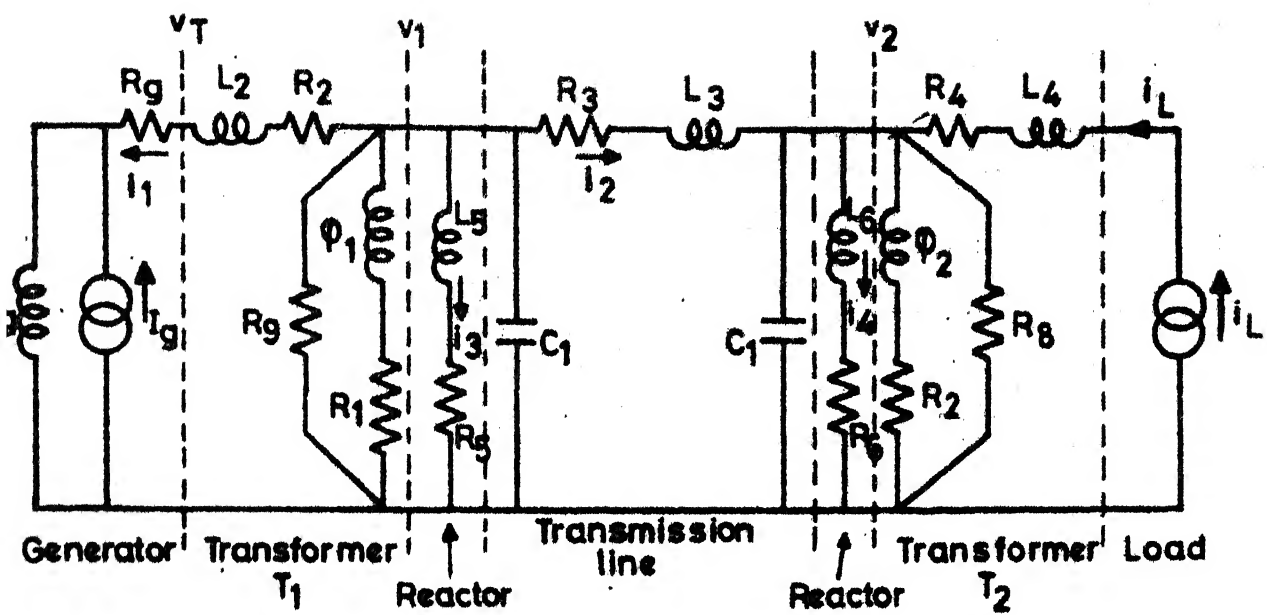


Fig. 3.8 Equivalent circuit of the system.

$$C_1 \dot{v}_1 = -i_1 - i_2 - i_3 - f_1(\varphi_1) - R_9^{-1} v_1 \quad (3.25)$$

$$C_1 \dot{v}_2 = i_2 - f_2(\varphi_2) - i_4 + i_L - R_8^{-1} v_2 \quad (3.26)$$

$$\dot{\varphi}_1 = v_1 - R_1 f_1(\varphi_1) \quad (3.27)$$

$$\dot{\varphi}_2 = v_2 - R_7 f_2(\varphi_2) \quad (3.28)$$

Equations (3.21) to (3.28) may be written in concise form as

$$[A] [\dot{X}_n] = f([X_n]) + [B][u(t)] \quad (3.29)$$

where

$$[X_n]^t = [i_1 \ i_2 \ i_3 \ i_4 \ v_1 \ v_2 \ \varphi_1 \ \varphi_2] \quad (3.30)$$

$$[u(t)]^t = [\dot{I}_g \ i_L] \quad (3.31)$$

$$f([X_n]) = \begin{vmatrix} -(R_2 + R_g) - v_1 \\ -R_3 i_2 + v_1 - v_2 \\ -R_5 i_3 + v_1 \\ -R_6 i_4 + v_2 \\ -i_1 - i_2 - i_3 - \frac{v_1}{R_9} - f_1(\varphi_1) \\ -i_2 - i_4 - \frac{v_2}{R_8} - f_2(\varphi_2) \\ v_1 - R_1 f_1(\varphi_1) \\ v_2 - R_7 f_2(\varphi_2) \end{vmatrix} \quad (3.32)$$

$$[A] = \begin{vmatrix} L_g + L_2 & 0 & 0 & 0 & 0 & 0 & 0 & 0 \\ 0 & L_3 & 0 & 0 & 0 & 0 & 0 & 0 \\ 0 & 0 & L_5 & 0 & 0 & 0 & 0 & 0 \\ 0 & 0 & 0 & L_6 & 0 & 0 & 0 & 0 \\ 0 & 0 & 0 & 0 & C_1 & 0 & 0 & 0 \\ 0 & 0 & 0 & 0 & 0 & C_1 & 0 & 0 \\ 0 & 0 & 0 & 0 & 0 & 0 & U & 0 \\ 0 & 0 & 0 & 0 & 0 & 0 & 0 & U \end{vmatrix} \quad (3.33)$$

and

$$[B] = \begin{vmatrix} -L_g & 0 \\ 0 & 0 \\ 0 & 0 \\ 0 & 0 \\ 0 & 0 \\ 0 & U \\ 0 & 0 \\ 0 & 0 \end{vmatrix} \quad (3.34)$$

It may be noted that the matrix $[A]$ is block diagonal, and hence, can be inverted easily. Equation (2.29) can be written as

$$[\dot{X}_n] = [A]^{-1} f([X_n]) + [A]^{-1} [B] [u(t)] \quad (3.35)$$

$$\text{or } [\dot{X}_n] = \phi([X_n]) + [D][u(t)] \quad (3.36)$$

where

$$\phi([X_n]) = [A]^{-1} f([X_n]) \quad (3.37)$$

$$\text{and} \quad [D] = [A]^{-1} [B] \quad (3.38)$$

3.4. SOLUTION PROCEDURE

Following load rejection, the set of eqns. given by (3.36) is required to be solved. The components of the forcing function $[u(t)]$ are the load current i_L , and the derivative of the dependent current source \dot{I}_g as given in eqn. (3.31). The load current i_L is known from the load data and is assumed to be a constant current source. The expression for \dot{I}_g has been given in eqn. (D-15). It may be observed that it depends upon the prime-mover speed and the generator d and q axes currents. Also it may be noted from eqns. (D-6) to (D-11) that these currents are dependent on the governor output P_m and the excitor voltage E_{fd} . The P_m and E_{fd} can be calculated by solving the generator, governor and excitation system state equations. The interconnection of various variables for each step of integration is shown in Fig. 3.9.

Before the integration procedure can be started, the initial values of various variables are needed. The procedure for the calculation of the initial conditions is given in Appendix-F.

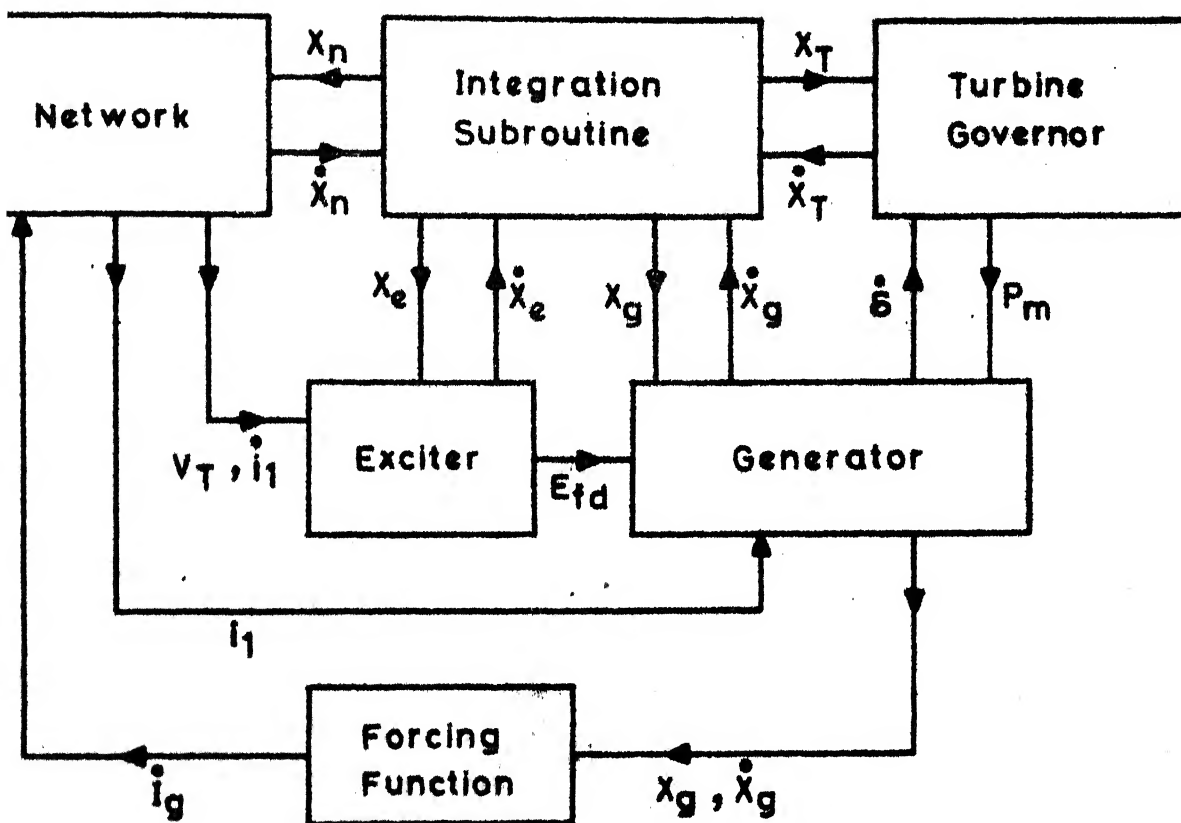


Fig. 3.9 Interconnection of system components for the digital simulation.

3.5. CALCULATION OF DYNAMIC OVERVOLTAGES

The calculation of dynamic overvoltages for both typical hydro and thermal systems are given below. The hydro system is found to be more prone to dynamic overvoltage because usually the hydro generators are smaller in size and are situated far away from the load centre leading to long EHV lines. Also the rise in speed on load rejection is more than for a comparable thermal system, which contributes to excessive overvoltages. However, the recent trend is to locate the thermal stations at the pit-heads and hence they may also become more prone to such overvoltages, especially when only one unit (small generation) is in operation.

3.5.1. Case Study 1 ; Hydro System

The single line diagram of the system studied is shown in Fig. 3.1. The data for the various components of the system i.e. the generator including its excitation and governor system, sending and receiving end transformers along with their saturation characteristics, shunt reactors and the transmission line is given in Appendix-E. It may be observed from Fig. 3.1 that the load may be rejected either by opening of the circuit breaker A (high side switching) or circuit breaker B (low side switching). The receiving end transformer is left connected to the system in the case of low side switching. Both high side and low side switching have been studied. It may be mentioned that if the low side switching

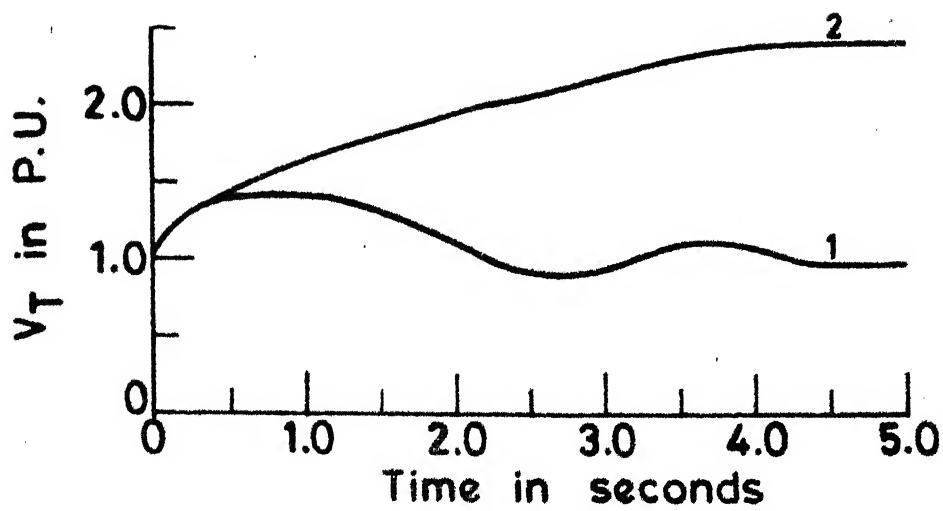
is permissible, the installation of the circuit breaker A could be deferred until more than one EHV line is commissioned.

3.5.1.1. High side switching : The results for this study are shown in Figs. 3.10 to 3.12, where both the excitation system (ES) blocked and active have been considered. While Fig. 3.10 shows the generator terminal voltage (v_T), change in speed ($\Delta\omega$) and field voltage (E_{fd}), Figs. 3.11 and 3.12 show the receiving end voltages on all the three phases.

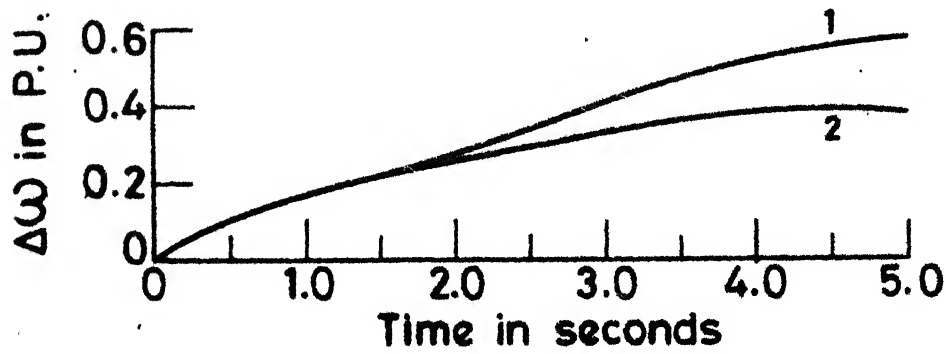
It may be noted from Fig. 3.10a that with ES blocked v_T slowly rises to 2.5 p.u. and this high voltage persists, indicating self-excitation. However, when ES is active, the maximum v_T is only about 1.45 p.u. and it settles down to 1.0 p.u. in an oscillatory manner showing the effectiveness of the ES in controlling the overvoltage due to self-excitation.

The rise in speed is about 40% when ES is blocked and it is about 60% when ES is active (Fig. 3.10b). This is in general agreement with the speed rise of 40% reported in the discussion of ref. [4] for a typical hydro system. The rise in speed is less when ES is blocked as the system losses are higher due to persistent overvoltages.

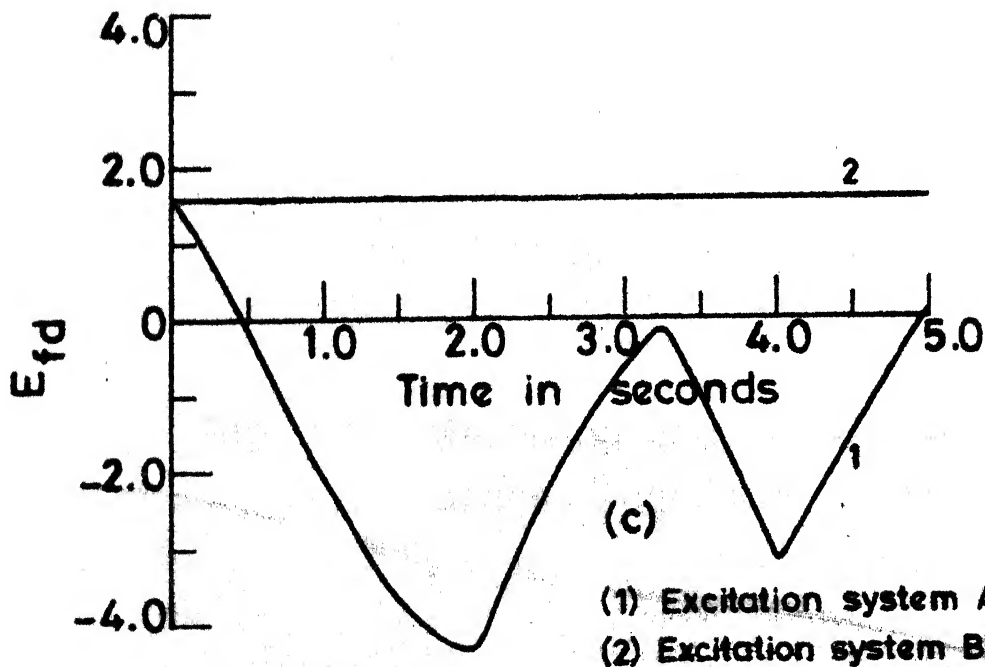
As shown in Fig. 3.10c, E_{fd} is held constant at the initial value when ES is blocked, while it hits the



(a)



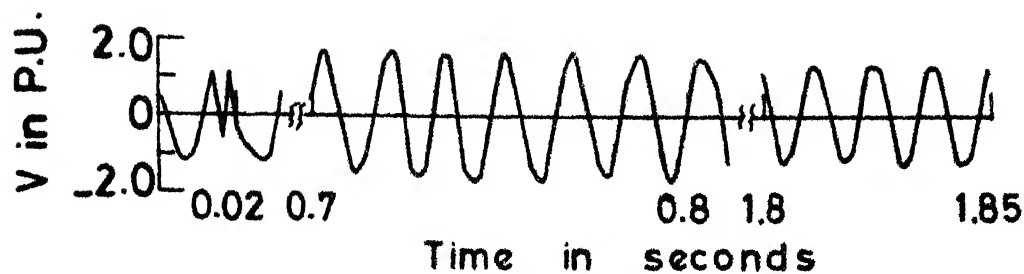
(b)



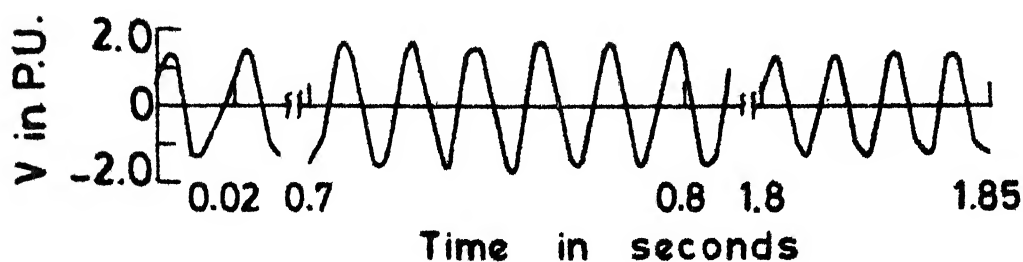
(c)

(1) Excitation system Active
(2) Excitation system Blocked

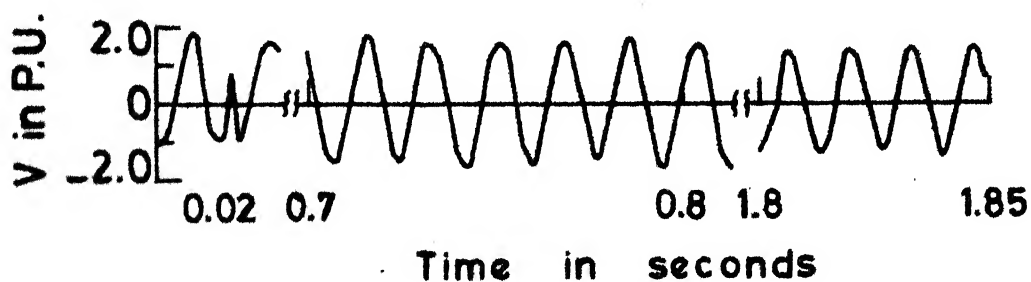
Fig.3.10 Variation of V_T , $\Delta\omega$ and E_{fd} with time. (High side switching).



(a) Phase 'a' voltage

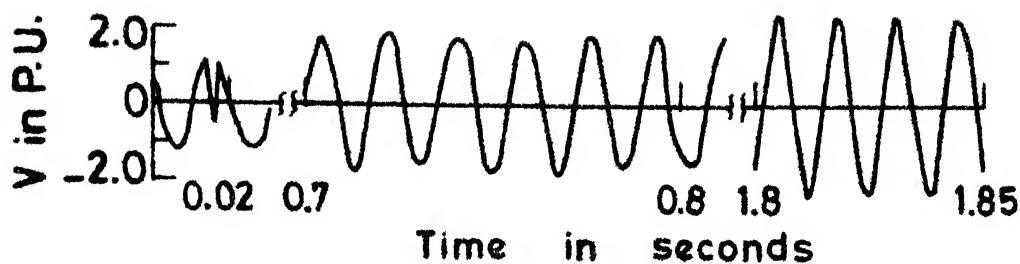


(b) Phase 'b' voltage

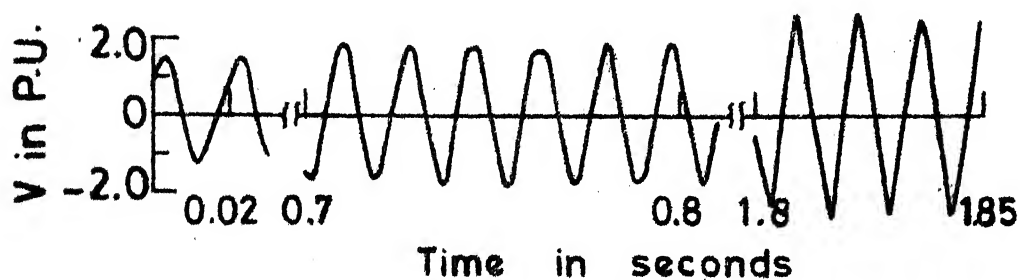


(c) Phase 'c' voltage

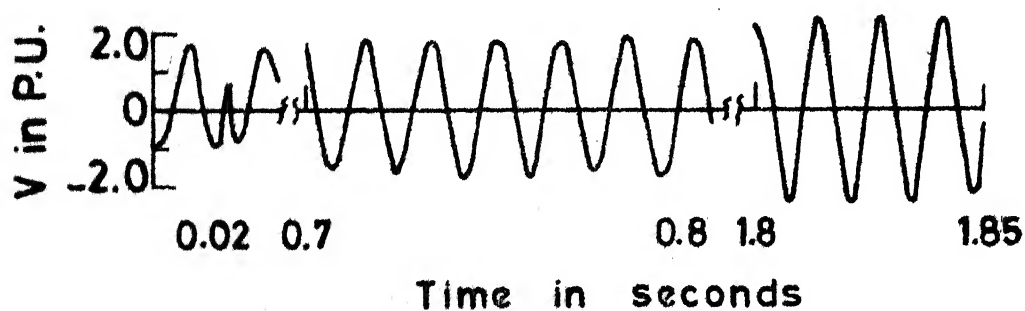
Fig. 3.11 Receiving end voltage with ES active (high side switching).



(a) Phase 'a' voltage



(b) Phase 'b' voltage



(c) Phase 'c' voltage

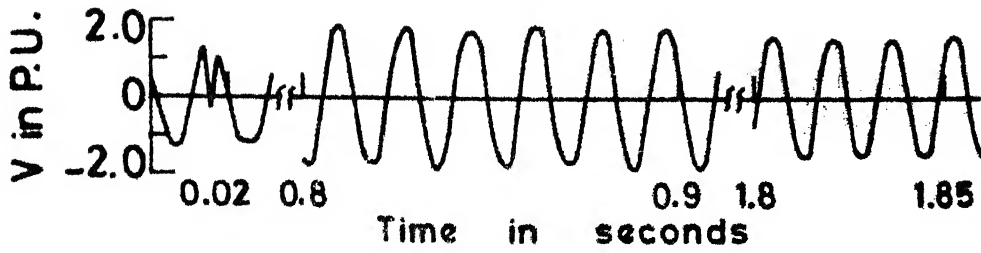
Fig. 3.12 Receiving end voltage with ES blocked (high side switching).

negative ceiling and varies in an oscillatory manner to bring the v_T to 1.0 p.u. when ES is active.

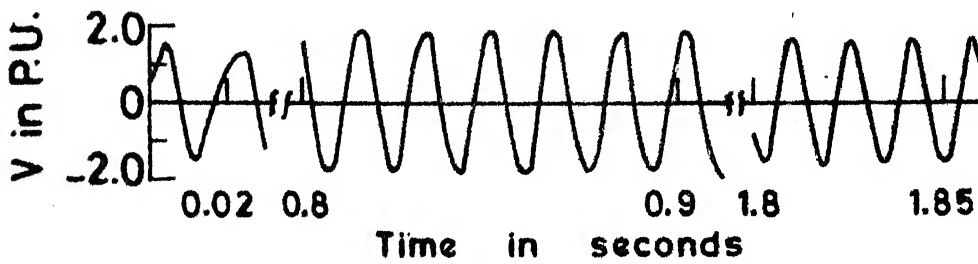
Figures 3.11 and 3.12 show the receiving end voltages with ES active and blocked respectively. As seen from Fig. 3.11, the maximum dynamic overvoltage (MDO) with ES active is 1.7 p.u., while with ES blocked it is more than 2.4 p.u. and still rising for the period of study (1.85 seconds). This further demonstrates the effectiveness of ES in controlling the MDO.

Effect of Shunt Reactor

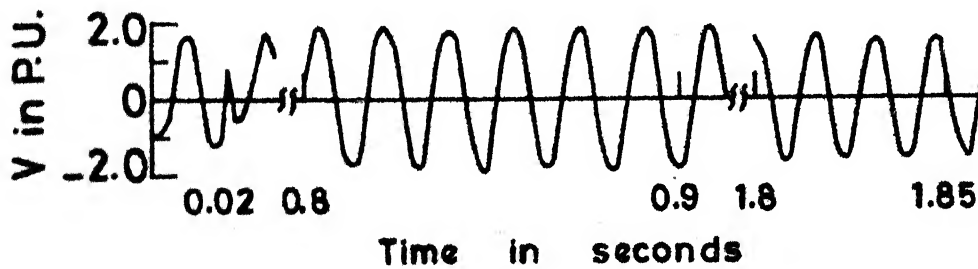
In order to study the effect of the shunt reactor, it was removed from the system, with all the other data (including load) remaining unchanged. The receiving end voltages for this case are shown in Fig. 3.13. As may be observed the MDO is found to be 1.95 p.u. as against 1.7 p.u. (Fig. 3.11) with shunt reactor. This demonstrates the effectiveness of shunt reactor in controlling the MDO. The shunt reactor also lowers the steady state voltage at the generator terminals for a given receiving end voltage and load at specified power factor. In the present study the generator terminal voltage is 1.05 p.u. and 1.12 p.u. with and without shunt reactor respectively. It may be mentioned that 1.12 p.u. voltage at the generator terminal may not be acceptable for steady state system operation.



(a) Phase 'a' voltage



(b) Phase 'b' voltage



(c) Phase 'c' voltage

Fig. 3.13 Receiving end voltage without any reactor (high side switching).

3.5.1.2. Low side switching : To study the effect of the receiving end transformer left connected to the system, the case of 'low side switching' was also studied. Again two cases are studied viz. both ES blocked and active. The receiving end voltages for these cases are given in Figs. 3.14 and 3.15 respectively.

It may be observed that the ferro-resonance takes place for both the cases with MDO equal to 2.0 p.u. However, it is controlled when ES is active (Fig. 3.15) and is persistent when ES is blocked (Fig. 3.14).

It may be concluded from above that it is not advisable to perform the 'low side switching' as it may lead to ferro-resonant mode. Although the ferro-resonance may be eventually controlled, the MDO and the duration for which the overvoltage occur may cause the damage.

3.5.2. Case Study 2 : Thermal System

The data for a typical thermal system, where single line diagram is shown in Fig. 3.1, is given in Appendix - E. Only 'high side switching' is considered as 'low side switching' is ruled out as given in Section 3.5.1.2.

For the basic system, where the EHV line length is 280 Km, the receiving end voltages on load rejection are given in Fig. 3.16. The MDO in this case is 1.6 p.u. It is clear that the overvoltages in this case are less severe as

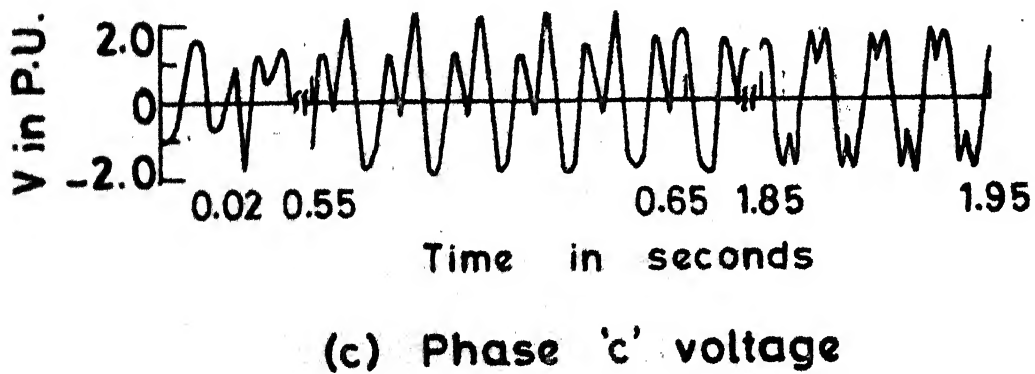
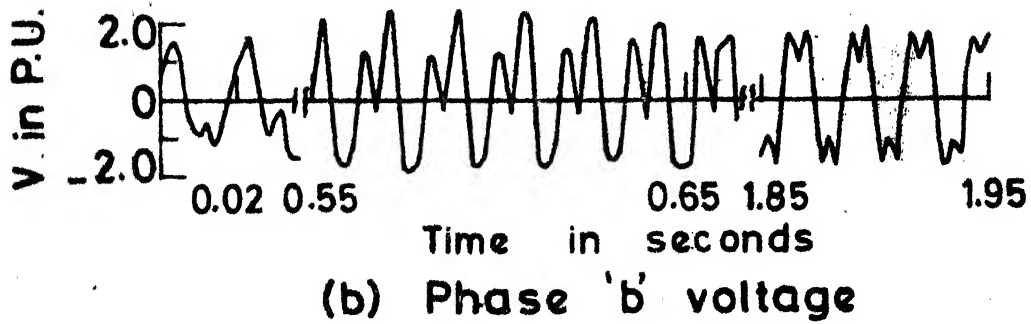
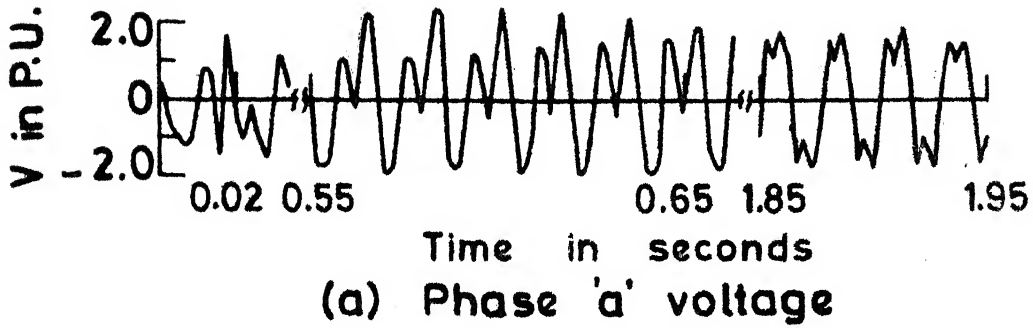
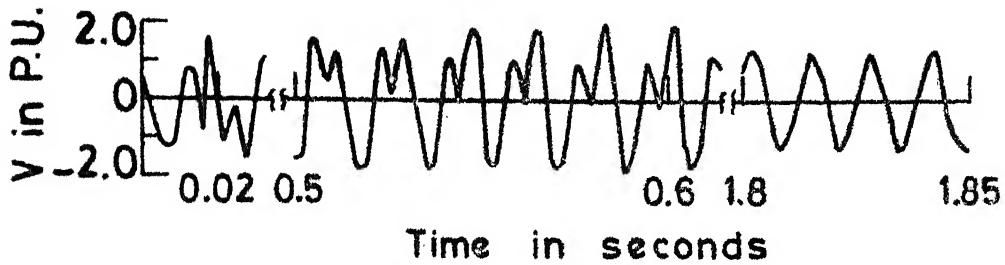
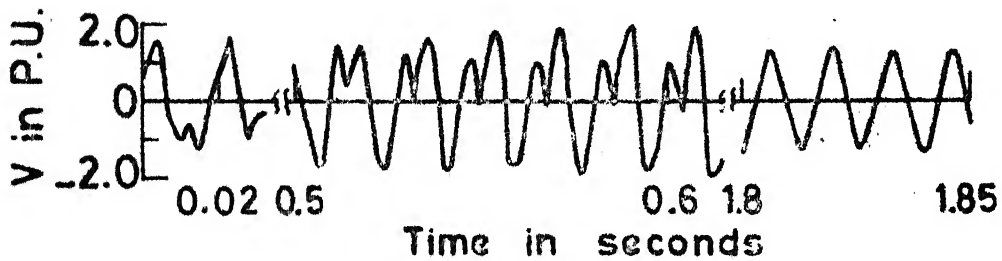


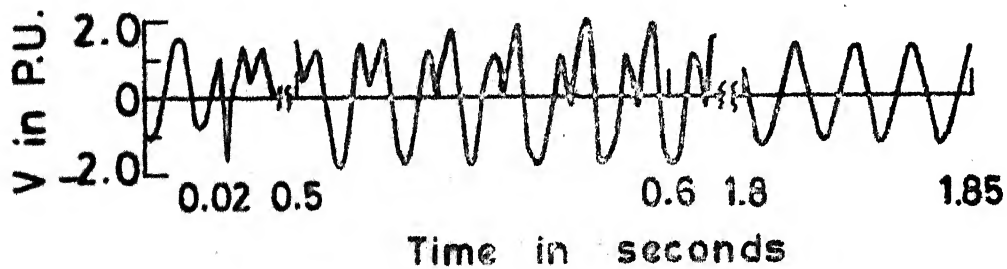
Fig. 3.14 Receiving end voltage with ES blocked (low side switching).



(a) Phase 'a' voltage

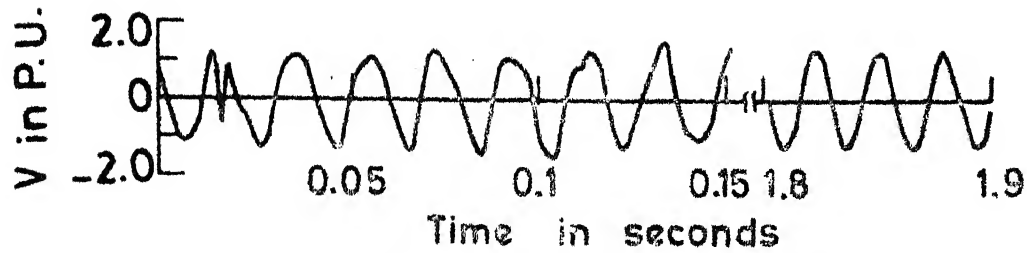


(b) Phase 'b' voltage

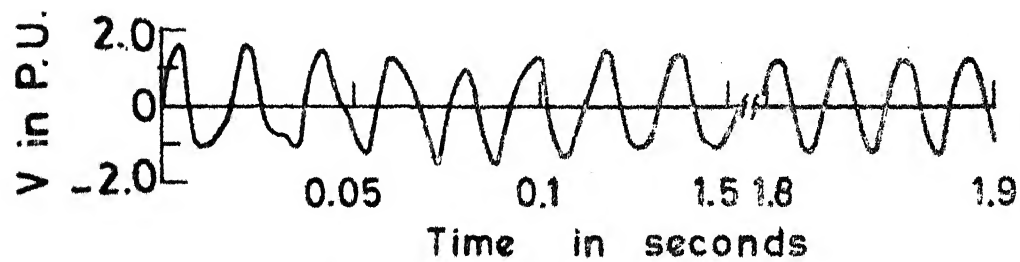


(c) Phase 'c' voltage

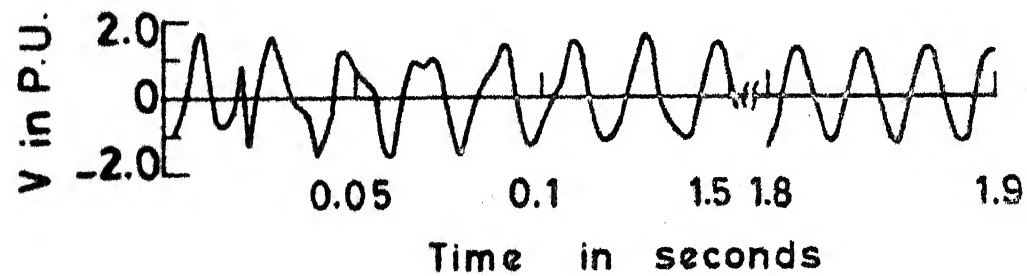
Fig. 3.15 Receiving end voltage with ES active (low side switching).



(a) Phase 'a' voltage



(b) Phase 'b' voltage



(c) Phase 'c' voltage

Fig. 3.16 Receiving end voltage for a thermal system (high side switching).

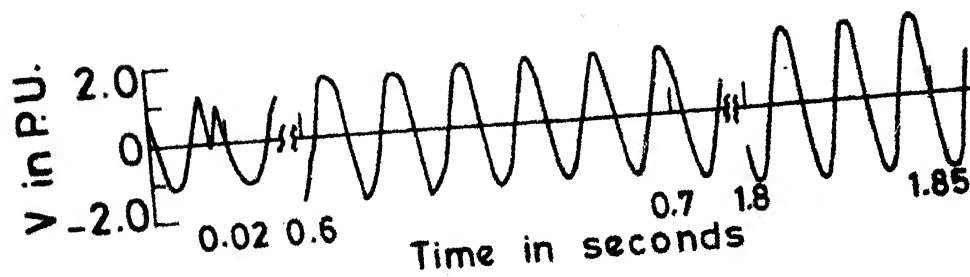
compared to the hydro system of approximately the same size (Fig. 3.11). However, when EHV line length is increased to 370 Km (shunt reactor compensation kept at 60% of line charging) the MDO is increased to 2.0 p.u. for both cases (Fig. 3.17) and the overvoltages are persistent.

This is because the thermal systems are more prone to self-excitation as they have less capability of supplying leading MVARs which is received through larger EHV lines. Also it may be observed that the ES can affect the flux along the generator d-axis only and hence it can not control the self-excitation if it occurs along the generator q-axis. This explains the persistent nature of overvoltage even when ES is active (Fig. 3.17).

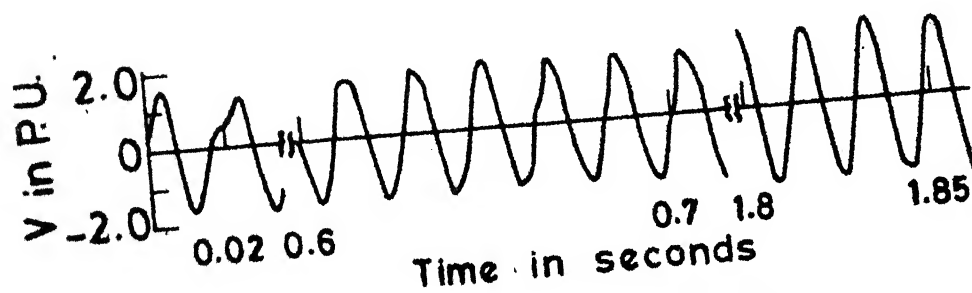
3.6. CONCLUSIONS

A single stage digital simulation technique for determinate dynamic overvoltages following load rejection has been developed and presented in this Chapter. The various components of the power system have been modelled in detail including the network transients on a 3-phase basis.

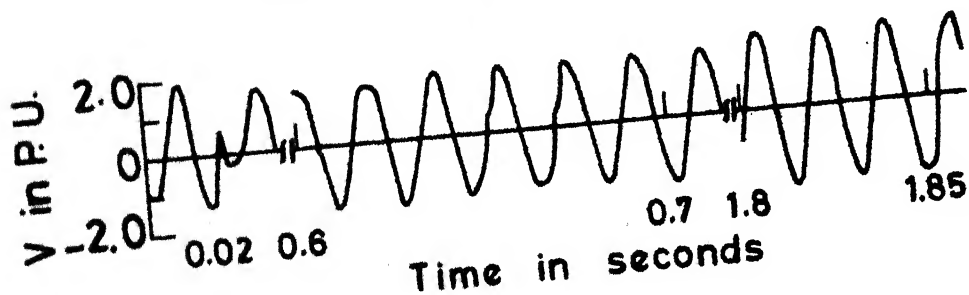
Both the hydro and thermal systems have been considered. It has been shown that the excitation system is effective in controlling the overvoltages caused by self-excitation as well as ferro-resonance. The effectiveness of



(a) Phase 'a' voltage



(b) Phase 'b' voltage



(c) Phase 'c' voltage

Fig. 3.17 Receiving end voltage of a thermal system with increased line length.

the shunt reactors in controlling the dynamic overvoltage is also demonstrated. It is also shown that the 'low side switching' may lead to ferro-resonant mode and, therefore, should be avoided.

CHAPTER - IV

TRANSIENT OVERVOLTAGES - STATE SPACE AND METHOD OF CHARACTERISTICS

4.1. INTRODUCTION

We have already studied the occurrence of the steady state power frequency and harmonic overvoltages in Chapter-II and dynamic overvoltages in Chapter-III. The topic which is yet to be covered is the study of transient overvoltages which can arise either due to switching or faults. An EHV system consists of transmission lines along with the components like transformers and generators etc. The transmission line modelling is quite complex for the calculation of switching transients. For this purpose several methods have been suggested in the past [6,7,8,9,10,11,12,20,21,29,31]. Perhaps the most popular method is due to Dommel [11,21,31] based upon the method of characteristics. It enables the transmission line to be represented by a resistive network along with the current sources, whose values are dependent upon the past history. Further, by using trapezoidal rule of integration, it is possible to represent the inductive and capacitive elements by resistances and current sources which depend upon the past history. Since the equivalent circuit

for a linear network (comprising of generators, transformers etc.) has only L's C's, voltage and current sources, it is obvious that the resultant network will be resistive. The network admittance matrix is constant as long as the time step of integration is not varied. Therefore the solution of the network is very simple, since the admittance matrix needs to be triangularized only once. However, when we wish to include non-linear elements, then the admittance matrix is not constant any more. Dommel has proposed Compensation Method [21] in such cases. The method works well in the case of one non-linear element. But if there are several non-linear elements, the resulting non-linear equations must be solved simultaneously. It is evident that the computation time per iteration may become excessive in such a case. For several non-linear elements, the state space approach may be better. Further, it enables the detailed generator representation with its amortisseur circuits, rotor dynamics and saturation along with voltage regulator and governor [28] as already described in Chapter -III.

In this Chapter the two alternatives as given below have been examined.

(a) To interface the transmission line model based upon the method of characteristics with the state space model for rest of the system.

(b) To use state space model for the transmission line as well, along with rest of the system.

4.2. SYSTEM ANALYSED

Since the main purpose of this Chapter is to examine the transmission line model as interfaced with rest of the system, it is adequate to represent the generator by its simplest representation, i.e. a voltage source behind a constant impedance.

The system analysed is shown in Fig. 4.1, which consists of a generator with unit transformer connected to an EHV transmission line with a shunt reactor at the receiving end. The representation of the generator, the unit transformer and the reactor is common in both alternatives 'a' and 'b' given above, whereas the transmission line modelling is different. An equivalent circuit of the system excluding the transmission line is shown in Fig. 4.2. As already mentioned, the generator is represented by a constant voltage (e_s) behind a constant impedance. The combined 'source' impedance $Z_c (=R_c + j\omega L_c)$ shown in Fig. 4.2 consists of the leakage impedance of the transformer along with the generator impedance. The transformer magnetising impedance Z_t is represented by $R_t + j\omega L_t$ and the reactor impedance Z_r is represented by $R_r + j\omega L_r$. The resistance R_b is the circuit breaker

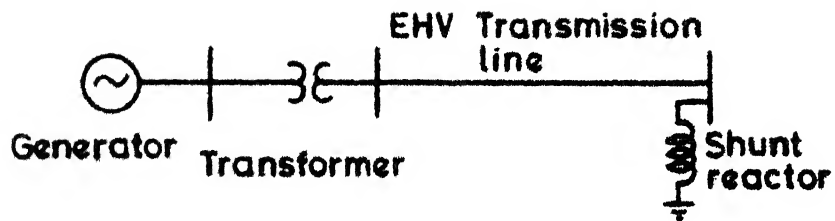


Fig.4.1 The system analysed.

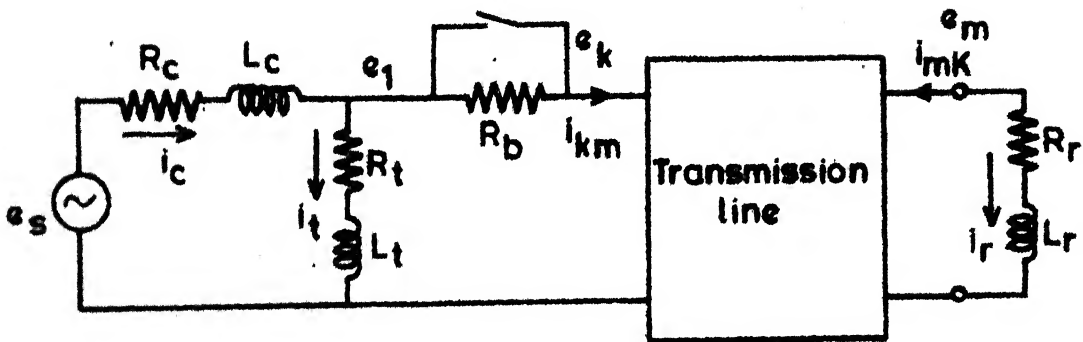


Fig.4.2 The equivalent circuit of the system.

closing resistor, which is inserted for a few milliseconds during the closing operations.

The resulting differential equations for the three phase system are

$$\frac{di_c}{dt} = L_c^{-1} (-R_c i_c + e_s - e_l) \quad (4.1)$$

$$\frac{di_t}{dt} = L_t^{-1} (-R_t i_t + e_l) \quad (4.2)$$

$$\frac{di_r}{dt} = L_r^{-1} (-R_r i_r + e_m) \quad (4.3)$$

$$\text{where } e_l = e_k + i_{km} R_b \quad (4.4)$$

$$i_{km} = i_c - i_t \quad (4.5)$$

$$i_{mk} = -i_r \quad (4.6)$$

The variable i_c , i_t , i_r , i_{km} , i_{mk} , e_s , e_l and e_k and e_m are 3×1 vectors and R_c , R_b , R_t , L_c and L_t are 3×3 matrices.

4.2.1. ALTERNATIVE 'a'

The transmission line model using the method of characteristics as given by Dommel [11] is shown in Fig. 4.3. By using a modal transformation, the three phase line currents and voltage can be converted into modal components. The transformation is given by

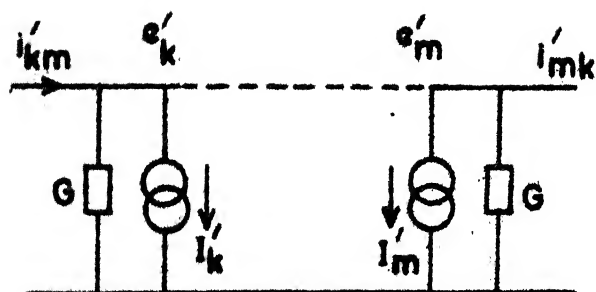


Fig.4.3 The transmission line model for "Alternative a".

$$e_{\text{phase}} \text{ or } i_{\text{phase}} = [T] e_{\text{mode}} \text{ or } i_{\text{mode}} \quad (4.7)$$

where

$$[T] = \begin{vmatrix} 1 & 1 & 1 \\ 1 & -2 & 1 \\ 1 & 1 & -2 \end{vmatrix} \quad (4.8)$$

This enables the three phase transmission line to be treated as equivalent to three independent single phase lines. The resultant equations for each mode, where the superscript 'prime' refers to modal quantities, are given by

$$i'_{km} = G. e'_k + I'_k (t - \tau) \quad (4.9)$$

$$i'_{mk} = G. e'_m + I'_m (t - \tau) \quad (4.10)$$

where

$$G = 1/(Z + R/4) \quad (4.11)$$

and i'_{km} , i'_{mk} , e'_k , and e'_m are the modal line currents and voltages at two ends of the line. $I'_k(t-\tau)$ and $I'_m(t-\tau)$ are the modal current sources which depend upon the past histories and ' τ ' is the modal propagation time. The Z and R in eqn. (4.11) are the modal surge impedance and resistance respectively.

$I'_k(t-\tau)$ and $I'_m(t-\tau)$ are given by

$$\begin{aligned} I'_k(t-\tau) &= \frac{1+h}{2} [-G. e'_m(t-\tau) - i'_{mk}(t-\tau)] \\ &+ \frac{1-h}{2} [-G. e'_k(t-\tau) - i'_{km}(t-\tau)] \end{aligned} \quad (4.12)$$

$$\begin{aligned}
 I'_m(t-\tau) = & \frac{1+h}{2} [-G. e'_k(t-\tau) - i'_{km}(t-\tau)] \\
 & + \frac{1-h}{2} [-G. e'_m(t-\tau) - i'_{mk}(t-\tau)] \quad (4.13)
 \end{aligned}$$

where

$$h = \frac{Z - R/4}{Z + R/4} \quad (4.14)$$

The eqns. (4.9) and (4.10) can be re-arranged as

$$e'_k = \frac{1}{G} [i'_{km} - I'_k(t-\tau)] \quad (4.15)$$

$$e'_m = \frac{1}{G} [i'_{mk} - I'_m(t-\tau)] \quad (4.16)$$

In the transmission line model presented above, there are four terminal quantities viz. e_k , e_m , i_{km} and i_{mk} . If any two of the above quantities are known, the other two can be calculated. In our case, first the currents i_{km} and i_{mk} are obtained from eqns. (4.5) and (4.6), and then the voltages e_k and e_m can be obtained from eqns. (4.15) and (4.16). Now it is required to integrate eqns. (4.1) and (4.2) using eqns. (4.3), (4.15) and (4.16). An integration scheme using the Modified Euler Method is given below :

Step 1 : Calculate derivatives i_c , i_t and i_r from eqns. (4.1) to (4.3).

- Step 2 : Increment the time.
- Step 3 : Obtain the first guess for the state variables i_c , i_t and i_r with the help of derivatives calculated in step 1.
- Step 4 : Obtain the first guess for the voltages e_k' and e_m' from eqns. (4.15) and (4.16). Note that the modal transformation given in eqn.(4.7) is required.
- Step 5 : Calculate the new values of the derivatives i_c , i_t and i_r from eqns. (4.1) to (4.3). It may be noted that the transformation back from modal to phase domain is required.
- Step 6 : Take the average of the derivatives calculated in steps (1) and (5), and use this to calculate final value of state variables i_c , i_t , and i_r .
- Step 7 : Calculate the final value of the voltages e_k' and e_m' from eqns. (4.15) and (4.16).

4.2.2. ALTERNATIVE 'b'

If we also employ the state space model for the transmission line, first alternative could be to use the π -section model. However, it is inefficient in applications requiring large band width, such as simulation of electromagnetic transients [11,12]. The undamped natural frequencies of a loss-less, open ended line are $\omega_k = \frac{k\pi}{\tau}$, $k = 1, 2 - -$,

whereas, a single π -section has an undamped natural frequency of $\omega = \frac{2}{\tau}$, which is considerably different than the line's lowest natural frequency. If we partition the line into two π -sections, then the undamped natural frequencies are $\omega_1 = \frac{2\sqrt{2}}{\tau}$ and $\omega_2 = \frac{4}{\tau}$, which is an improvement at the lowest natural frequency, but the error is large for the second frequency. As the line is partitioned into increasingly larger number of sections, the undamped natural frequency of the lowest pole approaches $\frac{\pi}{\tau}$. However, the number of state variables is much larger and hence the model is very inefficient.

The second alternative is to use the 'Fourier cosine series' transformation as given by Triesenberg [44], where he has shown that the line model based on the representation of distributed voltage has correct natural frequencies with both ends open circuited. The model is suited to the study of energisation transients and any other situation where the line is lightly loaded. It is efficient for the calculation of power frequency (steady state) conditions, since it will require a large number of terms in the cosine series. For this particular situation the dual model employing the 'Fourier cosine series' transformation for the spatially distributed current is more appropriate. In view of the above, we have employed the model based upon the transformation of distributed voltage.

If $v(x,t)$ is the three phase line voltage at a distance x measured from the sending end, then the 'Fourier cosine series' is given by

$$\mathcal{L}[v(x,t)] = V(x,s) = \frac{1}{\pi} V_0(s) + \frac{2}{\pi} \sum_{k=1}^n V_k(s) \cos(k\pi x/d) \quad (4.17)$$

where d is the line length and the coefficients $V_k(s)$, $k=0,1,2,3 \dots$ are found from the integral transform

$$V_k(s) = \frac{\pi}{d} \int_0^d V(x,s) \cdot \cos(k\pi x/d) dx \quad (4.18)$$

An approximate representation for eqn. (17) is

$$V(x,s) = \frac{1}{\pi} V_0(s) + \frac{2}{\pi} \sum_{k=1}^n V_k(s) \cdot \cos(k\pi x/d) \quad (4.19)$$

where 'n' is a finite integer.

Similar transformation can be made for the currents. As seen from eqn. (4.19) the voltage at any point of the line can be calculated by summing the various frequency components $[V_k(s), k=1,2,\dots,n]$. Thus, the Laplace transform of the end point voltages e_k and e_m (Fig. 4.2) are given by

$$\mathcal{L}[e_k(t)] = E_k(s) = \frac{1}{\pi} V_0(s) + \frac{2}{\pi} \sum_{k=1}^n V_k(s) \quad (4.20)$$

$$\mathcal{L}[e_m(t)] = E_m(s) = \frac{1}{\pi} V_0(s) + \frac{2}{\pi} \sum_{k=1}^n (-1)^k V_k(s) \quad (4.21)$$

A transfer function which relates the terminal currents $I_{km}(s)$ and $I_{mk}(s)$ to the component voltages V_k is derived in Appendix G. The structure of the line model based upon the eqns. (3-5), (4.20) and (4.21) is given in Fig. 4.4, where the value of 'n' is taken as three. The currents $I_{km}(s)$ and $I_{mk}(s)$ are shown in Fig. 4.4. The matrices R, L, C and G are 3 x 3 matrices for a 3-phase system.

For the sake of convenience, we define

$$x_1 = i_{km} - i_{mk} \quad (4.22)$$

$$x_2 = i_{km} + i_{mk} \quad (4.23)$$

$$x_3 = \frac{2}{\pi} v_0(t) \quad (4.24)$$

$$x_4 = \frac{2}{\pi} v_2(t) \quad (4.25)$$

$$x_5 = \frac{2}{\pi} v_1(t) \quad (4.26)$$

$$x_6 = \frac{2}{\pi} v_3(t) \quad (4.27)$$

where $x_1, x_2, x_3, x_4, x_5, x_6, v_0(t), v_1(t), v_2(t)$ and $v_3(t)$ are all 3 x 1 vectors.

Then from the block diagram given in Fig. 4.4 we have (ignoring the conductance G)

$$\dot{x}_3 = \frac{1}{d} C^{-1} x_1 \quad (4.28)$$

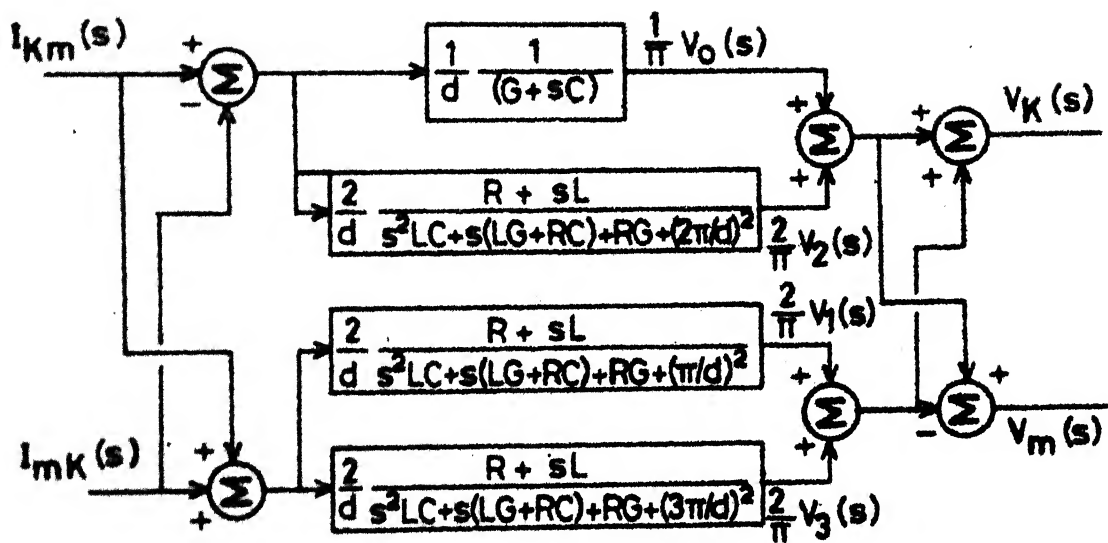


Fig. 4.4 The transmission line model for "Alternative b".

$$LC \ddot{x}_4 + RC \dot{x}_4 + \left(\frac{2\pi}{d}\right)^2 x_4 = \frac{2}{d} [R x_1 + L \dot{x}_1] \quad (4.29)$$

$$LC \ddot{x}_5 + RC \dot{x}_5 + \left(\frac{\pi}{d}\right)^2 x_5 = \frac{2}{d} [R x_2 + L \dot{x}_2] \quad (4.30)$$

and

$$LC \ddot{x}_6 + RC \dot{x}_6 + \left(\frac{3\pi}{d}\right)^2 x_6 = \frac{2}{d} [R x_2 + L \dot{x}_2] \quad (4.31)$$

Equation (4.28) to (4.31) can be written as a set of state equations as follows :

$$\begin{vmatrix} \dot{x}_3 \\ \dot{x}_4 \\ \dot{x}_5 \\ \dot{x}_6 \\ \dot{x}_7 \\ \dot{x}_8 \\ \dot{x}_9 \end{vmatrix} = \begin{vmatrix} 0 & 0 & 0 & 0 & 0 & 0 & 0 \\ 0 & 0 & 0 & 0 & U & 0 & 0 \\ 0 & 0 & 0 & 0 & 0 & U & 0 \\ 0 & 0 & 0 & 0 & 0 & 0 & U \\ 0 & 4b_1 & 0 & 0 & -L^{-1}R & 0 & 0 \\ 0 & 0 & b_1 & 0 & 0 & -L^{-1}R & 0 \\ 0 & 0 & 0 & 9b_1 & 0 & 0 & -L^{-1}R \end{vmatrix} \begin{vmatrix} x_3 \\ x_4 \\ x_5 \\ x_6 \\ x_7 \\ x_8 \\ x_9 \end{vmatrix}$$

$$+ \begin{vmatrix} \frac{1}{d}C^{-1} & 0 & 0 & 0 \\ 0 & 0 & 0 & 0 \\ 0 & 0 & 0 & 0 \\ 0 & 0 & 0 & 0 \\ b_2 & 0 & \frac{2}{d}C^{-1} & 0 \\ 0 & b_2 & 0 & \frac{2}{d}C^{-1} \\ 0 & b_2 & 0 & \frac{2}{d}C^{-1} \end{vmatrix} \begin{vmatrix} x_1 \\ x_2 \\ \dot{x}_1 \\ \dot{x}_2 \end{vmatrix} \quad (4.32)$$

where

$$b_1 = \left(\frac{\pi}{d}\right)^2 L^{-1} C^{-1} \quad (4.33)$$

$$b_2 = \left(\frac{2}{d}\right) L^{-1} C^{-1} R \quad (4.34)$$

$$x_7 = \dot{x}_4 \quad (4.35)$$

$$x_8 = \dot{x}_5 \quad (4.36)$$

$$x_9 = \dot{x}_6 \quad (4.37)$$

In the set of eqns. (4.32) the variables x_1 and x_2 and their derivatives are known as they depend upon network state variables as defined by eqns. (4.5), (4.6), (4.22) and (4.23). Now the set of eqns. (4.32) is solved by 'Modified Euler Method' (which has been already described) along with the eqns. (4.1) and (4.2). The line voltages e_k and e_m are given by

$$e_k = x_3 + x_4 + x_5 + x_6 \quad (4.38)$$

$$e_m = x_3 + x_4 - x_5 - x_6 \quad (4.39)$$

4.3. COMPARISON OF THE ALTERNATIVES

Both the alternatives are compared with the help of two examples given as follows :

Example - I

The system given in ref. [6] is considered first. The data for the system is given in Appendix H. The line energization voltage transients obtained by both the alternatives are shown in Fig. 4.5. It may be noted that the voltage for phase 'a' is in close agreement for both the alternatives (and with that reported in ref. [6]). For phases 'b' and 'c' also the voltage waveforms are in close agreement except that alternative 'b' give rise to superimposed high frequency oscillations. This may be attributed to the absence of the combined source impedance Z_c and truncation of the 'Fourier Series'.

Example - II

The second example is taken from ref. [27], which includes the source impedance Z_c and the transformer magnetising impedance Z_t . The trapped charge and non-simultaneous breaker pole closing is also considered. The data for this example is given in Appendix H. The receiving end voltage waveforms obtained without R_b and with R_b are shown in Figs. 4.6 and 4.7 respectively. There is a close agreement between the waveforms obtained by both the alternatives (and with that reported in ref. [27]). The superimposed high frequency oscillations shown earlier in Fig. 4.5,

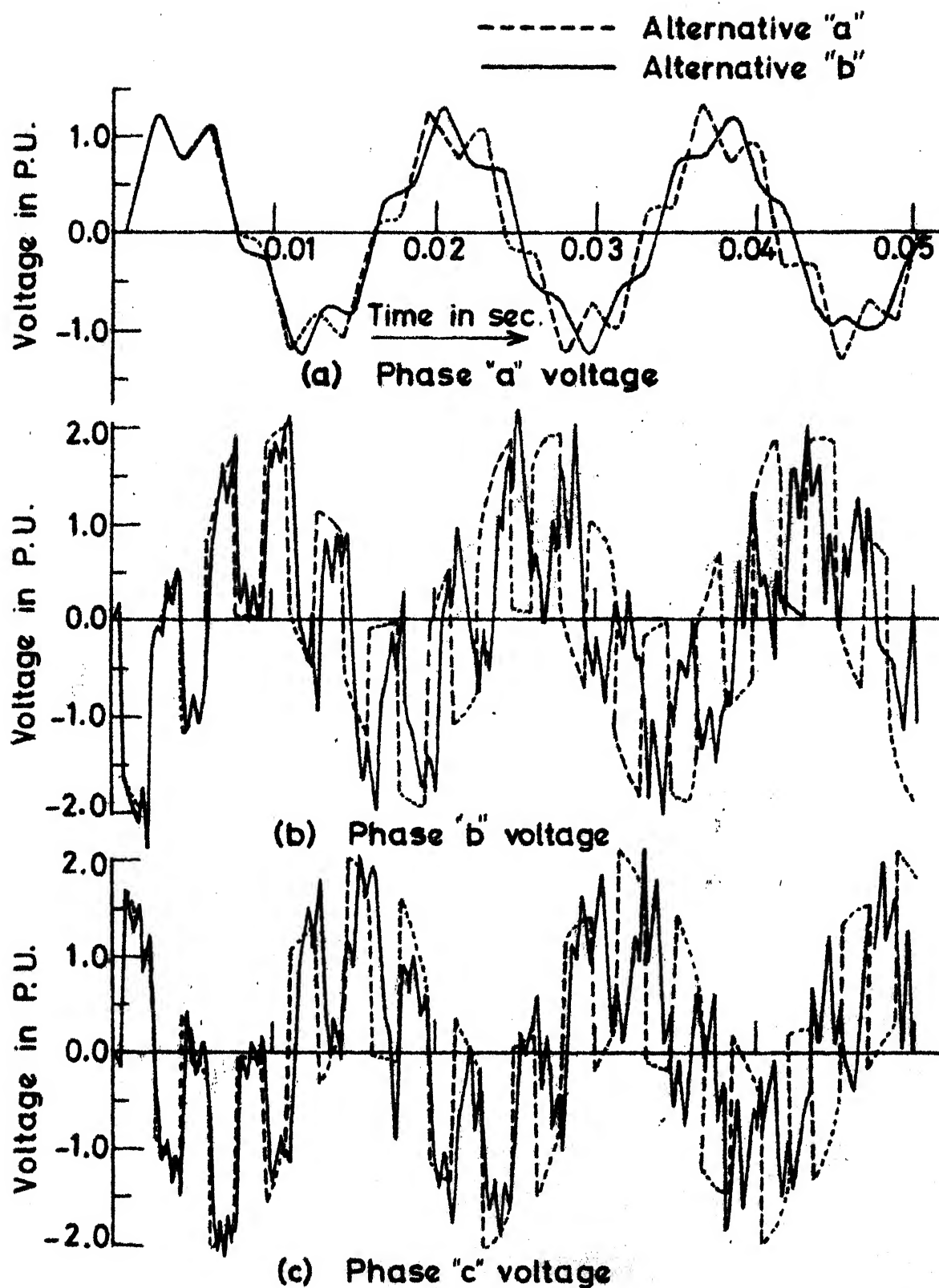


Fig. 4.5 Receiving end voltages of the line on energisation. (Example I).

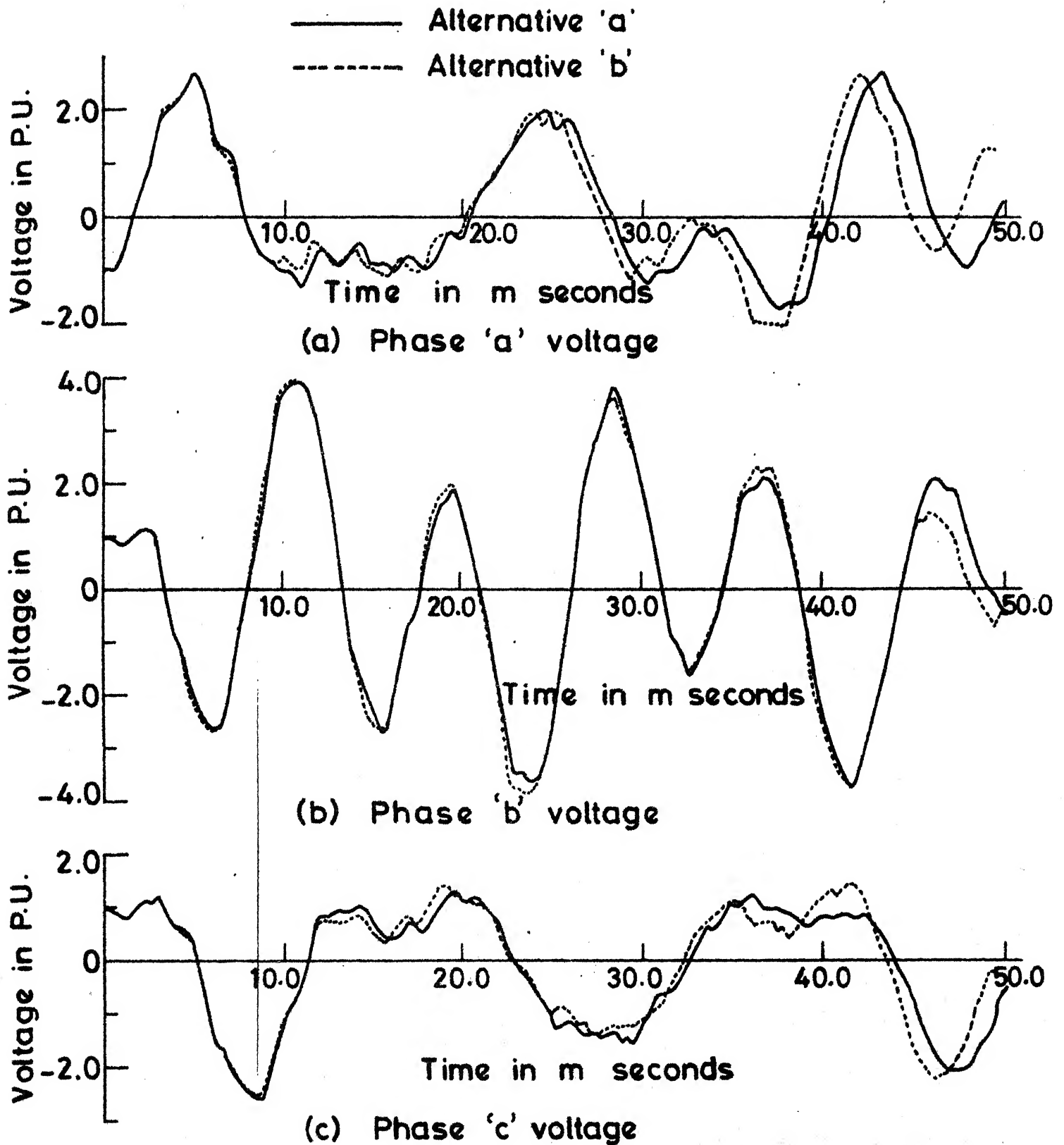


Fig. 4.6 Receiving end voltages on line energisation without closing resistance (Example-II)

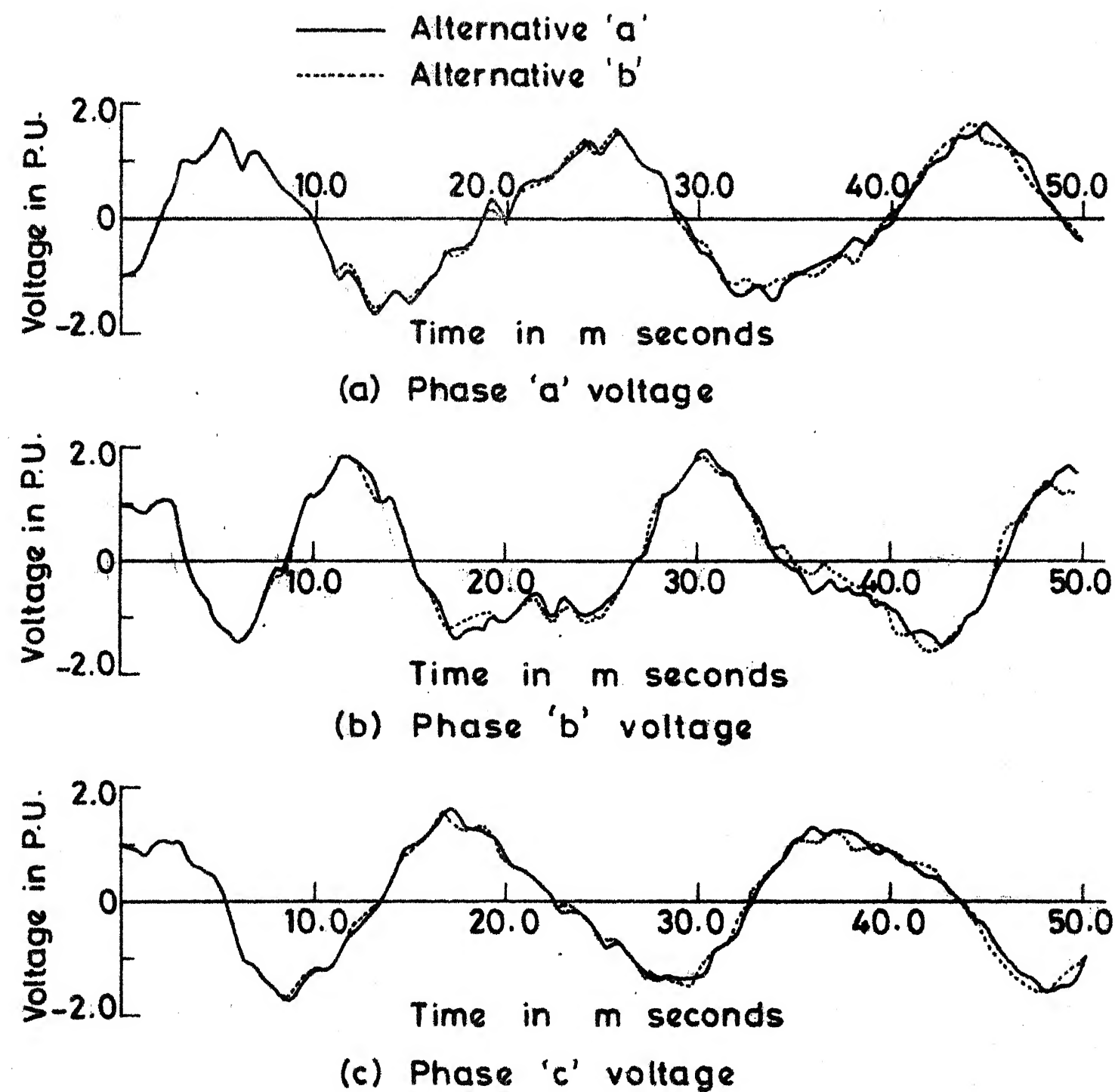


Fig. 4.7 Receiving end voltages on line energisation with closing resistance (Example-II)

while using the Alternative 'b' disappeared in this case. This is attributed to the presence of the combined source impedance Z_c .

A comparative statement of these two alternatives is given in Table 4.1. The Alternative 'a' has been found to be superior in terms of the computation time. The computation time is large in Alternative 'b' because of the larger computation time required per step and also the smaller step size. The larger (doubled) step size resulted in numerical instability for both the alternatives.

Table - 4.1

Comparative Statement for Alternative 'a' and 'b'

S.No.	Study	Step size in msec.	Total computation time in percent
1.	Alternative 'a'	0.05	100 percent
2.	Alternative 'b'	0.025	272 percent

4.4. CONCLUSION

For determining the transient overvoltages due to switching, the transmission line can be modelled either using the method of characteristics or the state space approach. However, when the system consists of several non-linear elements, barring transmission lines, the state space

approach is most desirable for the rest of the network. Thus, the two alternatives which need to be considered are (a) to interface the transmission line model based upon the method of characteristics with the state space model for rest of the system, and (b) to use the state space model also for the transmission line along with the rest of the system. It is shown that it is possible to employ either of the two alternatives. However, the Alternative 'b' has two drawbacks. If the source impedance is neglected, the resulting voltage waveforms may have high frequency oscillations superimposed on them. It is also shown that the total computation time for Alternative 'b' is approximately three times than that for Alternative 'a'. Thus it is concluded that the Alternative 'a' is superior to Alternative 'b'.

CHAPTER - V

TRANSIENT OVERVOLTAGES DUE TO FAULTS

5.1. INTRODUCTION

In Chapter IV, we have presented some modelling aspects for determination of the transient overvoltages in EHV systems. The conclusion was that if the EHV system has several non-linear elements which include generator and transformer saturation, the method of characteristics for the transmission line and the state space approach for the rest of the system should be used. In the majority of the EHV systems, the predominant transient overvoltages are those due to line energisation/~~re~~-energisation [19,26]. Such overvoltages can be controlled with the help of circuit breaker closing resistors. When the overvoltages due to line energisation/~~re~~-energisation are strongly controlled, the overvoltages due to fault inception and subsequent load rejection may become more important [15,16,17]. Further, if single pole switching is employed, special attention must be paid to the overvoltages on one of the unfaulted phases during a single line to ground fault. This is true, since a ground fault on one phase could cause a flashover from another phase to ground, thereby converting a single

line to ground fault into a double line to ground fault. The possibility of such an occurrences greatly diminishes the expected benefits of single pole switching.

The modelling of the synchronous generator for the determination of the above-mentioned overvoltages should be detailed since there can be fundamental frequency and natural frequency (of the system) components besides the harmonic components resulting from unbalanced currents flowing in the armature of the synchronous generator, especially if it is of the salient pole type [1].

A number of investigators [15,16,38] have used TNA to study the above-mentioned overvoltages. Some of the inherent drawbacks of the TNA, particularly the inability to have detailed generator representation, have already been pointed out in Sec. 3.1. A mathematical model for the digital simulation of single line to ground fault has been given in ref. [17]. The method is based upon the Laplace Transform technique and the fault is simulated by applying a voltage source equal and opposite in magnitude to the pre-fault voltage at the fault point and then making the use of superposition principle. Since superposition is only applicable to linear systems, this approach cannot be used for modelling when non-linear elements are present. A method simulating the line to ground fault using the

method of characteristics, which does not require superposition, has been developed and presented in this Chapter.

5.2. SYSTEM ANALYSIS

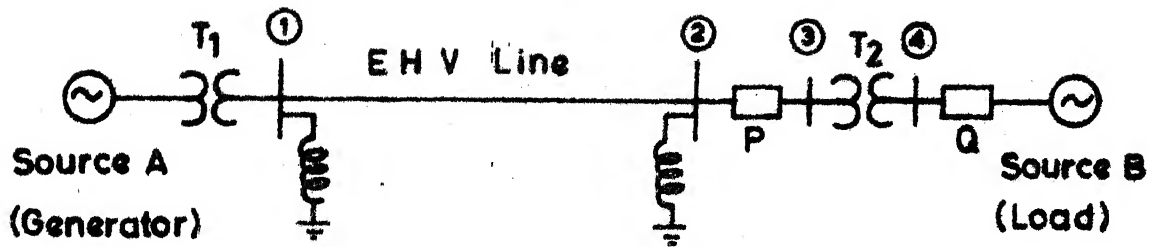
For the purpose of analysis, the system shown in Fig. 5.1 is considered. Here, the power flow is assumed from source A towards source B. Note that this figure is identical to Fig. 3.1 except that the load is represented by a voltage source. This is done because at the time of fault inception on the EHV line, there will also be a feed from the load side. An equivalent circuit for the system is given in Fig. 5.2, where the source A (generator) is represented in details as already explained in Chapter-III. The source B (load) is represented by a constant voltage source along with an impedance as determined by the short circuit MVA. A single line to ground fault is assumed to occur at point 'f' on the line as shown in Fig. 5.2. The fault simulation technique is given in Appendix - I.

The state equations describing the system during the fault on the EHV line are

$$(L_g + L_2) \dot{i}_1 = e_k - (R_2 + R_g)i_1 - L_g \dot{i}_g \quad (5.1)$$

$$L_5 \dot{i}_3 = e_k - R_5 i_3 \quad (5.2)$$

$$L_6 \dot{i}_4 = e_m - R_6 i_4 \quad (5.3)$$



T_1 = Sending end transformer

T_2 = Receiving end transformer

P and Q are circuit breakers

Fig. 5.1 System analysed for fault overvoltages.

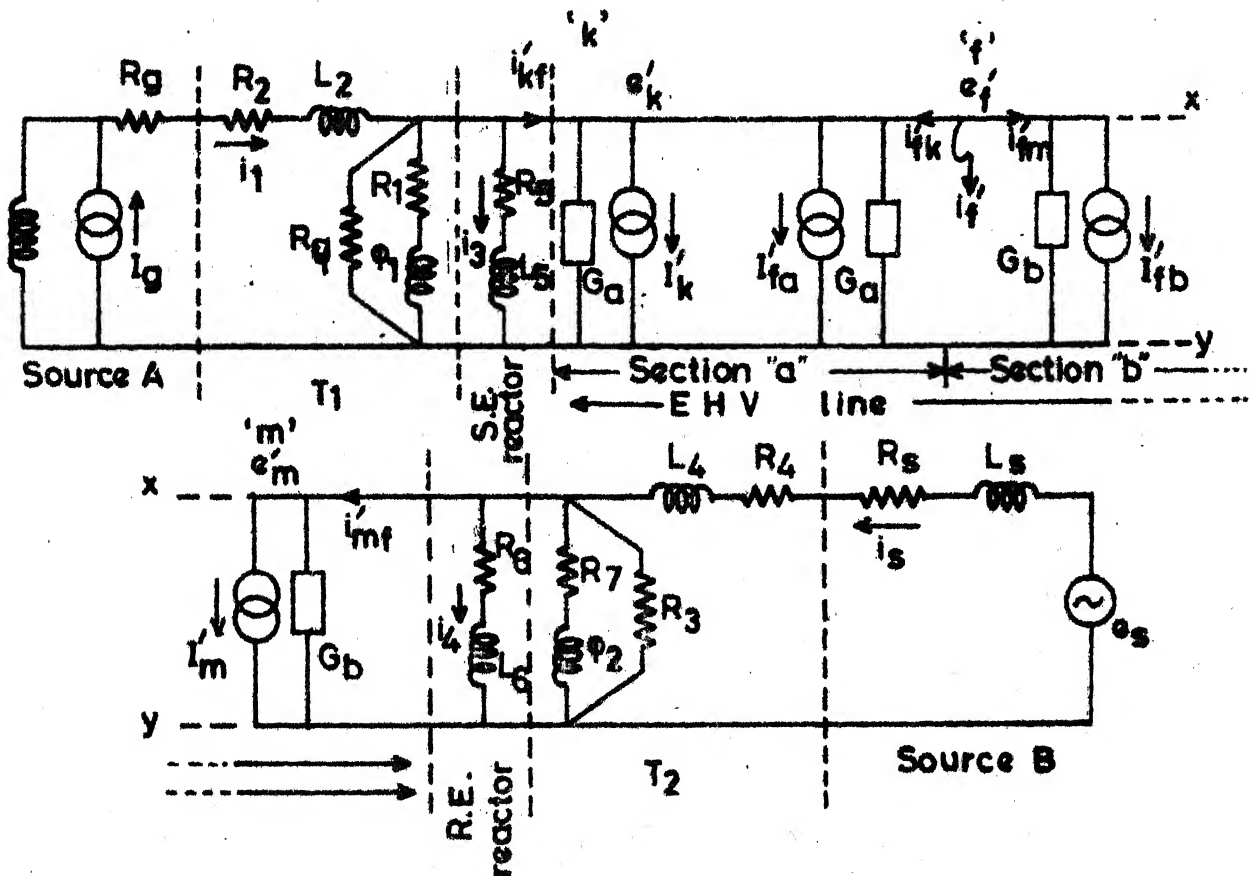


Fig. 5.2 Equivalent circuit for the system shown in Fig. 5.1

$$(L_4 + L_s) \dot{i}_s = e_s - e_m - (R_4 + R_s) i_s \quad (5.4)$$

$$\dot{\varphi}_1 = e_k - R_1 f_1(\varphi_1) \quad (5.5)$$

$$\dot{\varphi}_2 = e_m - R_7 f_2(\varphi_2) \quad (5.6)$$

Equations (5.1) to (5.6) can be written in concise form as

$$[A] \dot{x}_m = f'(x_m) + v' \quad (5.7)$$

where

$$[x_m]^t = [i_1 \ i_3 \ i_4 \ i_s \ \varphi_1 \ \varphi_2] \quad (5.8)$$

$$[v']^t = [(e_k - L_g \dot{i}_g) \ e_k \ e_m \ (e_s - e_m) \ e_k \ e_m] \quad (5.9)$$

$$f'(x_m) = \begin{bmatrix} -(R_2 + R_g) i_1 \\ -R_5 i_3 \\ -R_6 i_4 \\ -(R_4 + R_s) i_s \\ -R_1 f_1(\varphi_1) \\ -R_2 f_2(\varphi_2) \end{bmatrix} \quad (5.10)$$

$$[A] = \begin{bmatrix} L_g + L_2 & & & & & \\ & L_5 & & & & \\ & & L_6 & & & \\ & & & L_4 + L_s & & \\ & & & & U & \\ & & & & & U \end{bmatrix} \quad (5.11)$$

The set of eqns. given by (5.7) can be written as

$$\dot{x}_m = [A]^{-1} f'(x_m) + [A]^{-1} v' \quad (5.12)$$

$$\text{or } \dot{x}_m = f(x_m) + v \quad (5.13)$$

$$\text{where } f(x_m) = [A]^{-1} f'(x_m) \quad (5.14)$$

$$\text{and } v = [A]^{-1} v' \quad (5.15)$$

$[A]^{-1}$ needed in the above equations can be obtained easily, since $[A]$ is block diagonal.

If source A is also represented by a constant voltage source than only eqn. (5.1) will be modified and will be similar to eqn. (5.4).

If we wish to consider the load rejection overvoltage while the fault is still present, we will assume that in Fig. 5.1 the circuit breaker 'P' opens. This corresponds to high side switching as we have already concluded in Chapter - III that the low side switching is to be avoided. We will assume that the circuit breaker has opening resistors as suggested in ref. [23] for the control of load rejection overvoltages. For the above situation the equivalent circuit as given in Fig. 5.2 is still applicable except that a resistance R_b (opening resistor) is inserted between buses (2) and (3). The state equations describing the system are as follows.

$$(L_g + L_2) \dot{i}_1 = e_k - (R_2 + R_g) i_1 - L_g \dot{i}_g \quad (5.16)$$

$$L_5 \dot{i}_3 = e_k - R_5 i_3 \quad (5.17)$$

$$L_6 \dot{i}_4 = e_m - R_6 i_4 \quad (5.18)$$

$$(L_4 + L_s) \dot{i}_s = e_s - v_2 - (R_4 + R_s) i_s \quad (5.19)$$

$$\dot{\phi}_1 = e_k - R_1 f_1(\phi_1) \quad (5.20)$$

$$\dot{\phi}_2 = v_2 - R_7 f_2(\phi_2) \quad (5.21)$$

$$\text{where} \quad v_2 = e_m + R_b(i_{mf} + i_4) \quad (5.22)$$

It may be noted that the eqns. (5.16) to (5.21) are same as eqns. (5.1) to (5.6) except that the term ' e_m ' in eqns. (5.4) and (5.6) is replaced by ' v_2 ' which is defined by eqn. (5.22)

$$[A] \dot{x}_m = f'(x_m) + u' \quad (5.23)$$

where $[x_m]^t$, $f'(x_m)$ and $[A]$ are already defined by eqns. (5.8), (5.10) and (5.11) respectively and

$$[u']^t = [(e_k - L_g \dot{i}_g) e_k e_m (e_s - v_2) e_k v_2] \quad (5.24)$$

The set of eqns. (5.23) can be written as

$$\dot{x}_m = f(x_m) + u \quad (5.25)$$

where $f(x_m)$ is already defined by eqn. (5.14) and

$$u = [A]^{-1} u' \quad (5.26)$$

With reference to Fig. 5.2, the circuit breaker opening resistance R_b will not be present between buses (2) and (3) when the breaker P is completely opened. This implies disconnection of the load along with the transformer T_2 from rest of the system. In this situation eqns. (5.19) and (5.22) are to be ignored.

5.3. SOLUTION PROCEDURE

The solution of eqn. (5.13) or (5.25) will require \dot{I}_g , e_s , e_k and e_m which are components of the vector 'v' or 'u'. The \dot{I}_g is calculated by eqn. (D-15) as already discussed in Sec. 3.4 and the source voltage e_s is given. The voltages e_k and e_m are obtained from eqns. (I-13) and (I-14). It may be noted that these equations are in modal domain and transformation from modal to phase domain can be done by eqn. (4.7). The terminal currents i_{kf} and i_{mf} needed in eqns. (I-13) and (I-14) are given by

$$i_{kf} = -i_3 - i_2 - f_1(\varphi_1) - e_k/R_9 \quad (5.27)$$

and when the

(a) circuit breaker P poles are closed

$$i_{mf} = -i_s - i_4 - f_2(\varphi_2) - e_m/R_8 \quad (5.28)$$

(b) with the opening resistor R_b inserted between poles

$$i_{mf} = -i_s - i_4 - f_2(\varphi_2) - v_2/R_8 \quad (5.29)$$

(c) with the poles completely open

$$i_{mf} = -i_4 \quad (5.30)$$

The solution procedure utilizing the modified Euler Method for the solution of the set of eqns. (5.13) or (5.29), (I-13) and (I-14) is similar to as given in Sec. 4.2.1.

5.4. SYSTEM STUDIES

Based on the theory presented so far, a computer program was developed. To gain confidence in the program the system studied in ref. [15] was simulated. The system consists of an EHV line connected to sources at both ends, which were simulated by constant voltage source representation. The line to ground fault was assumed to occur at middle of the EHV line. In ref. [15] two values for the combined source inductance 'L', which consists of the source and transformer leakage inductance ($L_4 + L_s$ in Fig. 5.2), have been taken. They are 0 and 40 mH respectively. It may be mentioned that in eqn. (5.11), the matrix [A] has a term $L_4 + L_s$. This term can not be taken as zero, as otherwise $[A]^{-1}$ can not be obtained. Therefore, we chose

a value of 3.2 mH compared to zero in ref. [15]. This corresponds to an inductive reactance of 0.001 ohm at 50 Hertz. Compared to the maximum overvoltage (at fault location) of 2.1 and 2.0 p.u. in ref. [15] for $L = 0$ and $L = 40$ mH respectively, we got values of 2.0 and 1.9 p.u. respectively.

Further, studies were made on the system shown in Fig. 5.1, whose data is given in Appendix E except for the source B (load), which is given in Appendix J. The generator is assumed to be hydro because it is expected to give more overvoltages due to saliency [1]. Both fault inception and **subsequent load rejection overvoltages** have been considered and are presented below.

5.4.1. FAULT INCEPTION OVERVOLTAGES

Three studies with source A consisting of one or two generators in parallel, with line to ground fault located at the sending end or middle of the line and detailed (Case - I) as well as constant voltage source (Case - II) representation for the source A (generator) were conducted.

The results obtained are summarized in Table 5.1, which shows the maximum voltage along with time of its occurrence at the sending end, receiving end and fault location. The maximum of these overvoltages (MOV) for each study for both Cases I and II have been underlined. The

TABLE - 5.1

Overvoltages on healthy phases due to fault inception on
Phase 'a'*

Study No.	Study details	Case No.	Maximum voltage in p.u. (Time of occurrence in m.second)					
			Sending end		Receiving end		Fault location	
			Phase 'b'	Phase 'c'	Phase 'b'	Phase 'c'	Phase 'b'	Phase 'b'
I	Two generators operating in parallel. Fault at the sending end of the line	I	1.61 (4.68)	<u>-2.08</u> (2.52)	1.35 (5.04)	-1.34 (1.44)	-	-
		II	-1.39 (15.12)	<u>-1.90</u> (2.52)	1.23 (4.32)	-1.46 (11.88)	-	-
II	Two generators operating in parallel. Fault at the middle of the line	I	1.59 (4.68)	<u>-1.94</u> (1.44)	-1.68 (14.76)	-1.48 (0.72)	1.5 (4.68)	-1.62 (1.80)
		II	1.58 (5.4)	<u>-1.76</u> (0.72)	-1.39 (14.76)	-1.48 (0.72)	-1.39 (15.12)	1.44 (11.16)
III	One generator operation. Fault at the middle of the line.	I	-1.63 (14.76)	<u>-1.87</u> (1.44)	1.56 (2.88)	-1.45 (2.88)	-1.47 (6.12)	-1.53 (1.8)
		II	-1.63 (14.76)	<u>-1.72</u> (0.72)	1.45 (7.2)	-1.34 (4.32)	-1.31 (14.76)	-1.33 (1.8)

* The fault is created when the voltage on phase 'a' at the fault point is passing through its maximum.

high lights of these studies are as follows :

- (1) It may be observed that Case I (detailed generator representation) always gave rise to higher MOV compared to Case II (constant voltage source representation). This can be primarily attributed to harmonic overvoltages because of the unbalanced currents flowing through the armature of the generator, which are ignored in Case II.
- (2) It is also observed that most severe case is when the fault occurs at the sending end. This can be attributed to the fact that in this case the effect of saliency is maximum at the generator terminals, because the external line reactance which reduces the percentage difference between the direct and quadrature axis reactances is zero.
- (3) The two generators operating in parallel i.e. high source MVA, give rise to higher overvoltages as compared to only one generator in operation. This may be explained as follows. The fault inception results into the initiation of travelling waves, which get reflected back and forth at the line ends. With high source MVA, the source impedance will be lower giving rise to higher reflection coefficient and consequent higher overvoltage.

For Study I, the three phase voltage waveforms at the sending end (where MOV occurred) are shown in Figs. 5.3 and 5.4 for Cases I and II respectively. Similarly for Studies II and III, Cases I and II, Figs. 5.5 through 5.8 show the phase c voltage waveforms at the sending end where the MOV occurred.

5.4.2. FAULT OVERVOLTAGES FOLLOWING LOAD REJECTION

The case of load rejection overvoltages following a fault on the EHV line is very important [23]. In Fig. 5.1, it is simulated by opening of the circuit breaker P while the fault is still on the line. In view of the results obtained in Sec. 5.4.1, the detailed representation for the generator (Source A) has been employed as it will give higher overvoltage compared with the constant voltage source representation. The results of this study are given in Table 5.2. It may be observed that the MOV in this case is 2.5 p.u.

TABLE - 5.2

Overvoltage due to load rejection following fault

Study No.	Fault location in percent of line length from sending end.	Maximum overvoltages (MOV) (The letters in parenthesis indicate the phase)	
		Without R_b	With $R_b (=400)$
I	50	1.8 (b)	1.7 (b)
II	80	2.4 (b)	1.9 (b)
III	90	2.5 (b)	2.2 (b)

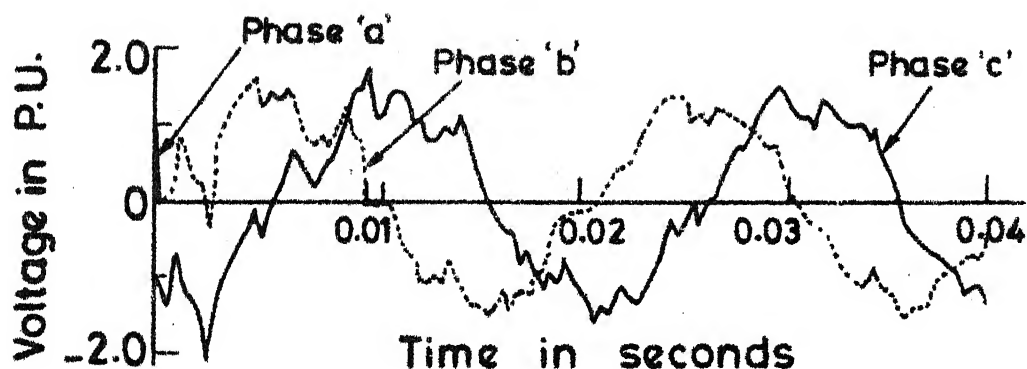


Fig. 5.3 Fault inception voltage waveform at the sending end of the line for Case-I and Study-I.

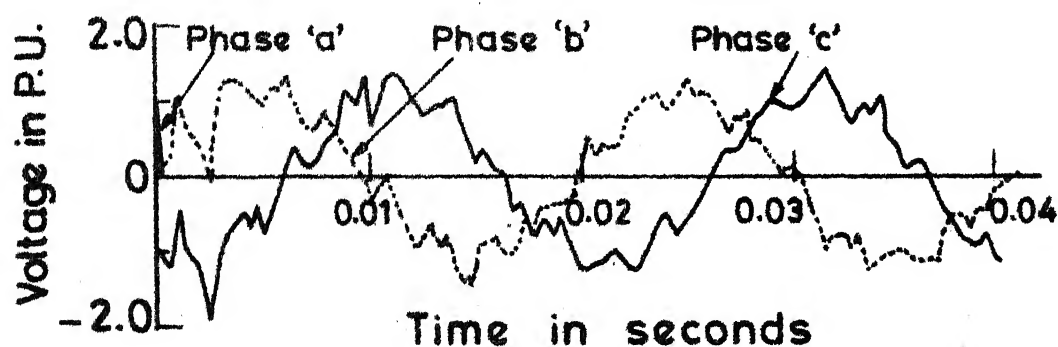


Fig. 5.4 Fault inception voltage waveform at the sending end of the line for Case-II and Study-I.

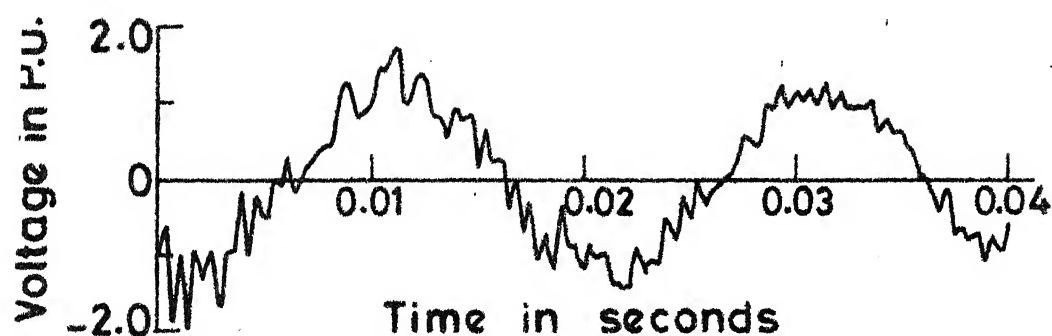


Fig. 5.5 Fault inception voltage waveform on phase c at sending end of the line for Case-I and Study-II.

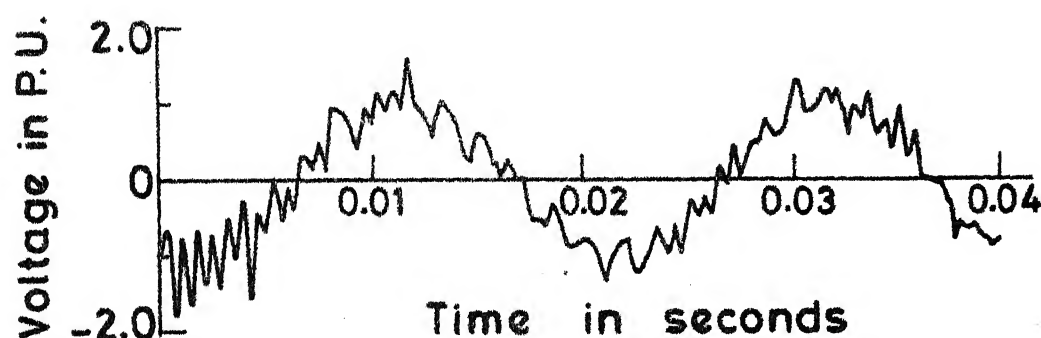


Fig. 5.6 Fault inception voltage waveform on phase c at sending end of the line for Case-II and Study-II.

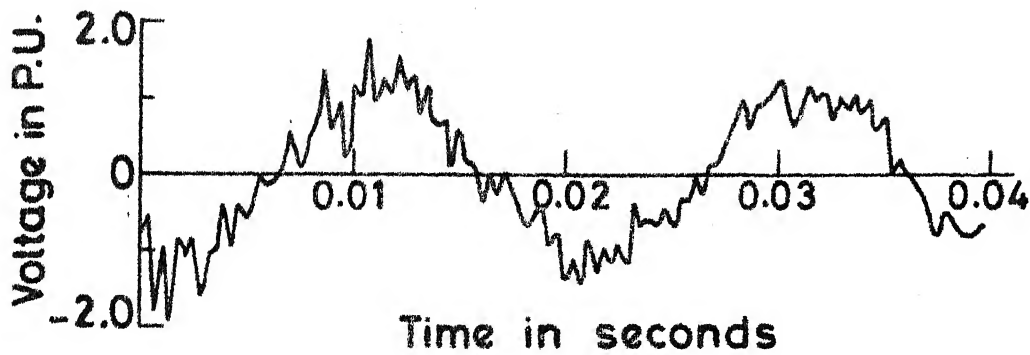


Fig. 5.7 Fault inception voltage waveform on phase 'c' at sending end of the line for Case-I and Study-III.

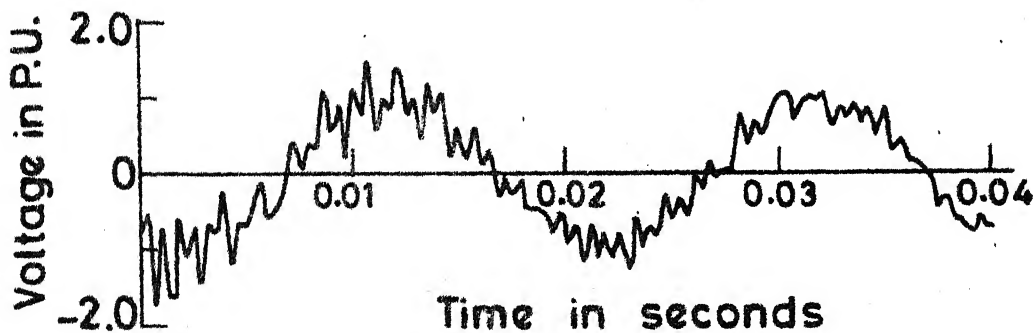


Fig. 5.8 Fault inception voltage waveform on phase c at sending end of the line for Case-II and Study-III .

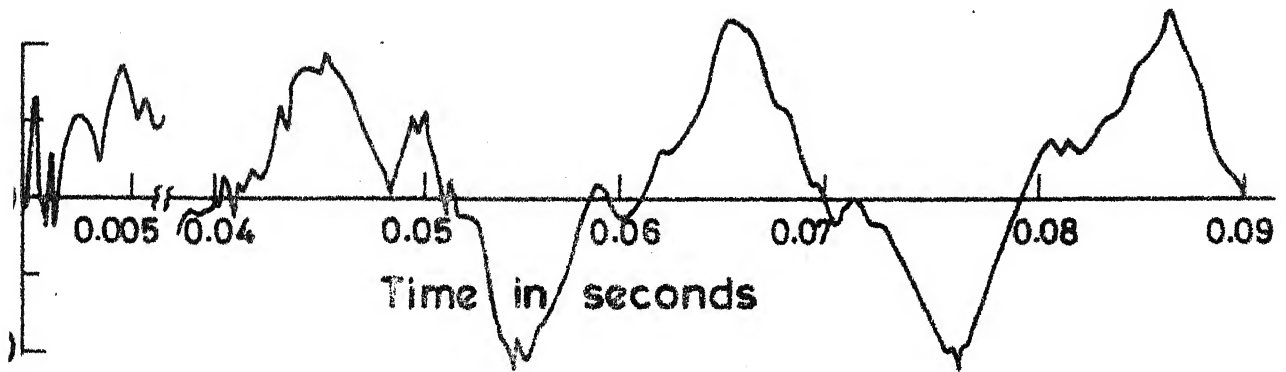


Fig. 5.9 Fault overvoltage due to load rejection on phase 'b' at receiving end of the line without CB opening resistance for study-III.

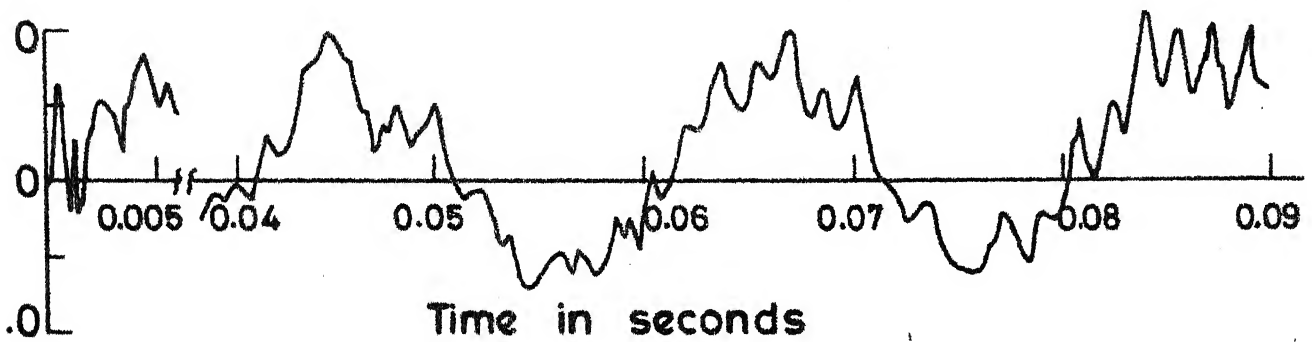


Fig. 5.10 Fault overvoltage due to load rejection on phase 'b' at receiving end of the line with CB opening resistance for study-III.

compared with 2.08 p.u. for the fault inception case and 1.8 p.u. for the case of load rejection without any fault (Chapter -III). These overvoltages were reduced to 2.2 p.u. with circuit breaker opening resistor, demonstrating its usefulness.

These overvoltages were found to be maximum at the receiving end irrespective of fault location. As seen in Table 5.2, the maximum overvoltage occurred with the fault closer to the receiving end.

For Study -III, the receiving end phase 'b' voltage waveforms, where MOV occurred, with and without R_b have been given in Figs. 5.9 and 5.10 respectively.

5.5. CONCLUSIONS

The transient overvoltages due to fault inception and subsequent load rejection have been studied. A digital simulation technique, based on the method of characteristics, has been presented for the simulation of the line faults. The technique does not require the principle of superposition and is, therefore, applicable even if the system has non-linear elements.

It is shown that the detailed generator representation compared with constant voltage source representation is

necessary as otherwise the overvoltages may be lower by about 10 percent. The load throw-off overvoltages following fault could be more severe compared with fault inception or load throw-off without any fault. They can be, however, controlled by circuit breaker opening resistors.

CHAPTER - VI

C O N C L U S I O N S

6.1. GENERAL

This thesis has been aimed at developing improved or new methods for the calculation of steady state, dynamic and transient overvoltages in EHV systems. This is important for the proper determination of the insulation level.

We give below a review of the significant work done and also scope for further work.

6.2. REVIEW OF THE SIGNIFICANT WORK

Chapter II deals with the determination of steady state overvoltages. The failure of an electromagnetic voltage transformer in a practical system, when a circuit breaker fitted with grading capacitors was used for switching, has been analysed. The analytical studies were carried out using the principle of 'Harmonic Balance', which gave excellent agreement with results obtained in the field. The above technique is superior compared to the describing function and state space techniques employed earlier to analyse the problem. Based upon the data collected for several makes of the transformers and circuit breakers, it has been shown

that the steady state overvoltages can be kept to a low value if the transformer saturation characteristic is controlled.

Chapter III deals with the determination of dynamic overvoltages following load rejection. A single stage digital simulation method has been developed for this purpose. The simulation includes the network representation on a three phase basis and detailed generator representation along with its excitation system and prime mover governor. The generator and transformer saturation is also included. It is believed to be more accurate and detailed than those reported in the literature. It is capable of predicting the generator self-excitation and/or ferroresonance phenomena in a single simulation. The effect of excitation system and prime mover governor parameters, transformer saturation and shunt reactors etc., on controlling the dynamic overvoltages can be studied. A number of typical studies for both hydro and thermal systems, which demonstrate the effectiveness of the excitation system and shunt reactors in controlling the overvoltages as given. It is also shown that the receiving end transformer should be disconnected on load rejection.

Chapter IV deals with modelling aspects for the determination of transient overvoltages when several non-linear elements are present in the EHV system. It is shown

that in such a case it is best to model the transmission line based upon the method of characteristics and rest of the system using state space model.

Chapter V deals with the determination of over-voltages due to fault inception and load throw-off subsequent to the fault occurrence. A technique for the simulation of the fault using the method of characteristics has been developed. This is superior compared to the older methods which employed superposition principle for fault simulation, as in that case we must linearise the non-linear elements present in the EHV system. The fault inception overvoltages have been calculated both for simplified and detailed generator representation. The work reported in the literature does not include detailed generator representation. It is shown that the simplified generator representation leads to optimistic results.

6.3. SCOPE FOR FURTHER WORK

While determining the steady state overvoltages in Chapter II it was found out that the occurrence of high voltage or low voltage mode depends on the initial conditions. This particular part of the analysis was carried out using standard state space techniques. A solution had to be obtained for each particular initial condition. This is obviously a laborious process especially when one wishes to change some

of the circuit parameters. A phase plane analysis should be attempted.

Thyrister controlled static shunt compensators have lately become popular. Their role in the control of dynamic overvoltages should be investigated.

We have not considered series compensated EHV transmission lines while calculating the various overvoltages. This aspect should be studied further.

APPENDIX - A

FOURIER EXPRESSION FOR $f(\varphi)$

In Fig. A-1, it is illustrated how $f(\varphi)$ can be obtained from φ -i characteristic. Analytical value of $f(\varphi)$ is calculated piecewise.

From 0 to u_1

$$\begin{aligned} i = f(\varphi) &= \frac{\varphi_1}{L_1} + \frac{\varphi_2 - \varphi_1}{L_2} + \frac{X \cos u - \varphi_2}{L_3} \\ &= K_1 + \frac{X \cos u}{L_3} \end{aligned} \quad (A-1)$$

where

$$K_1 = \frac{\varphi_1 (L_2 - L_1)}{L_1 L_2} + \frac{\varphi_2 (L_3 - L_2)}{L_2 L_3} \quad (A-2)$$

From u_1 to u_2

$$\begin{aligned} i = f(\varphi) &= \frac{\varphi_1}{L_1} + \frac{X \cos u - \varphi_1}{L_2} \\ &= K_2 + \frac{X \cos u}{L_2} \end{aligned} \quad (A-3)$$

where

$$K_2 = \frac{\varphi_1 (L_2 - L_1)}{L_1 L_2} \quad (A-4)$$

From u_2 to $\pi/2$

$$i = f(\varphi) = \frac{X \cos u}{L_1} \quad (A-5)$$

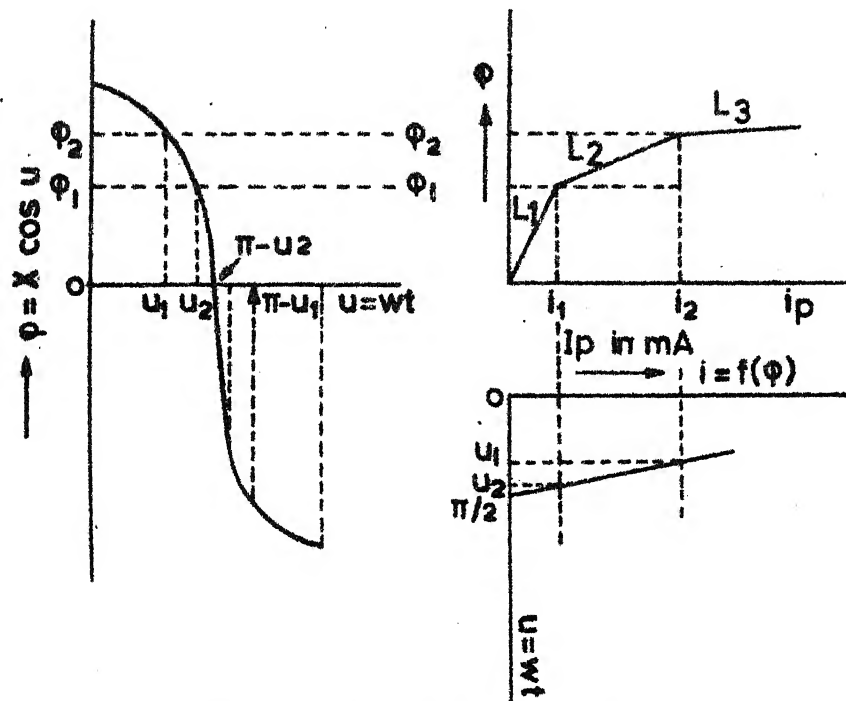


FIG. A.1 DERIVATION OF $i(\phi)$ FROM ϕ

From $\pi/2 < u < \pi$, the derivation is similar to above. The Fourier coefficient B_1 is given by

$$B_1 = \frac{1}{2\pi} \int_0^{\pi} f(\varphi) \cos u \, du \quad (A-6)$$

Substituting the values of $f(\varphi)$ from the eqns.(A-1) through (A-5) and similar equations for $\pi/2 < u < \pi$ in eqn. (A-6), we have

$$\begin{aligned} B_1 = & \frac{2}{\pi} \left[\int_0^{u_1} \left(K_1 + \frac{X \cos u}{L_3} \right) \cos u \, du + \int_{u_1}^{u_2} \left(K_2 + \frac{X \cos u}{L_2} \right) \right. \\ & \left. \cos u \, du + \int_{u_2}^{\pi-u_2} \frac{X \cos u}{L_1} \cos u \, du + \int_{\pi-u_2}^{\pi-u_1} \left(-K_2 + \frac{X \cos u}{L_2} \right) \right. \\ & \left. \cos u \, du + \int_{\pi-u_1}^{\pi} \left(-K_1 + \frac{X \cos u}{L_3} \right) \cos u \, du \right] \quad (A-7) \end{aligned}$$

By simplification

$$\begin{aligned} B_1 = & \frac{2}{\pi} \left[\frac{X}{L_3} \left(u_1 + \frac{\sin 2u_1}{2} \right) + \frac{X}{L_2} (u_2 - u_1) + \frac{1}{2} (\sin 2u_2 - \sin 2u_1) \right. \\ & \left. + \frac{X}{L_1} \left(\frac{\pi}{2} - u_2 \right) - \frac{\sin 2u_2}{2} + 2(K_1 - K_2) \sin u_1 + K_2 \sin u_2 \right] \quad (A-8) \end{aligned}$$

where

$$u_1 = \cos^{-1} \frac{\varphi_2}{X} \quad (A-9)$$

$$u_2 = \cos^{-1} \frac{\varphi_1}{X} \quad (A-10)$$

APPENDIX - BSECANT METHOD

We wish to solve the non-linear equation

$$f(X) = 0 \quad (B-1)$$

In Newton's method, we employ the iterative scheme

$$X_{i+1} = X_i - \frac{f(X_i)}{f'(X_i)} \quad (B-2)$$

where

$$f'(X_i) = \frac{f(X_i) - f(X_{i-1})}{X_i - X_{i-1}} \quad (B-3)$$

Substituting (B-3) in (B-2), we get

$$X_{i+1} = \frac{X_{i-1} f(X_i) - X_i f(X_{i-1})}{f(X_i) - f(X_{i-1})} \quad (B-4)$$

The above iterative scheme is known as 'Secant' method.

APPENDIX - C

CONDITION OF STABILITY

Let the solution of the equation

$$\ddot{\varphi} + k\dot{\varphi} + \frac{f(\varphi)}{C_{th}} = G \cos(\omega t) \quad (C-1)$$

for the fundamental component be

$$\varphi = X(t) \cos \omega t + Y(t) \sin \omega t \quad (C-2)$$

where

$$f(\varphi) = B_1 \cos \omega t + A_1 \sin \omega t \quad (C-3)$$

In the steady state, the amplitudes $X(t)$ and $Y(t)$ in eqn.(C-2) are constant. From the above equations under the assumption that $X(t)$ and $Y(t)$ vary slowly we can get [3]

$$\frac{dX(t)}{dt} = M(X,Y) = -\omega^2 X + k\omega Y + \frac{B_1}{C_{th}} - G = 0 \quad (C-4)$$

$$\frac{dY(t)}{dt} = N(X,Y) = -\omega^2 Y + k\omega X + \frac{A_1}{C_{th}} = 0 \quad (C-5)$$

Let the steady state solution for X and Y be X_0 and Y_0 . If we consider small variations α and β from the solutions X_0 and Y_0 , these deviations approach zero with increase of the time t , if the system is stable.

From eqns. (C-4) and (C-5)

$$\frac{d\alpha}{dt} = \frac{\partial M}{\partial X} \alpha + \frac{\partial M}{\partial Y} \beta \quad (C-6)$$

$$\frac{d\beta}{dt} = \frac{\partial N}{\partial X} \alpha + \frac{\partial N}{\partial Y} \beta \quad (C-7)$$

The solutions of these simultaneous equations have the form $\exp(\lambda t)$ where λ is determined by characteristic equation

$$\begin{vmatrix} \frac{\partial M}{\partial X} - \lambda & \frac{\partial M}{\partial Y} \\ \frac{\partial N}{\partial X} & \frac{\partial N}{\partial Y} - \lambda \end{vmatrix} = 0 \quad (C-8)$$

The variations α and β will approach zero with increase in time, provided the real part of λ is negative. This is given by Hurwitz criterion as

$$-\frac{\partial M}{\partial X} - \frac{\partial N}{\partial Y} > 0 \quad (C-9)$$

and

$$\frac{\partial M}{\partial X} \frac{\partial N}{\partial Y} - \frac{\partial M}{\partial Y} \frac{\partial N}{\partial X} > 0 \quad (C-10)$$

APPENDIX - D

GENERATOR EQUIVALENT CIRCUIT

The generator winding arrangement is shown in Fig. D-1. The dependent current source model of the generator is shown in Fig. 3.2.

The dependent current source vector I_g having 3-phase components is expressed as

$$I_g = I_d \underline{c} + I_q \underline{s} \quad (D-1)$$

The transformation matrices \underline{c} and \underline{s} are defined as

$$\underline{c}^T = \sqrt{2/3} [\cos \theta_r \cos(\theta_r - 2\pi/3) \cos(\theta_r + 2\pi/3)] \quad (D-2)$$

$$\underline{s}^T = \sqrt{2/3} [\sin \theta_r \sin(\theta_r - 2\pi/3) \sin(\theta_r + 2\pi/3)] \quad (D-3)$$

The generator terminal current i_1 can also be split in its d-q components as

$$i_d = \underline{c}^T i_1 \quad (D-4)$$

$$i_q = \underline{s}^T i_1 \quad (D-5)$$

Now the final equations describing the machine can be written. Here ϕ refers to flux linkage and the subscripts refer to winding shown in Fig. D-1.

$$I_d = c_1 \phi_f + c_2 \phi_h \quad (D-6)$$

$$I_q = c_3 \phi_g + c_4 \phi_k \quad (D-7)$$

$$\dot{\phi}_f = a_1 \phi_f + a_2 \phi_h + b_1 E_{fd} + b_2 i_d \quad (D-8)$$

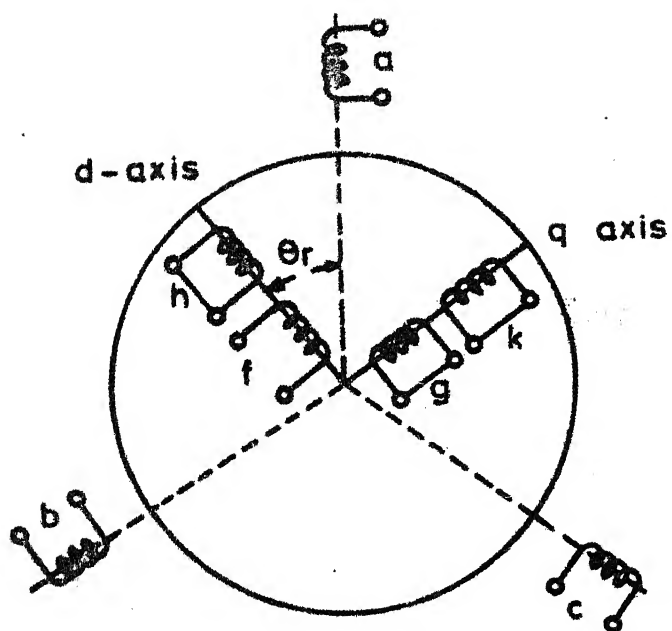


Fig.D-1 The generator

$$\dot{\phi}_h = a_3 \phi_f + a_4 \phi_h + b_3 i_d \quad (D-9)$$

$$\dot{\phi}_g = a_5 \phi_g + a_6 \phi_k + b_5 i_q \quad (D-10)$$

$$\dot{\phi}_k = a_7 \phi_g + a_8 \phi_k + b_6 i_q \quad (D-11)$$

The electro-mechanical power is

$$P_e = -x_d'' (i_d I_q - i_q I_d) \quad (D-12)$$

where x_d'' is sub-transient reactance. Further,

$$\dot{\delta} = \frac{d\delta}{dt} \quad (D-13)$$

$$\ddot{\delta} = \frac{\omega_o}{2H} (-D\dot{\delta} + P_m - P_e) \quad (D-14)$$

The various coefficients shown in above equations are dependent on self and mutual reactances of the windings shown in Fig. D-1. Details are available in ref. [28].

$\phi_f, \phi_h, \phi_g, \phi_k$, and $\dot{\delta}$ are the state variables.

The derivative of I_g , which is required for the calculation of forcing function, is obtained by differentiating eqn.(D-1) with respect to time.

$$\dot{I}_g = (\dot{I}_d + \omega I_q) \underline{c} + (\dot{I}_q - \omega I_d) \underline{s} \quad (D-15)$$

APPENDIX - ESYSTEM DATA FOR DYNAMIC OVERVOLTAGE STUDY

Data for both the cases of study, viz., hydro and thermal systems are given below. All the data is on 100 MVA base.

a) Case Study I - Hydro SystemGenerator parameters

Rating 173.7 MVA, 11 KV, 50 Hz

x_d	=	0.607	;	x'_d	=	0.135
x''_d	=	0.0853	;	x_q	=	0.336
x'_q	=	-	;	x''_q	=	0.1325
x_o	=	0.065	;	R_a	=	0.00158
T'_{do}	=	8.84	;	T''_{do}	=	0.03
T'_{qo}	=	-	;	T''_{qo}	=	0.03
H_c	=	4.56	;	D_c	=	0.0
K_1	=	0.035	;	K_2	=	7.358
K_3	=	0.8				

Line parameters

One three phase transposed single circuit, 400 KV, 260 Km long line. The line parameters are as follows :

$$z_1 = 0.0048 + j 0.0517 \text{ p.u.}$$

$$z_0 = 0.0375 + j 0.1351 \text{ p.u.}$$

$$y_1 = j 1.475$$

$$y_0 = j 0.985 \text{ p.u.}$$

These symmetrical component parameters are converted into self and mutual impedances in the digital programme.

Transformer parameters

A typical non-linear saturation characteristic is taken from ref. [23] and is shown in Fig. E-1. This characteristic is voltage versus current which is converted into flux versus current. The characteristic is taken as piecewise linear by four straight line segments as shown in Fig. E-1.

Sending end transformer

Rating : 180 MVA, 11 KV/400 KV

$$R_2 = 0.0 \text{ p.u.} ; X_2 = 0.0833 \text{ p.u.}$$

$$R_9 = 277.7 \text{ p.u.} \quad (\text{accounts for a loss of } 0.65 \text{ MW})$$

$$R_1 = 4.0 \text{ p.u.} \quad (\text{accounts for a loss of } 0.09 \text{ MW})$$

Magnetising current at no load = 1.25 percent

With reference to Fig. E-1 where magnetising characteristic is shown

$$\varphi_a = 0.0032 \text{ p.u.} ; \varphi_b = 0.00352 \text{ p.u.}$$

$$\varphi_c = 0.00382 \text{ p.u.} ; S_1 = 0.2525$$

$$S_2 = 0.0075 \quad S_3 = 0.00245$$

$$S_4 = 0.0011$$

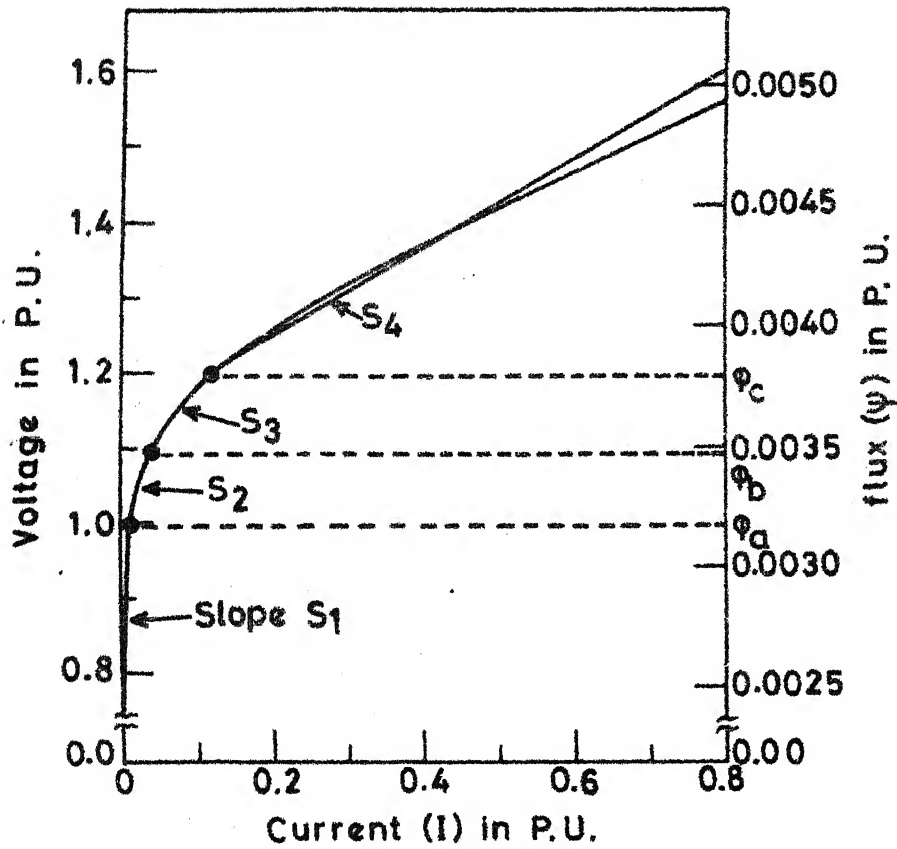


Fig.E-1 Magnetising characteristic of the transformer.

Receiving end Transformer

Rating : 450 MVA , 400 KV/200 KV

$$R_4 = 0.00 \text{ p.u.} ; X_4 = 0.0334 \text{ p.u.}$$

$$R_\theta = 800.0 \text{ p.u. (Accounts for a loss of 0.562 MW)}$$

$$R_7 = 0.79 \text{ p.u. (Accounts for a loss of 0.350 MW)}$$

The nature of magnetising characteristic is same as that of sending end transformer. The break point fluxes and the slopes are

$$\varphi_a = 0.0032 \text{ p.u.} ; \varphi_b = 0.00353$$

$$\varphi_c = 0.00382 \text{ p.u.} ; S_1 = 0.101$$

$$S_2 = 0.003 \quad S_3 = 0.00098$$

$$S_4 = 0.00044$$

Voltage regulator parameters

$$K_a = 400 ; T_a = 0.05 \text{ sec}$$

$$K_e = -0.17 ; T_e = 0.95 \text{ sec}$$

$$K_f = 0.04 ; T_f = 1.0 \text{ sec}$$

$$S_a = 0.00027 ; S_b = 1.304$$

$$V_{R \text{ max}} = 3.5 ; V_{R \text{ min}} = -3.5$$

Hydraulic Governor parameters

$$T_r = 5.0 \text{ sec} ; T_w = 1.0 \text{ sec}$$

$$T_s = 0.2 \text{ sec} ; \sigma = 0.05$$

$$G_{h \text{ min}} = 0.0 ; G_{h \text{ max}} = 1.0$$

$$\alpha = 0.3 ; \dot{G}_{h \text{ min}} = -5.0$$

$$\dot{G}_{h \text{ max}} = 5.0$$

Shunt Reactor at Receiving end

Rating : 65 MVAR

$X = 1.34 \text{ p.u.}$; $R = 0.0077 \text{ p.u.}$

Load

1.5 p.u. at $|V| = 1.0$ and power factor = 0.95 lag.

b) Case Study II - Thermal SystemGenerator parameters (Data on 100 MVA base)

Rating : 250 MVA ; 50 Hz

$x_d = 0.8468 \text{ p.u.}$; $x'_d = 0.1178 \text{ p.u.}$

$x''_d = 0.0816 \text{ p.u.}$; $x_q = 0.8468 \text{ p.u.}$

$x'_q = 0.1178 \text{ p.u.}$; $x''_q = 0.0816 \text{ p.u.}$

$x_1 = 0.0652 \text{ p.u.}$; $x_0 = 0.044 \text{ p.u.}$

$T'_{do} = 7.0 \text{ sec}$; $T''_{do} = 0.1 \text{ sec}$

$T'_{qo} = 0.5 \text{ sec}$; $T''_{qo} = 0.05 \text{ sec}$

$R_a = 0.00072 \text{ p.u.}$; $H_c = 2.2$

$D_c = 0.0$; $K_1 = 0.035$

$K_2 = 7.358$; $K_3 = 0.8$

Line parameters

One three phase, single circuit, transposed, 400 KV and 280 Km long line. The parameters are as follows :

$z_1 = 0.0052 + j 0.0575 \text{ p.u.}$

$z_0 = 0.0452 + j 0.1760 \text{ p.u.}$

$y_1 = j 1.495 \text{ p.u.}$

$y_0 = j 1.03 \text{ p.u.}$

Sending End Transformer parameters

Rating : 250 MVA, 11 KV/400 KV

$$R_2 = 0.0 ; X_2 = 0.0639$$

$$R_6 = 722.00 \text{ p.u. (Corresponding to a loss of .137 MW)}$$

$$R_7 = 2.88 \text{ p.u. (Corresponding to a loss of .082 MW)}$$

Details of magnetising characteristics (Fig.E-1)

$$\varphi_a = 0.0032 ; \varphi_b = 0.00351$$

$$\varphi_c = 0.00382 ; S_1 = 0.1818$$

$$S_2 = 0.0054 ; S_3 = 0.001764$$

$$S_4 = 0.000792$$

Receiving end Transformer parameters

Not considered.

Voltage Regulator parameters

$$T_e = 0.7 \text{ sec} ; K_e = 1.0$$

$$T_a = 0.5 \text{ sec} ; K_a = 0.12$$

$$T_f = 2.0 \text{ sec} ; K_f = 200$$

$$S_a = 0.0 ; S_b = 0.0$$

$$V_{R \text{ max}} = 4.0 ; V_{R \text{ min}} = -4.0$$

Thermal governor parameters

$$T_{sl} = 0.425 \text{ sec} ; R_o = 0.04$$

$$T_{hp} = 0.2 \text{ sec} ; F_{hp} = 0.62$$

$$T_{ip} = 4.0 \text{ sec} ; F_{ip} = 0.38$$

$$T_{lp} = 100.0 \text{ sec} ; F_{lp} = 0.0$$

$$G_{th \text{ min}} = -1.18 ; G_{th \text{ max}} = 0.59$$

$$G_{th \text{ min}} = 0.0 ; G_{th \text{ max}} = 0.85$$

Shunt Reactors at Both ends

Rating : 45 MVAR calculated at voltage 1.05 p.u.

$$X = 2.45 \quad ; \quad R = 0.008$$

Load

2.0 p.u. at $|V| = 0.95$ and power factor = 0.95 lag.

APPENDIX - F

CALCULATION OF INITIAL CONDITIONS

Network Initial conditions

Since the load conditions are known, the various voltages and currents can be calculated by performing the load flow. The entire network is symmetrical and balanced. The voltages and currents are calculated in **phasor** form and then the instantaneous values for each phase are calculated. The load current is chosen as a reference **phasor**.

Generator Initial conditions

The vector diagram for the generator is shown in Fig. F-1. The terminal voltage v_T and current i_l is known in **phasor** form from the initial conditions of the network variables. The field voltage E_{fd} and the angle δ , are calculated with the help of the following

$$C_{vt} = v_T - i_l \cdot (R_a + j x_q) \quad (F-1)$$

$$\delta = \angle C_{vt} - \pi/2 \quad (F-2)$$

$$E_{fd} = |C_{vt} - i_d (x_d - x_q)| \quad (F-3)$$

Now the initial value of other variables are given by :

$$I_f = \frac{E_{fd}}{x_{df}} \quad (F-4)$$

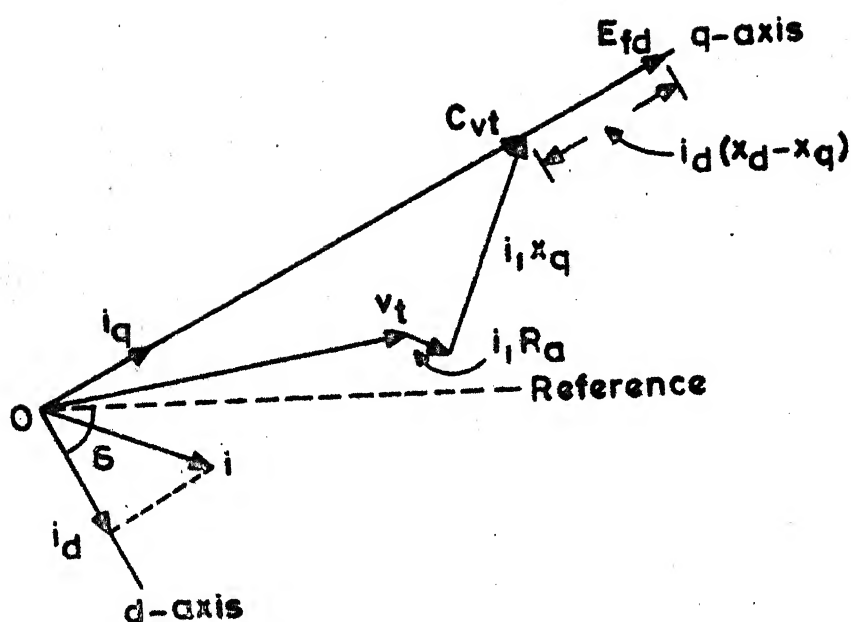


Fig. F-1 Generator vector diagram at steady state.

$$\varphi_f = x_f \cdot I_f + x_{df} \cdot i_d \quad (F-5)$$

$$\varphi_h = x_{dh} \cdot i_d + x_{fh} \cdot I_f \quad (F-6)$$

$$\varphi_g = x_q \cdot g \cdot i_q \quad (F-7)$$

$$\varphi_k = x_q \cdot K \cdot i_q \quad (F-8)$$

$$\delta = 0.0 \quad (F-9)$$

Governor Initial conditions

The equations for calculating initial conditions are given below for both hydro and thermal governors.

Hydro Governor

$$X_{h1} = G_h \quad (F-10)$$

$$X_{h2} = \delta \cdot G_h \quad (F-11)$$

$$X_{h3} = \frac{3}{2} \cdot G_h \quad (F-12)$$

where

$$G_h = \frac{100}{P_{base}} \cdot P_m \quad (F-13)$$

Under steady state conditions $P_m = P_e$

Thermal Governor

$$X_{s1} = G_{th} \quad (F-14)$$

$$X_{s2} = G_{th} \quad (F-15)$$

$$X_{s3} = G_{th} \quad (F-16)$$

$$X_{s4} = G_{th} \quad (F-17)$$

$$\text{where } G_{th} = \frac{100}{P_{base}} \cdot \frac{P_m}{F_{hp} + F_{ip} + F_{lp}} \quad (F-18)$$

Excitor Initial conditions

The equations are as follows :

$$X_{e1} = 0.0 \quad (F-19)$$

$$X_{e2} = (S_e + K_e) E_{fd} \quad (F-20)$$

APPENDIX - G

DERIVATION OF THE TRANSFER FUNCTION RELATING TERMINAL CURRENTS TO THE COMPONENT VOLTAGES OF 'FOURIER COSINE SERIES'

The basic equations for a transmission line in Laplace transform domain are :

$$Z(s) \quad I(x,s) = - \frac{d}{dx} V(x,s) \quad (G-1)$$

$$Y(s) \quad V(x,s) = - \frac{d}{dx} I(x,s) \quad (G-2)$$

Differentiating the eqn. (G-1) and substituting in eqn. (A-2) we get

$$Z(s) \quad Y(s) \quad V(x,s) = \frac{d^2}{dx^2} V(x,s) \quad (G-3)$$

If both sides of eqn. (G-3) are transformed by eqn. (4.16) then we get

$$\begin{aligned} Z(s) \quad Y(s) \quad V_k(s) = & -(k\pi/d)V_k(s) \frac{\pi}{d} \frac{d}{dx} E_k(s) \\ & + \frac{\pi}{d}(-1)^k \frac{d}{dx} E_m(s) \end{aligned} \quad (G-4)$$

Finally, substituting eqn. (G-1) for the derivatives in eqn. (G-4).

$$V_k(s) = \frac{\pi}{d} [Z(s) Y(s) + (k\pi/d)^2 U]^{-1} Z(s) [I_{km}(s) - (-1)^k I_{mk}(s)] \quad (G-5)$$

APPENDIX - HDATA FOR SYSTEM CONSIDERED IN CHAPTER IVExample - I

All the data as given in ref. [6] is on a 345 KV and 100 MVA base.

$$R_1 = 0.00918 \text{ p.u.} \quad R_o = 0.0509 \text{ p.u.}$$

$$X_1 = 0.258 \text{ p.u.} \quad X_o = 0.099 \text{ p.u.}$$

$$Y_1 = 1.64 \text{ p.u.} \quad Y_o = 0.96 \text{ p.u.}$$

The source impedance Z_c and the transformer magnetising impedance Z_t are neglected.

Circuit breaker closing resistor R_b and the trapped charges were taken as zero. All the circuit breaker poles closed simultaneous. The source voltage e_s which is considered to be balanced three phase, is given below.

$$e_s = \begin{bmatrix} 1.0 \sin(377t) \\ 1.0 \sin(377t - 2\pi/3) \\ 1.0 \sin(377t + 2\pi/3) \end{bmatrix}$$

Example - II

The data as given in ref. [2] is given on a 400 KV and 100 MVA base.

The line data

$$R_1 = 0.0048 \text{ p.u.}$$

$$X_1 = 0.0517 \text{ p.u.}$$

$$Y_1 = 1.4706 \text{ p.u.}$$

$$R_o = 0.0375 \text{ p.u.}$$

$$X_o = 0.1551 \text{ p.u.}$$

$$Y_o = 0.9804 \text{ p.u.}$$

System data

$$R_c = 0.000 \text{ p.u.}$$

$$R_t = 0.000 \text{ p.u.}$$

$$R_r = 0.0077 \text{ p.u.}$$

$$R_b = 0.25 \text{ p.u.}$$

$$X_c = 0.1313 \text{ p.u.}$$

$$X_t = 80.0 \text{ p.u.}$$

$$X_r = 1.54 \text{ p.u.}$$

Pole closing span in msec. = 0, 2, 4

Trapped charge in p.u. = -1.0, 1.0, 1.0

$$e_s = \begin{vmatrix} 1.148 & \sin(314t + \varphi) \\ 1.148 & \sin(314t - 2\pi/3 + \varphi) \\ 1.148 & \sin(314t + 2\pi/3 + \varphi) \end{vmatrix}$$

where $\varphi = 280$ degrees (this corresponds to the source angle which gave rise to maximum overvoltage).

APPENDIX - I

SIMULATION OF THE TRANSMISSION LINE FAULTS

With reference to Fig. 5.2, the fault is assumed to occur at point 'f' on the transmission line connected between terminals k and m. The transmission line is sectioned into sections 'a' and 'b' at the fault point as shown in the figure. Each section is represented as given in ref. [21]. The equations in modal domain (primed variables) for both the sections are as follows :

$$i'_{kf} = G_a \cdot e'_k + I'_k (t - \tau) \quad (I-1)$$

$$i'_{fk} = G_a \cdot e'_f + I'_{fa} (t - \tau) \quad (I-2)$$

$$i'_{fm} = G_b \cdot e'_f + I'_{fb} (t - \tau) \quad (I-3)$$

$$i'_{mf} = G_b \cdot e'_m + I'_m (t - \tau) \quad (I-3)$$

where

$$G_a = \frac{1}{Z_a + R_a/4} \quad (I-5)$$

$$G_b = \frac{1}{Z_b + R_b/4} \quad (I-6)$$

$$I'_k(t-\tau) = \frac{1+h_a}{2} [-G_a \cdot e'_f(t-\tau) - i'_{fk}(t-\tau)] + \frac{1-h_a}{2} [-G_a \cdot e'_k(t-\tau) - i'_{kf}(t-\tau)] \quad (I-7)$$

$$I'_{fa}(t-\tau) = \frac{1+h_a}{2}[-G_a \cdot e'_k(t-\tau) - i'_{kf}(t-\tau)] + \frac{1-h_a}{2}[-G_a e'_f(t-\tau) - i'_{fk}(t-\tau)] \quad (I-8)$$

$$I'_{fb}(t-\tau) = \frac{1+h_b}{2}[-G_b e'_f(t-\tau) - i'_{mf}(t-\tau)] + \frac{1-h_b}{2}[-G_b \cdot e'_m(t-\tau) - i'_{fm}(t-\tau)] \quad (I-9)$$

$$I'_m(t-\tau) = \frac{1+h_b}{2}[-G_b e'_m(t-\tau) - i'_{fm}(t-\tau)] + \frac{1-h_b}{2}[-G_b \cdot e'_f(t-\tau) - i'_{mf}(t-\tau)] \quad (I-10)$$

$$h_a = \frac{G_a - R_a/4}{G_a + R_a/4} \quad (I-11)$$

$$h_b = \frac{G_b - R_b/4}{G_b + R_b/4} \quad (I-12)$$

By re-arranging the eqns. (I-1) and (I-4) we get

$$e'_k = \frac{1}{G_a} [i'_{kf} - I'_k(t-\tau)] \quad (I-13)$$

$$e'_m = \frac{1}{G_b} [i'_{mf} - I'_m(t-\tau)] \quad (I-14)$$

Equations (I-13) and (I-14) are similar to eqns. (4.15) and (4.16) and can be solved as discussed in Chapter IV. The determination of the terms $I'_k(t-\tau)$ and $I'_m(t-\tau)$

will require the past histories of voltage e_f' and currents i_{kf}' , i_{fk}' , i_{fm}' and i_{mf}' . The currents i_{kf}' and i_{mf}' are known by eqns. (5.27) to (5.30) whereas the currents i_{fk}' and i_{fm}' are calculated by eqns. (I-2) and (I-3). The expression for e_f' will be different under different system conditions and is derived below.

(a) No fault condition :

It may be observed from Fig. 5.2, that under no fault condition we have

$$i_f' = 0 \quad (I-15)$$

$$i_{fk}' = -i_{fm}' \quad (I-16)$$

From eqns. (I-1), (I-2), (I-15) and (I-16) we have

$$e_f' = - \frac{I_{fa}'(t-\tau) + I_{fb}'(t-\tau)}{G_a + G_b} \quad (I-17)$$

(b) Line to ground fault

A line to ground fault is created by forcing the voltage on phase 'a' at the fault point to zero. The faults ~~to on~~ ~~are~~ phases 'b' and 'c' will be obviously zero.

$$e_{fa} = 0 \quad (I-18)$$

$$\text{and } i_{fb} = i_{fc} = 0 \quad (I-19)$$

From eqns. (4.7), the modal quantities 1,2,3 are given by

$$\begin{bmatrix} e_{f1} \\ e_{f2} \\ e_{f3} \end{bmatrix} = \frac{1}{3} \begin{bmatrix} 1 & 1 & 1 \\ 1 & -1 & 0 \\ 1 & 0 & -1 \end{bmatrix} \begin{bmatrix} e_{fa} \\ e_{fb} \\ e_{fc} \end{bmatrix} \quad (I-20)$$

From eqns. (I-18) and (I-20) we get

$$e_{fa} = e_{f1} + e_{f2} + e_{f3} = 0 \quad (I-21)$$

The fault current i_f in terms of its modal components is

$$\begin{bmatrix} i_{f1} \\ i_{f2} \\ i_{f3} \end{bmatrix} = \frac{1}{3} \begin{bmatrix} 1 & 1 & 1 \\ 1 & -1 & 0 \\ 1 & 0 & -1 \end{bmatrix} \begin{bmatrix} i_{fa} \\ i_{fb} \\ i_{fc} \end{bmatrix} \quad (I-22)$$

From eqns. (I-19) and (I-22) we get

$$i_{f1} = i_{f2} = i_{f3} = i_{fa}/3 \quad (I-23)$$

At the fault point 'f'

$$i'_{fk} + i'_{fm} + i'_f = 0 \quad (I-24)$$

From eqns. (I-2), (I-3) and (I-24) we get

$$e'_f = - [i'_f + I'_{fa}(t-\tau) + I'_{fb}(t-\tau)] / (G_a + G_b) \quad (I-25)$$

and from eqns. (I-21), (I-23) and (I-25)

$$i_{f1} = -\frac{D_1}{D_4} [I_{fa1}(t-\tau) + I_{fb1}(t-\tau)] - \frac{D_2}{D_4} [I_{fa2}(t-\tau) + I_{fb2}(t-\tau)] - \frac{D_3}{D_4} [I_{fa3}(t-\tau) + I_{fb3}(t-\tau)] \quad (I-26)$$

where

$$D_1 = (G_{a2} + G_{b2})(G_{a3} + G_{b3}) \quad (I-27)$$

$$D_2 = (G_{a3} + G_{b3})(G_{a1} + G_{b1}) \quad (I-28)$$

$$D_3 = (G_{a1} + G_{b1})(G_{a2} + G_{b2}) \quad (I-29)$$

$$\text{and } D_4 = D_1 + D_2 + D_3 \quad (I-30)$$

The suffix 1,2,3 indicate the modal component of the quantities.

(c) Double line to ground fault

A double line to ground fault is simulated by forcing the voltage on phases 'b' and 'c' at the fault point to zero. The fault current on phase 'a' i_{fa} will obviously be zero.

$$e_{fb} = e_{fc} = 0 \quad (I-31)$$

$$\text{and } i_{fa} = 0 \quad (I-32)$$

Substituting the eqns. (I-31) and (I-32) in eqns. (I-20) and (I-22) respectively we get

$$e_{f1} = e_{f2} = e_{f3} = e_{fa}/3 \quad (I-33)$$

$$\text{and } i_{fa} = i_{f1} + i_{f2} + i_{f3} = 0 \quad (I-34)$$

From eqns. (I-25), (I-33) and (I-34) we get

$$e_{fa} = -\frac{1}{D_5} [I_{fa1}(t-\tau) + I_{fa2}(t-\tau) + I_{fa3}(t-\tau) + I_{fb1}(t-\tau) + I_{fb2}(t-\tau) + I_{fb3}(t-\tau)] \quad (I-35)$$

$$\text{where } D_5 = G_{a1} + G_{a2} + G_{a3} + G_{b1} + G_{b2} + G_{b3} \quad (I-36)$$

Re-arranging eqn. (I-25), we get

$$i'_f = -[I'_{fa}(t-\tau) + I'_{fb}(t-\tau)] - (G_a + G_b) \cdot e'_f \quad (I-37)$$

APPENDIX - JDATA FOR SOURCE B CONSIDERED IN CHAPTER - V

All data is on 100 MVA base.

(a) Fault Inception overvoltagesStudy - I

Positive sequence impedance = $0.0008 + j 0.0426$ p.u.
 Zero sequence impedance = $0.0015 + j 0.065$ p.u.
 Voltage at bus (4) = 1.0 p.u.
 Power transfer = $3.0 + j 1.0$ p.u.

Study - II

Same as Study - I.

Study - III

Positive sequence impedance = $0.0016 + j 0.085$ p.u.
 Zero sequence impedance = $0.0030 + j 0.13$ p.u.
 Voltage at bus (4) = 1.0 p.u.
 Power transfer = $1.5 + j 0.5$ p.u.

(b) Fault overvoltages following load throw-off :

For all the Studies - I, II and III the source B data is same as that of Study - I of the fault inception overvoltages.

The **CB opening** resistance is taken as 400 ohms and is inserted for 8 m.seconds.

LIST OF REFERENCES

1. H.A. Peterson, 'Transients in Power Systems', John Wiley and Sons, Inc. NY 1951.
2. G.Hayashi, 'Forced Oscillations with Non-linear Restoring Force', Journal of Applied Physics, Vol. 24, Number 2, Feb. 1953.
3. W.J. Cunningham, 'An Introduction to Non-linear Analysis', McGraw Hill Book Company 1958.
4. F.P. Demello, A.C. Dolbec, D.A. Swann and M. Temoshok, 'Analog Computer Studies of System Overvoltages Following Load Rejections', AIEE Trans on Power Apparatus and Systems, Vol. PAS-82, pp. 42-49, April 1963.
5. G.Jancke, 'The Development of Swedish 400 KV Network', IEEE Trans. on Power Apparatus and Systems, Vol. PAS-83, pp. 197-205, March 1964.
6. R. Uram and R.W. Miller, 'Mathematical Analysis and Solution of Transmission Line Transients-I Theory', IEEE Trans. on Power Apparatus and Systems, Vol. PAS-83, pp. 1116-1123, Nov. 1964.
7. S.J.Day, N.Mullineux and J.R.Reed, 'Developments in Obtaining Transient Response Using Fourier Transform Part-I - Gibb's Phenomenon and Fourier Integral', International Journal of Electrical Engineering Education, Vol. 3, pp.501-506, 1965.

8. E.W. Stafford, D.J.Evans and N.G.Hingorani, 'Calculation of Travelling Waves on Transmission Lines by Finite Differences', Proc. of IEE , Vol.112, pp.941-947, 1965.
9. S.J.Day, N.Mullinex and J.R.Reed, 'Developments in Obtaining Transient Response Using Fourier Transform Part-II- Use of Modified Fourier Transforms', International Journal of Electrical Engineering Education, Vol.4, pp.31-40, 1966.
- 10.J.P. Bickford and P.S. Doepel, 'Calculation of Switching Transients With Particular Reference to the Line Energisation, Proc. IEE, Vol.114, No.4, pp. 465-477, April 1967.
- 11.H.W.Dommel, 'Digital Computer Simulation of Electromagnetic Transients in Single and Multiphase Network', IEEE Trans. on Power Apparatus and Systems, Vol.PAS-88, pp. 388-399, April 1969.
- 12.L.M. Wedpohl and S.E.T. Mohammad, 'Multiconductor Transmission Lines - Theory of Natural Modes and Fourier Integral Applied to Transient Analysis', Proc. IEE, Vol. 116, pp. 1553-1563, Sept. 1969.
- 13.Glen, W.Swift, 'An Analytical Approach to Ferroresonance', IEEE trans. on Power Apparatus and Systems, Vol. PAS-88, pp. 42-46, January 1969.
- 14.A. Hausperg, G.S. Vessel, G.I.Stillman, J.H.Charkov and J.C.Haahr, 'Overvoltages on the AEP 765 KV System', IEEE Trans. on Power Apparatus and Systems. Vol. PAS-88, pp. 1329-1342, Sept. 1969.

15. E.W. Kimbark and A.C. Legate, 'Fault Surge Versus Switching Surge : A Study of Transient Overvoltages Caused by Line - to - Ground Faults', IEEE trans. on Power Apparatus and Systems, Vol.PAS-87, p. 1762, 1969.
16. A Clerici and A. Taschini, 'Overvoltages due to Line Energisation and Re-energisation Versus Overvoltages Caused by Faults and Fault Clearing in EHV Systems', IEEE Trans. on Power Apparatus and Systems, Vol. PAS-89, pp. 932-941, May/June 1970.
17. C. Boonyubal, C.Calabrese and J.R. Tuder, 'A Mathematical Analysis of Transmission Line Transients Related to Fault Surges', IEEE Trans. of Power Apparatus and System. Vol. PAS-89, pp. 1207-1215, July/August 1970.
18. Alan Greenwood, 'Electrical Transients in the Power Systems', John Wiley and Sons. 1971.
19. H.B. Thoren, 'Reduction of Switching Overvoltages in EHV and UHV Systems', IEEE Trans. on Power Apparatus and Systems, Vol.PAS-90, pp.1321-1328, May/June, 1971.
20. R.Raghavan and V.R. Sastri, 'Digital Calculation of Transient Phenomena in EHV Systems Part-I', IEEE Trans. on Power Apparatus and Systems, Vol.PAS-90, pp.2072-2076, Sept./Oct. 1971.
21. H.E. Dommel, 'Non-linear and Time Varying Elements in Digital Simulation of Electromagnetic Transients', Paper Presented at the 1971 PICA Conference held in NY in May 1971.

22. U.H. Welle, C.H. Thomas, L.A. Burkhard, W.R. Lund, R.A. Hedin and A.E. Kilgour, 'Parallel EHV Untransposed Transmission Lines Studied For Overvoltages Due to Switching and Resonance', IEEE Trans. on Power Apparatus and Systems Vol. PAS-91, pp. 190-194, Jan./Feb. 1972.
23. A Clerici and C.H. Didriksen Jr., 'Dynamic Overvoltages and Ferroresonance Found in Switching Surge Studied for Irqn 400 KV Systems', IEEE Trans.on Power Apparatus and Systems, Vol. PAS-91, pp. 195-203, Jan/Feb. 1972.
24. E.Dolan, D.Gillies and E.W. Kimbark, 'Ferroresonance in a Transformer Switched with an EHV Line', IEEE Trans. on Power Apparatus and Systems, Vol. PAS-91, 1273-1280, May/June 1972.
25. Ferroresonance Observations in High Voltage Sub-station, Laborelec Report 2/304 July 1970, 2/2027 July 1971, and 2/20212 August 1972.
26. R.P.Aggarwal, I.B.S.Chauhan and V.P.Sinha, 'Method to Determine dynamic overvoltages due to sudden load rejection on EHV system, Journal of Institution Engineers (India), Vol. 54, EL-2, pp. 67-70, Dec. 1973.
27. Switching Surge Overvoltages Study of EHV System under Beas Project Part-I, IIT Kanpur Report 1972.
28. R.S. Ramshaw and K.R. Padiyar, 'Generalised System Model for Slip-ring Machines', Proc.of IEE, Vol. 120, No.6, pp. 647-658, June 1973.

29. R.G.Wasley and S.Selvavinayagamoorthy, 'Approximate Analytic Formulae for Transmission Line Forward and Backward Response Functions in the Time Domain', IEEE Trans.on Power Apparatus and Systems, Vol. PAS-93, pp.1731, Nov./Dec. 1974.
30. S.J.Balser and P.C. Krause, 'Single Pole Switching- A Study of System Transients With Transposed and untransposed Lines', IEEE Trans. on Power Apparatus and Systems, Vol. PAS-93, pp. 1208-1212, July/August 1974.
31. W.S. Meyer and H.W. Dommel, 'Numerical Modelling of Frequency Dependent Transmission Line Parameters in an Electromagnetic Transient Program', IEEE trans. on Power Apparatus and Systems, Vol. PAS-93, pp. 1401-1409, Sept./Oct. 1974.
32. Voltage Transformer Failure at Rishikesh Sub-station of UPSEB', BHEL Report, 1977.
33. Ferro-resonance of a High Tension Transformer with the Capacity of an open circuit breaker, Laborlec Report July 1977.
34. N.Germay, S.Mastere and J.Uroman, 'Review of the Ferro-resonance Phenomena in High Voltage Power System and Presentation of a Voltage Transformer Model for Predetermining Them, CIGRE, Paper No.33-18, 1974.
35. Prusty and Sanyal, ' A New Approach for Study of Ferro-resonance', Proc. of IEE, Vol.123, No.9, pp.906-918, Sept. 1976.

36. F.P.Demello, L.M.Lewzinger and R.J.Mills, 'Load Rejection Overvoltages as Affected by Excitation System Control', IEEE Trans.on Power Apparatus and Systems, Vol. PAS-94, pp.280-287, March/April 1975.
37. 'Electrical Engineering Handbook', Published by Siemens Aktiengesellschaft and Heydon and Sons Limited 1969, 1976.
38. A.Clerici, G.Santagostino and A.Magagnoli, 'Influence of Fault Initiation and Fault Clearing Overvoltages on the Insulation of UHV Lines', IEEE Trans. on Power Apparatus and Systems, Vol. PAS-94, pp. 802-809, May/June 1975.
39. V.Brandwajn and H.W. Dommel, 'A New Method for Interfacing Generator Model With Electromagnetic Transient Program', Presented at 1977, PICA held on May 1977, pp. 280-265.
40. V. Madzarevic, F.K. Tseng, D.H.Woo, W.D.Niebuhr and R.G. Rocamora, 'Overvoltages on EHV Transmission lines Due to Faults and Subsequent by Passing of Series Capacitors', IEEE Trans. PAS-96, pp.1847-1855, Nov./Dec. 1977.
41. Y.A. Tsirel and V.S. Polyakov, 'Ferroresonance Phenomena in Networks with a Dead-grounded Neutral and Measures to Prevent Them', Soviet Power Engineering, No.3, March 1977, pp. 180-184.
42. J.M.Feldman, 'On the Accuracy and Utility of Piecewise Linear Model of Ferroresonance', IEEE Trans.on Power Apparatus and Systems, Vol.PAS-97, pp. 469-477 March/April 1978.

43. M.R. Nigli, W.E. Yturralde, W.O. Niebuhr, V.Madzarevic and R.G. Rocamora, 'Fault Clearing Overvoltages on Long Transformer Terminated Lines', IEEE Trans. on Power Apparatus and Systems, Vol. PAS-98, pp.667-678, March/April 1979.
44. D.M.Triezenberg, 'An Efficient State Variable transmission Line Model', IEEE Trans. on Power Apparatus and Systems, Vol. PAS-98, pp.484-492, March/April 1979.
45. IEEE Committee Report, 'Computer Representation of Excitation Systems', IEEE Trans. on Power Apparatus and Systems, Vol. PAS-87, June 1968.
46. IEEE Committee Report, 'Dynamic Models for Steam and Hydro Turbines in System Studies, ' IEEE Trans of Power Apparatus and Systems, Vol. PAS-92, pp. 1904-1915, Nov./Dec. 1973.
47. Correspondence with M/s HITACHI Ltd.
48. T. Onu and H. Matsubara, 'Number of Sections Necessary for Transmission Line Model Used for Transient Network Analyzer', Electrical Engineering in Japan, Vol. 95, No.5, pp. 26-33, 1975.
49. G.L. Wilson and K.A. Schmid, 'Transmission Line Models for Switching Studies; Design Criteria II : Selection of Line Length, Model Design and Tests', IEEE Trans. on Power Apparatus and Systems, Vol. 93, pp. 389-395, Jan/Feb. 1974